

**EFFECTS OF RESIDUAL STRESS, WELD TOE NOTCH AND WELD
DEFECTS ON FATIGUE OF WELDED STEEL STRUCTURES**

Wenyu Shen

B.S. Beijing University, China, 1982

M.S. Chinese Academy of Science, China, 1987

**A dissertation submitted to the faculty
of the Oregon Graduate Institute of Science & Technology
in partial fulfillment of the degree
Doctor of Philosophy
in
Materials Science and Engineering
April, 1992**

The dissertation "Effects of Residual Stress, Weld Toe Notch and Weld Defects on Fatigue of Welded Steel Structures" by Wenyu Shen has been examined and approved by the following Examination Committee:

Paul Clayton
Professor and Thesis Advisor

Milton Scholl
Assistant Professor

Lemmy Meekisho
Assistant Professor

Grzegorz Glinka
Professor
University of Waterloo, Canada

Oscar Orringer
Senior Mechanical Engineer
U. S. Department of Transportation

ACKNOWLEDGEMENTS

I would like to acknowledge Federal Railroad Administration (FRA) Office of Research and Development for sponsoring this project.

I am deeply grateful to my advisor, Dr. Paul Clayton, for his encouragement and guidance throughout this work. Particularly, I appreciate his patience and understanding. I would like to express my special thanks to Dr. Milton Scholl for his help in test design and providing lots of technique support. I would like to thank Bob Turpin for his help in welding operation and testing arrangement; thank Dr. Lemmy Meekisho, Dr. Grzegorz Glinka and Dr. Oscar Orringer for spending time to evaluate my thesis and providing many useful discussions.

Also, I wish to thank Ken Burns, Andy Villeneuve, Douglas Davis for the assistance in experiments; thank Sylvia Berkowitz for the editing work; and specially, thank Xuqiu Tan for the concern and emotional support.

Finally, I would like to appreciate all the student, staff and faculty members in the Department of Materials Science and Engineering and in the Oregon Graduate Institute of Science & Technology for their help and friendship during the past four years.

To my parents

献给我的父母

TABLE OF CONTENTS

TITLE	i
APPROVAL	ii
ACKNOWLEDGEMENTS	iii
DEDICATION	iv
TABLE OF CONTENTS	v
LIST OF FIGURES	x
LIST OF TABLES	xiv
ABSTRACT	xv
CHAPTER 1 INTRODUCTION	1
CHAPTER 2 BACKGROUND	7
2.1 Fatigue fracture	7
2.2 Residual stress	17
2.3 Fatigue of welded joints	22
2.4 Mean stress effect on fatigue of unwelded steel	25
2.5 Welding residual stress effect on fatigue of welded steel	37
2.6 Residual stress measurement method	45
2.7 Sectioning residual stress measurement	49
2.8 Hole-drilling residual stress measurement	54
CHAPTER 3 EXPERIMENTAL	60
3.1 General test program	60
3.2 Material	62

3.3 Specimen preparation	64
3.3.1 Pad-on-plate weld specimen	64
3.3.2 Simple weld specimen	64
3.4 Fatigue test design	68
3.4.1 Testing machine	68
3.4.2 Grip system	68
3.4.3 Fatigue test condition	69
3.4.4 Crack propagation measurement	69
3.5 Application of Sectioning method	74
3.5.1 Sectioning operation	74
3.5.2 Calibration test	74
3.6 Application of Hole-drilling method	77
3.6.1 Hole drilling operation	77
3.6.2 Calibration constants	77
3.6.3 Hole drilling machining stress	79
3.6.4 High stress application	79
3.6.5 Accuracy of Hole-drilling method	80
3.7 Residual stress measurement	84
3.7.1 Residual stress in as-received A515 steel plate	84
3.7.2 Residual stress in as-welded pad-on-plate specimen	84
3.7.3 Residual stress in as-welded simple specimen	85
3.7.4 Residual stress in stress-relieved simple specimen	85
3.7.5 Residual stress in cyclic loaded simple specimen	86
3.8 Weld toe stress concentration	89
3.9 Metallurgical analysis	94
3.9.1 Microstructure and microhardness	94

3.9.2	Welding defects	94
3.9.3	Fracture surface analysis	95
CHAPTER 4	RESULTS	96
4.1	Sectioning calibration	96
4.2	Hole-drilling calibration	97
4.2.1	Calibration constant	97
4.2.2	Hole drilling machining stress	97
4.2.3	High stress correction	98
4.2.4	Accuracy of Hole-drilling method	99
4.3	Residual stress measurement	105
4.3.1	As-received plate	105
4.3.2	As-welded pad-on-plate specimen	105
4.3.3	As-welded simple specimen	106
4.3.4	Stress-relieved simple specimen	107
4.3.5	Effect of cyclic load	107
4.4	Fatigue test	122
4.4.1	S-N relationship	122
4.4.2	Crack propagation property	122
4.5	Stress concentration factor	133
4.6	Metallurgical analysis	136
4.6.1	Microstructure and microhardness analysis	136
4.6.2	Weld defect analysis	137
4.6.3	Visual fracture surface analysis	137
4.6.4	SEM fracture surface analysis	138
CHAPTER 5	CALCULATION	155
5.1	Stress intensity factor	155

5.1.1	Semi-elliptic crack	155
5.1.2	Through-thickness crack	156
5.2	Fatigue crack propagation	160
CHAPTER 6 DISCUSSION		165
6.1	Residual Stresses	165
6.1.1	Measurement method	165
6.1.2	Residual stress measurement	166
6.1.3	Specimen width effect	169
6.1.4	Residual stress relaxation effect	169
6.1.5	Heat treatment effect	170
6.2	Fatigue test	174
6.2.1	S-N test result	174
6.2.2	Welding residual stress effect	175
6.2.3	Literature comparison	175
6.2.4	Effect of weld toe notch and weld defect	176
6.2.5	Crack profile analysis	177
6.2.6	Tank car problem	177
6.3	Fatigue crack propagation	181
6.3.1	The concept of equivalent crack	181
6.3.2	Determination of equivalent crack	182
6.3.3	Crack propagation analysis	187
6.3.4	Future work	188
CHAPTER 7 CONCLUSION		196
REFERENCE		198
APPENDIX		205
1.	Program for sectioning residual stress analysis	205

2. Program for hole-drilling residual stress analysis	207
3. Program for stress intensity factors of semi-elliptic crack	210
4. Program for stress intensity factors of through-thickness crack	212
5. Program for fatigue propagation life of semi-elliptic crack	213
6. Program for fatigue propagation life of through-thickness crack	215
BIOGRAPHIC NOTE	216

LIST OF FIGURES

	<i>Page</i>
1.1 Tank Car Structure	4
1.2 Pad-on-shell weld detail	5
1.3 Computed residual stress patterns at the weld end	6
2.1 Sinusoidal cyclic fatigue load	13
2.2 Stress-life (S-N) curve for steel	14
2.3 Strain-life (ϵ -N) curve for steel	15
2.4 Crack propagation property ($\frac{da}{dN} - \Delta K$) curve for steel	16
2.5 Residual stresses and welding distortion in butt welded plate	21
2.6 Mean stress effect on fatigue strength	31
2.7 Mean stress effect on strain-life curve	32
2.8 Mean stress effect on crack propagation of A516 steel	33
2.9 Mean stress effect on crack propagation of mild steel	34
2.10 Mean stress effect on crack propagation of high strength steel	35
2.11 Mean stress effect on threshold stress intensity factor	36
2.12 Gurney's S-N results	43
2.13 Maddox's S-N results	44
2.14 Sectioning configuration	53
2.15 Hole-drilling configuration	59
3.1 Pad-on-plate weld specimen	66

3.2	Bead-on-plate and fillet simple weld specimens	67
3.3	Fatigue testing machine	71
3.4	Grip system	72
3.5	Crack propagation gage and its principle	73
3.6	Strain gage rosette for sectioning measurement	76
3.7	Strain gage rosette for hole-drilling measurement	81
3.8	Hole-drilling fixture	82
3.9	Tensile bar configuration	83
3.10	Local coordinate system for residual stress measurement	87
3.11	Measurement points distribution	88
3.12	Specimen for SCF measurement	92
3.13	Principle of SCF measurement	93
4.1	Stress-strain curve for hole-drilling calibration	102
4.2	Stress-strain curve for high stress hole-drilling calibration	103
4.3	Calibration constants as a function of stress level	104
4.4	Residual stresses in pad-on-plate weld specimens	113
4.5	Residual stress patterns in pad-on-plate weld specimens	114-116
4.6	Effect of specimen width on residual stress	117
4.7	Residual stresses in simple weld specimens	118
4.8	Cyclic load effect on longitudinal residual stress (3D plotting)	119
4.9	Cyclic load effect on longitudinal residual stress (2D plotting)	120
4.10	Cyclic load effect on transverse residual stress	121
4.11	Crack propagation measurement	130

4.12	Crack length as a function of load cycles	131
4.13	Overload effect on crack growth rate	132
4.14	Stress concentration factor measurement	135
4.15	Microstructure of as-welded A515 weld joint	141-142
4.16	Microstructure of stress-relieved A515 weld joint	143-144
4.17	Weld defect (slag inclusion)	145
4.18	Weld defect (porosity)	146
4.19	Weld defect (lack of fusion)	147
4.20	Fracture surface feature (top view)	148
4.21	Fracture surface feature (surface view of initiation site)	149
4.22	Fracture surface feature (section view)	150
4.23	Fracture surface feature (surface view of crack profile)	151
4.24	SEM picture of crack initiation site	152
4.25	SEM picture of magnified initiation site	153
4.26	SEM picture of crack surface	154
5.1	Center semi-elliptic crack configuration	158
5.2	Calculated SIF as a function of crack length	159
5.3	Crack propagation property of A515 steel	163
5.4	Crack propagation calculation under load 0 to 13 Ksi	164
6.1	Residual stress in skip weld specimen	172
6.2	Different weld profile	173
6.3	Comparison of S-N test result and Gurney's result	179
6.4	Comparison of S-N test result and Maddox's result	180

6.5	Equivalent crack concept	190
6.6	Comparison with general ferrite-pearlite steels	191
6.7	Crack propagation calculation with $m=2$	192
6.8	Crack propagation calculation with $m=3$	193
6.9	Crack propagation calculation comparison	194
6.10	Comparison with A516 steel	195

LIST OF TABLES

	<i>Page</i>
2.1 Mean stress effect on fatigue of unwelded steel	30
2.2 Residual stress effect on fatigue of welded steel	41
2.3 Fatigue test result from Maddox	42
3.1 Chemical compositions of A515 and A283 steel	63
3.2 Tensile properties of A515 and A283 steel	63
4.1 Hole-drilling calibration	100
4.2 Hole-drilling machining stress	101
4.3 Accuracy of Hole-drilling technique	101
4.4 Residual stress in as-received A515 plate	108
4.5 Residual stress in as-welded pad-on-plate specimen	109
4.6 Residual stress in as-welded simple weld specimen	110
4.7 Residual stress in stress-relieved specimen	111
4.8 Effect of cyclic load on residual stress	112
4.9 Fatigue test of fillet welded A515 steel specimen	124
4.10 Fatigue crack propagation measurement	125-129
4.11 Average stress concentration factor measurement	134
4.12 Microhardness measurement	140
4.13 Geometrical feature of fatigue crack	140
6.1 Semi-elliptic crack propagation life calculation	189
6.2 Through-thickness crack propagation life calculation	189

ABSTRACT

Effects of Residual Stress, Weld Toe Notch and Weld Defects on Fatigue of Welded Steel Structures

Wenyu Shen, Ph.D.

Oregon Graduate Institute of Science & Technology, 1992

Supervising Professor: Paul Clayton

In studying the fatigue behavior of fillet welded railroad tank car shell structures, the effects of welding residual stress, weld toe notch and weld defects on the fatigue of fillet welded A515 steel specimens were evaluated.

Both hole-drilling and sectioning measurement techniques were used to obtain residual stress information. Pad-on-plate weld specimens were designed to simulate the tank car structure for welding residual stress measurement. Simple bead-on-plate and fillet weld specimens, which have similar welding residual stresses near the weld end toe to the pad-on-plate specimens, were designed to be as compact as possible for fatigue testing.

As-welded and stress-relieved simple weld specimens were tested under pulsed tension and alternating cyclic load conditions to determine stress-life and fatigue crack propagation properties. Weld toe stress concentration effects were determined by strain gage measurement. Fracture surface features and crack initiation sites were studied by visual analysis, scanning electron microscopy and optical microscopy.

Welding residual stresses were found to be biaxial tension-compression near the weld end toe and biaxial tension-tension near the weld center toe. Longitudinal tensile residual stress was significantly relieved when the applied longitudinal tensile cyclic load was greater than 14 Ksi. Test results did not show a consistent effect of tensile residual stress on the fatigue strength under pulsed tension loads. However, tensile residual stress had a significant influence on the fatigue strength under alternating cyclic loads.

The weld end toe was associated with a stress concentration factor of approximately 3 and was the most critical factor in initiating fatigue cracks. Weld defects, such as slag inclusions, lack of fusion, and porosity were found to significantly affect the fatigue strength of a welded joint when the load magnitude or mean stress was low. An equivalent crack concept, based on linear elastic fracture mechanics theory, was introduced to quantify the weld toe stress concentration effect. This concept was shown to be effective for fatigue design and fatigue life prediction of welded structures.

CHAPTER 1

INTRODUCTION

Welding is the most efficient and economical way to permanently join metal parts. It has wide applications in manufacturing and in the repair industry. Because of the influence of weld geometry, weld defects and welding residual stress, the mechanical performance of a welded joint is usually not the same as that of the parent material. In the applications of pressure vessels, off-shore structures, railway equipment, reaction boilers and pipe lines, fatigue fracture at a welded joint is a common failure mode. Since these structures are often employed to transport or to store hazardous materials, it is important to evaluate the fatigue behavior of welded joints for both safety and economical reasons.

A group of DOT 111A/100W tank cars, Figure 1.1, manufactured with 7/16 inch thick ASTM A515 grade 70 structural steel plate in 1967, were used to carry non-pressurized hazardous materials, such as ethylene oxide and gasoline. Between 1979-1981, these tank cars were required to be reinforced by welding spanning stiffeners onto the underbelly in order to improve the overall buckling resistance. Figure 1.2 shows the detailed welding repair dimensions. The stiffener was continuously fillet welded onto a 0.5 inch thick A283 steel pad, and the pad was skip fillet welded onto the tank car shell. The alteration specifications for the pad-on-shell welding required that each skip fillet weld not exceed 3 inches in length and that the throat thickness not exceed 1/4 inch.

During a safety inspection in 1986, it was found that some of the welded joints were not in conformance with the specifications. For example, some skip fillet welds were up to 8 inches in length and some throat thicknesses exceeded 1/4 inch. The Federal Railroad Administration (FRA) Office of Safety asked the Transportation Systems Center (TSC) to form a task force to evaluate the effect of non-conforming stiffeners on the structural integrity of tank car shells. The evaluation was performed by developing a theoretical model to calculate the welding residual stress patterns around a welded joint and determining the effect of non-specified welding conditions on the residual stress [1,2]. The results showed that the shell residual stress was insensitive to the fillet weld length and the weld throat thickness. However, the calculated results showed that the shell welding residual stress was of yield magnitude in a biaxial tension-tension mode within a critical zone, about 1/4 inch in diameter, at the weld end toe area, Figure 1.3. The service loads on a tank car include static weight load, vertical vibration load and horizontal drawing load. The result of a finite element analysis has shown that the total service loads on the tank car shell surface are low amplitude fluctuations within a range of -25 to +15 Ksi [3]. Combined with the welding residual stress, the overall loads on the fillet welds of a tank car shell are low amplitude cyclic stresses with high mean stress. This raises a concern that the high tensile residual stress might significantly reduce the fatigue resistance of the tank car shell since a through crack was identified in a tank car shell in one instance.

The effect of residual stress on the fatigue behavior of a welded structure is an interesting and long debated subject. Some investigators believe that a tensile residual stress would degrade the fatigue strength of a welded joint, and

that relieving the as-welded tensile residual stress would improve the fatigue strength of a welded joint [1,4]. However, other investigators believe that the tensile welding residual stress is not always detrimental, and that relieving tensile welding residual stress will not improve the fatigue strength of a welded joint if the applied cyclic load is fully tensile [5-8]. Since each study deals with different materials, specimen types and test conditions, they are not necessarily systematically related. The fatigue strength of a welded joint is not only dependent on residual stress but is also dependent on the material, geometry, weld defects and the nominal load [9,10]. Also, the residual stress itself is variable, depending on the load and the crack length during the fatigue process. Although there has been a tremendous effort to reveal the mysterious role of residual stress, there is still some confusion and there has been no consistent conclusion on the issue.

For the tank car problem, a research program was carried out to evaluate the effect of welding residual stress on the fatigue behavior of a fillet welded tank car shell. Considering that except welding residual stress, a welded joint also subjects to the effects of weld geometry and weld defects which are considered important factors to affect the fatigue strength of a welded joint. With the tank car program as a basis, a quantitative study of the roles of welding residual stress, weld toe notch and weld defects on the fatigue behavior of welded joints has been carried out in the current work. Major objectives include experimental measurement of welding residual stress and weld toe stress concentration, fatigue testing of as-welded and stress-relieved weld specimens, fracture surface analysis, and fatigue crack propagation calculations.

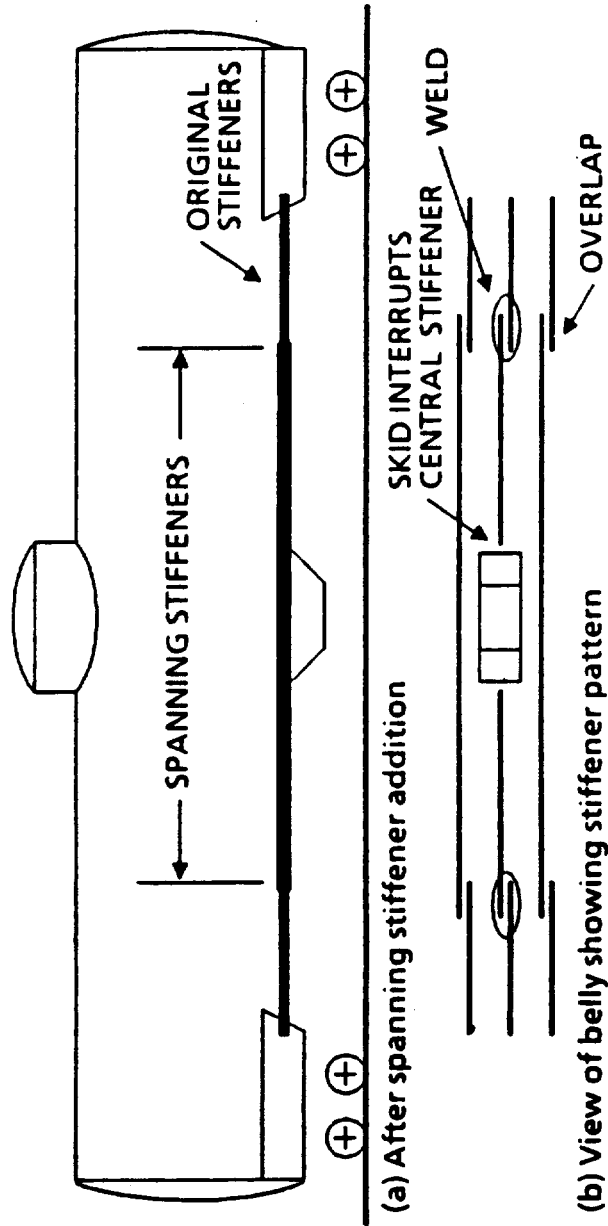


Figure 1.1 Tank Car Structure

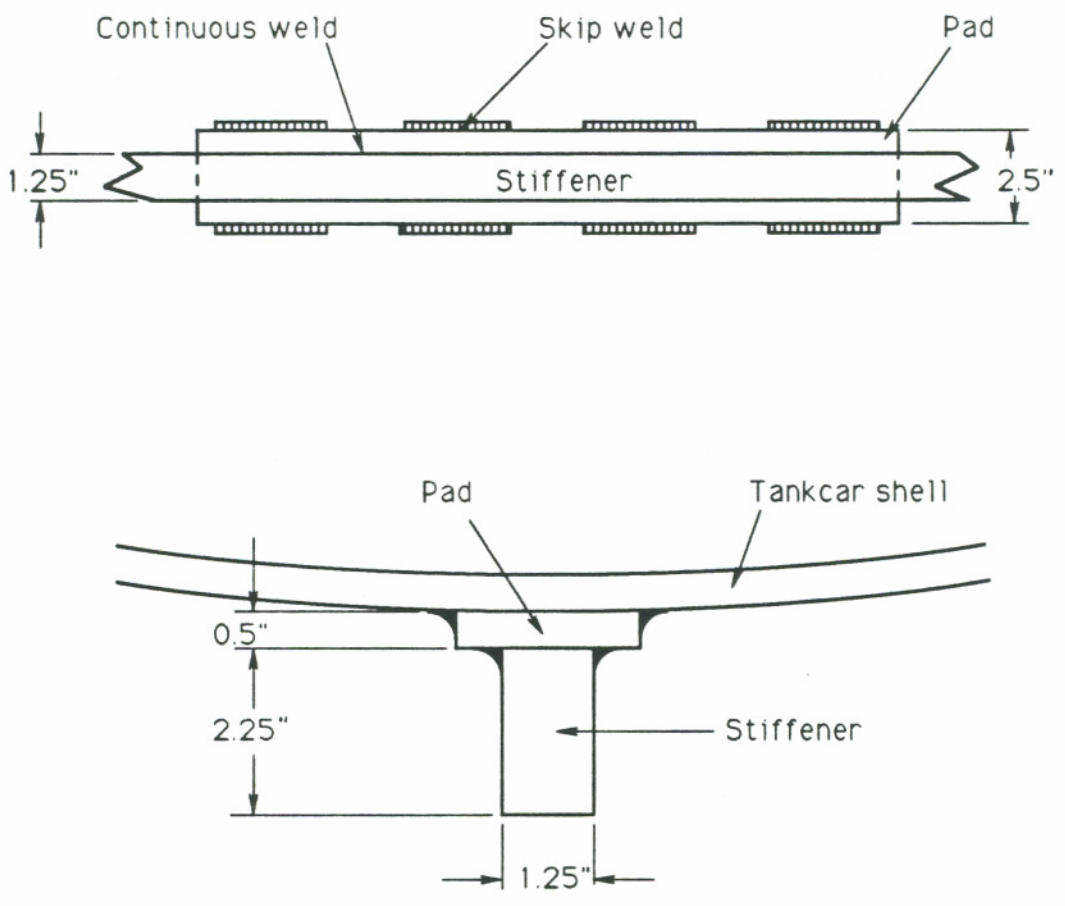
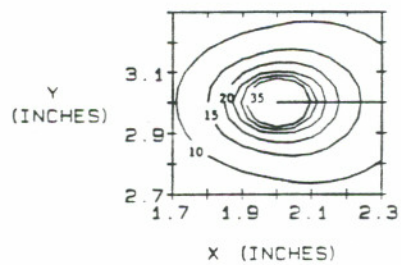
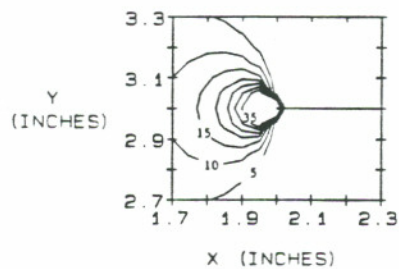
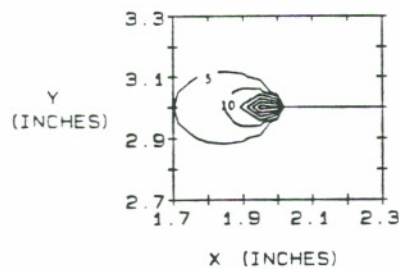


Figure 1.2 Pad-on-shell Weld Detail



(a) Mises-Hencky Equivalent Stress

(b) Normal Stress S_{xx} (c) Normal Stress S_{yy}

STRESS CONTOURS NEAR THE END OF A SKIP WELD
(STRESS CONTOURS IN KSI; 1 KSI = 6.895 Mpa)

Figure 1.3 Computed Residual Stress Patterns at the Weld End [2]

CHAPTER 2

BACKGROUND

2.1 Fatigue fracture

Fatigue is a process in which a material suffers progressive plastic damage due to a fluctuating stress. The fatigue failure which is of the greatest engineering concern is fatigue fracture. It is the failure mode involved with crack nucleation and crack propagation in a material. Since there are always defects in a material, there are always local stress concentrations in a stressed material. If a high enough fluctuating stress is applied, alternating microplastic slip movement will occur at those defects as a result of local yielding. It is the accumulation of these microplastic deformations that causes progressive plastic damage and crack formation in the material, and further causes the crack to propagate.

The plastic deformation around a fatigue crack is usually small and the fatigue fracture surface typically shows brittle fracture features. Under detailed fracture surface examination, two types of surface appearances may be identified [11,12]. In one, the fracture surface is smooth and flat with little indication of plastic deformation. This usually occurs when the cracked surface is perpendicular to the maximum tensile stress, such as during the propagation of a well developed crack. The other type of fracture surface is rough with indications of large plastic deformation. This occurs when the crack surface is

inclined to the maximum tensile stress, such as during the initiation of a crack.

Fatigue life is defined as the number of stress cycles required to cause failure by fracture, and is sometimes divided into crack initiation life and crack propagation life. The crack initiation life is usually defined as the number of stress cycles required to develop a certain size crack. The crack propagation life is usually defined as the number of stress cycles required to drive the crack from initiation to final failure. Because crack initiation is a process of microplastic damage accumulation, there is no clear boundary between crack initiation and crack propagation. Different investigators use different crack sizes to define crack initiation, and no consistent standard has been established.

Fatigue load may be any cyclic stress with variable ranges and frequencies. Since any load-time spectrum can be theoretically decomposed into a combination of several simpler sinusoidal load-time spectra, a sinusoidal load-time spectrum is typically used as a fatigue load in most fundamental fatigue studies. Figure 2.1 shows a sinusoidal load-time spectrum normally used in laboratory fatigue tests. The major parameters of the load are:

maximum stress, σ_{\max}

minimum stress, σ_{\min}

mean stress, $\sigma_m = (\sigma_{\max} + \sigma_{\min})/2$

stress amplitude, $\sigma_a = (\sigma_{\max} - \sigma_{\min})/2$

stress ratio, $R = \sigma_{\min}/\sigma_{\max}$

stress range, $\Delta\sigma = \sigma_{\max} - \sigma_{\min}$

Load frequency is also a load parameter. Since when the load frequency is far less than the resonant frequency of the structure, its effect on fatigue strength is usually insignificant for steels at room temperature and in noncorrosive environments [13-15]. Therefore, only two of these load parameters are independent and any two can be used to represent the fatigue loading spectrum in fatigue studies.

There are three major methods used in fatigue life prediction: the Stress-Life approach, the Strain-Life approach and the Linear Elastic Fracture Mechanics approach [16]. Any of these methods may be used for fatigue design of new structures and fatigue life prediction of existing structures. Each of the methods has its advantages and disadvantages in application.

Stress-Life Approach (S-N):

This approach is commonly used for high cycle fatigue tests under load controlled conditions and is used to determine the relationship between fatigue life and an applied constant stress level. Test data are presented by plotting fatigue failure life versus stress level on a log-log diagram. The stress level could be σ_{\max} , σ_a or $\Delta\sigma$ with a fixed mean stress σ_m or stress ratio R. This approach neglects the fracture mechanisms in crack initiation and crack propagation processes. Although it is considered the most accurate approach for a particular practical problem, it is a purely empirical method for fatigue design and fatigue life prediction. The experiments to generate the test data are expensive and time consuming, and the results obtained under one set of conditions cannot easily be used for fatigue predictions in another. Figure 2.2 shows a typical S-N curve for steels. The relationship between stress and

fatigue life is nearly linear. The curve becomes horizontal at the point when infinite life is reached. This minimum stress for fatigue failure is known as the fatigue endurance limit, S_e . The empirical equation for the stress-life relationship is:

$$S_n = S_e (N/n)^k \quad (2.1)$$

where S_n is the fatigue strength computed at n failure cycles, N is the number of cycles to define the fatigue endurance limit S_e (N is usually taken as 2 million cycles) and K is a constant which depends on the material and loading conditions.

Strain-Life Approach (ϵ - N):

This approach is used for low cycle fatigue tests under strain controlled conditions, and it determines the relationship between fatigue life and an applied constant strain level. Test data are presented by plotting fatigue failure life versus strain level on a log-log diagram. The fatigue failure life is theoretically determined from the true stress-strain behavior of the material under cyclic load. Since this condition is similar to the crack initiation from a notch, this approach is typically used for crack initiation life prediction. Since it is based on elastic and plastic theory, the test results from the strain-life approach are non-specific of the test conditions. Test results from small, simple specimens may be used to predict fatigue properties of large, complex structures. Figure 2.3 shows a generalized ϵ - N curve for steel. The equation for this relationship is:

$$\frac{\Delta\epsilon}{2} = \frac{\sigma'_f}{E} (2N_f)^b + \epsilon'_f (2N_f)^c \quad (2.2)$$

where $\frac{\Delta\epsilon}{2}$ is the strain amplitude, E is Young's modulus, σ'_f is the fatigue strength coefficient, b is the fatigue strength exponent, ϵ'_f is the fatigue ductility coefficient, c is the fatigue ductility exponent and $2N_f$ is number of reversals to failure. The fatigue strength exponent b usually varies between -0.05 to -0.12 and the fatigue ductility exponent c usually varies between -0.5 to -0.7.

Linear Elastic Fracture Mechanics Approach (LEFM):

The LEFM approach is commonly used for fatigue crack propagation tests under load controlled conditions. This approach determines the relationship between the crack propagation rate and the crack tip stress intensity factor. Test data are presented by plotting crack propagation rate versus stress intensity factor range on a log-log diagram. Based on LEFM theory, some empirical relationships between the fatigue crack propagation rate and the crack tip stress intensity factor can be established. These relationships can be used for prediction of the fatigue crack propagation life of a cracked structure. This approach has gained wide acceptance due to its direct relationship with the observable physical crack length. Figure 2.4 shows a typical $\frac{da}{dN} - \Delta K$ curve for steels. The curve usually consists of three regions: Region I, near threshold crack growth region; Region II, power law crack growth region; and Region III, rapid unstable crack growth region. Fatigue crack propagation in Region I is slow and is sensitive to the mean stress of the applied cyclic load (see section 2.4). Although a few empirical relationships have been established for region I crack propagation prediction, none has been proved effective. A simple relationship for fatigue crack propagation in Region II is the well known Paris law:

$$\frac{da}{dN} = C (\Delta K)^m \quad (2.3)$$

where $\frac{da}{dN}$ is the crack propagation rate, ΔK is the stress intensity factor range, C and m are material constants. This relationship has proven to be a reasonable approach for the prediction of fatigue crack propagation in most materials. Crack growth in Region III is generally not of interest since the crack propagation life is short and the fracture mode is no longer a fatigue problem.

Some important considerations in fatigue crack propagation studies are the threshold stress intensity factor, K_{th} , and transition stress intensity factor between region I and region II, K_{tr} . When the applied stress intensity factor range is below K_{th} , the crack will either stop or grow too slowly to be identified. When the applied stress intensity factor range is lower or higher than K_{tr} , the crack propagation rate will behave differently (see Figure 2.4).

The fatigue strength of a structure depends on factors such as load, residual stress, defects, geometry, material and environment. Load, as a driving force, provides the necessary energy for crack growth. Residual stress is an additional load. Defects, as a factor of stress concentration, have an effect on the local load which then affects fatigue crack initiation. Geometry affects the crack tip plastic zone size and the crack tip residual stress. The mechanical properties of the material, as a measure of strength and deformation ability, affect the crack initiation and crack propagation. The environment can affect material properties as well.

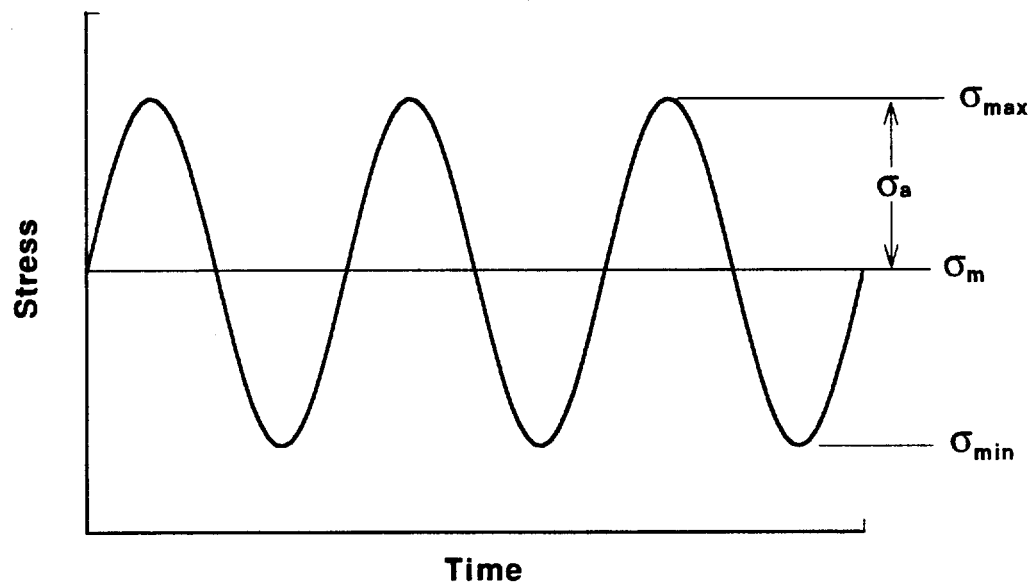


Figure 2.1 Sinusoidal Cyclic Fatigue Load

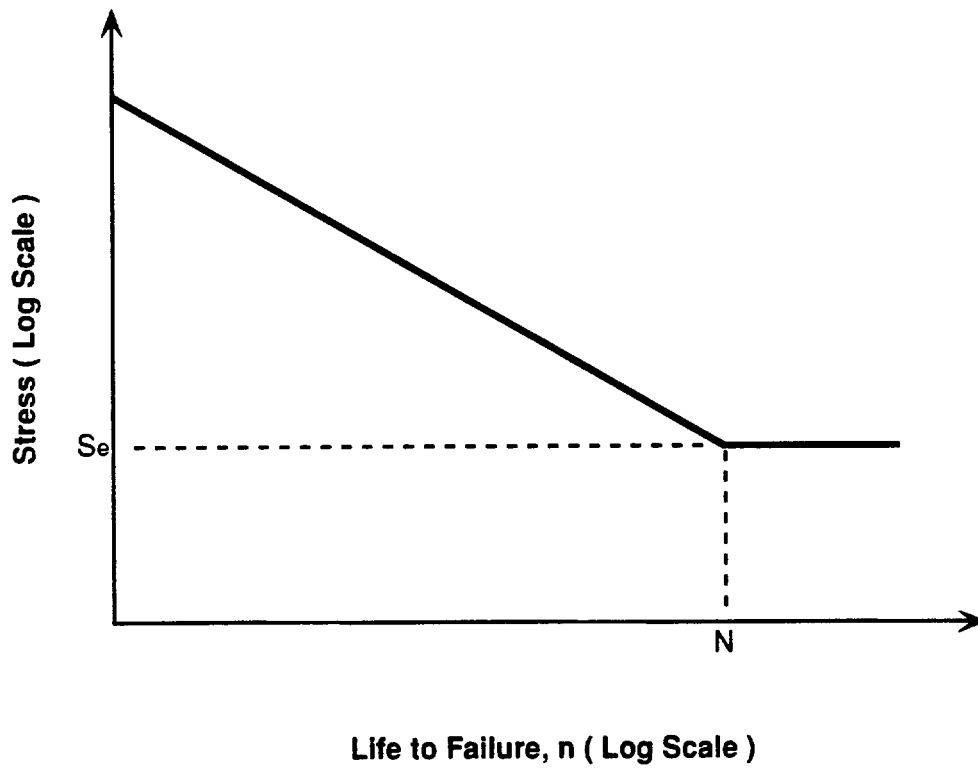


Figure 2.2 Stress-life (S-N) Curve for Steel

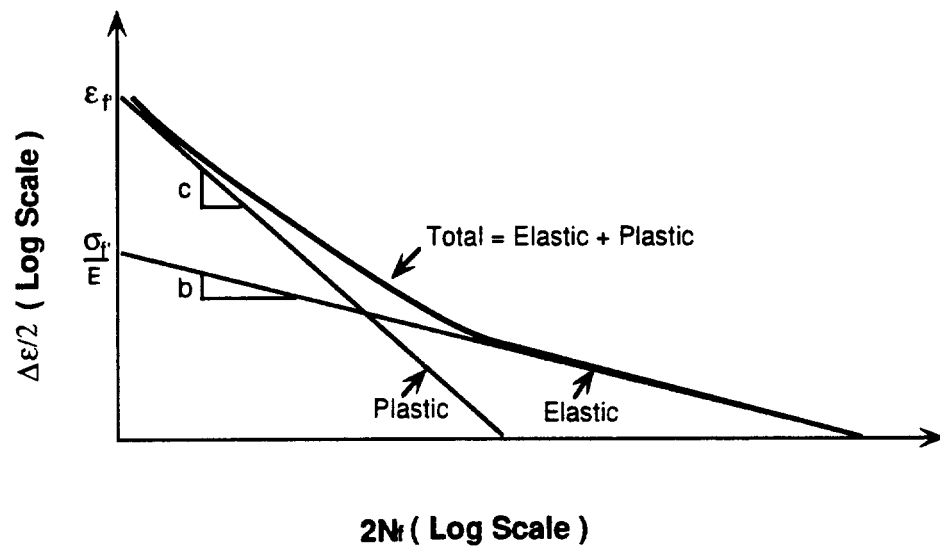


Figure 2.3 Strain-life (ϵ - N) Curve for Steel

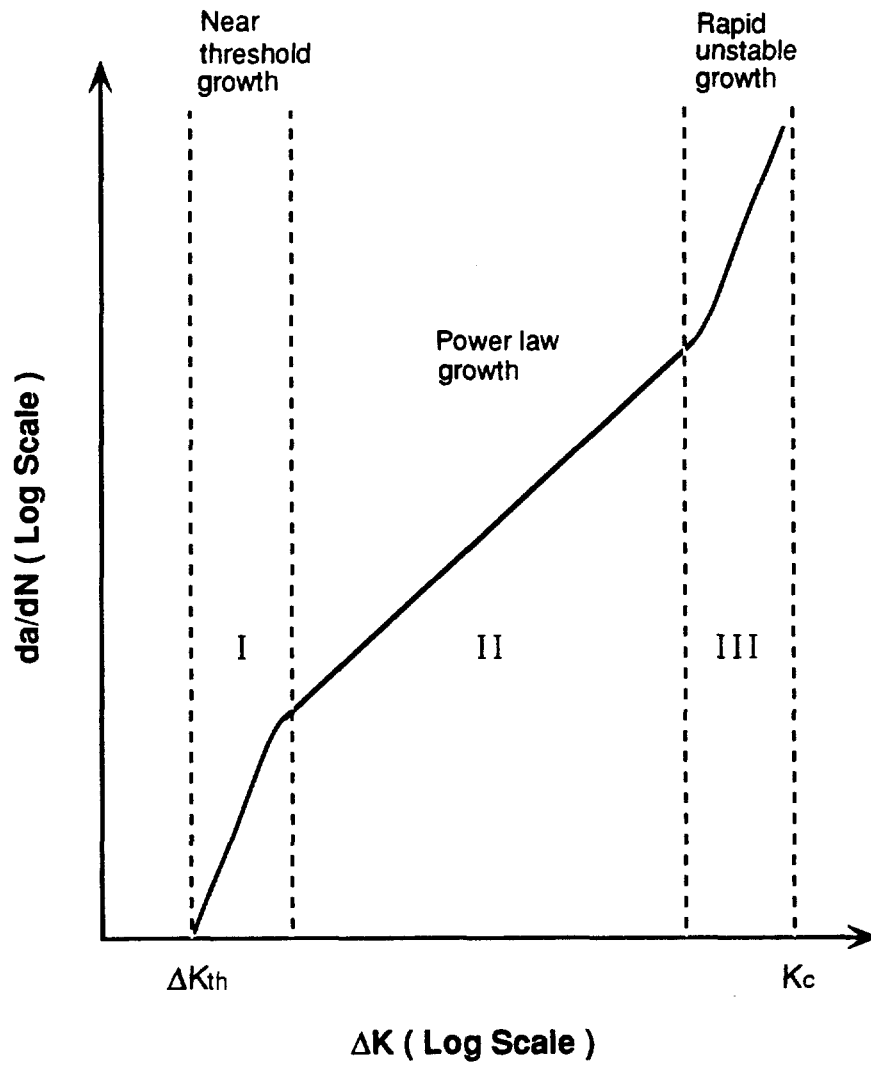


Figure 2.4 Crack Propagation Property ($\frac{da}{dN}$ - ΔK) Curve for Steel

2.2 Residual stress

Residual stress is due to restricted elastic deformation. A major feature of residual stress is that it exists in a structure in a self-balanced mode without any external load. It is usually classified as macro-residual stress and micro-residual stress [17,18]. Macro-residual stress is balanced on a large scale and is due to welding, assembling and metal forming processes. It can be directly related to the mechanical failure of structures and is commonly of engineering concern. Micro-residual stress is balanced within a small region that can be as small as a few grains or even a group of atoms. It originates from microstructural distortion or a localized defect. It has no direct relation to the overall mechanical property of a structure but it can be related to the local failure mechanism of the material.

During welding, distortion and residual stress will inevitably be caused by the shrinkage of melted weld material and the thermal expansion and contraction of the base material. Figure 2.5 shows typical welding residual stress distribution patterns and bending distortions in a butt welded plate. The longitudinal residual stress is tensile near the weld and compressive away from the weld. The transverse residual stress is tensile near the weld center and compressive at the weld ends.

When welding residual stress is involved as part of the overall load in the fatigue of a welded joint, the total loading conditions become complex since the residual stress will change to match with the nominal load and crack length. In order to predict the effect of welding residual stress on the fatigue behavior of a welded joint, the following facts need to be kept in mind:

- a). Welding residual stress varies with location, Figure 2.5, due to its self-balancing nature.
- b). When the magnitude of the welding residual stress plus the external load is greater than the yield strength of the material, local plastic deformation will occur, causing partial residual stress relaxation and a redistribution of residual stress [5].
- c). With crack growth, the welding residual stress will be relieved along the crack surface. The whole residual stress pattern will be redistributed to form a new self-balanced pattern at the crack front [19].
- d). Residual stress from other sources may interfere with the effect of welding residual stress. Such sources include the new residual stress developed at the crack tip due to local yielding and the micro-residual stress due to local defects.

All these factors have significant effects on the true fatigue load. They cause the loading condition to become complicated and make the fatigue process difficult to analyze. Some successful approaches for predicting the effect of welding residual stress have been reported in the study of the effect of residual stress on fatigue crack propagation. Residual stress σ_{res} was considered as a contribution to the external stress. The true stress ratio or effective stress

ratio is then: $R_{eff} = \frac{\sigma_{min} + \sigma_{res}}{\sigma_{max} + \sigma_{res}}$. Because a crack will propagate when the crack

tip is under tensile stress load, in some cases only part of the external load will

cause crack growth. The crack opening ratio, defined as $U = \frac{\sigma_{max} - \sigma_{op}}{\sigma_{max} - \sigma_{min}}$, is

then dependent on the effective stress ratio R_{eff} ; where σ_{op} is the minimum stress required to cause crack opening. Therefore, the effective stress intensity factor range is $\Delta K_{eff} = U \Delta K$ and is also a function of R_{eff} . It is interesting to note that the plotted $\frac{da}{dN} - \Delta K_{eff}$ diagrams for as-welded specimens and unwelded specimens are consistent under a range of nominal stress ratios. Some investigators have concluded that the effect of welding residual stress on the fatigue crack propagation rate is equivalent to the effect of mean stress or stress ratio [20-23]. This signifies that although the effect of residual stress on the overall fatigue property is variable and a detailed analysis is required for each condition, the effect of residual stress is always equivalent to some sort of mean stress. By appropriately taking into account the contribution of residual stress to the nominal fatigue load, an accurate prediction of the effect of residual stress might be expected.

The plastic zone size at a fatigue crack tip is an important factor closely related to the fatigue crack growth properties of the material. From an energy point of view, the greater the plastic deformation in the fatigue process, the greater the energy required for crack growth, and consequently, the greater the fatigue strength of the material might be. Since the crack tip plastic deformation is also related to the crack tip residual stress, it would be interesting to examine their relationships to the fatigue properties. When a tensile load is applied to a cracked component, a yielding zone is created at the crack tip due to the stress singularity. When the load is removed, a new balanced stress state between the plastically deformed material and the surrounding elastically deformed material will be reached. This will result in a compressive residual

stress remaining at the crack tip. For the same material and specimen geometry, the larger the load, the larger the yielded zone size, and consequently, the larger the compressive residual stress and its territory at the crack tip will be. This will have a significant effect on the crack growth behavior. An example of this phenomenon is crack retardation which occurs when an overload is applied to a fatigued specimen that has been loaded under constant cyclic load [24]. The relationship between the crack tip residual stress and the crack tip plastic zone size is complex and dependent on the material and the geometry. Experimental results show that residual stress has a significant effect on the fatigue behavior of thick specimens or brittle materials but has little effect on the fatigue behavior of thin specimens or ductile materials [25,26]. Fracture mechanics concepts show that [27] the plastic zone size of a thin specimen under plane stress loading conditions is greater than that for a thick specimen under plane strain loading conditions. Also, a ductile material is usually associated with a larger plastic deformation on the fracture surface than a brittle material. It is therefore concluded that the intrinsic relationship between the crack tip plastic zone and residual stress is a measure of toughness and it is this toughness that controls the fracture behavior of the material. Thick and brittle materials that correspond to a low toughness are therefore more sensitive to the effects of the crack tip residual stress.

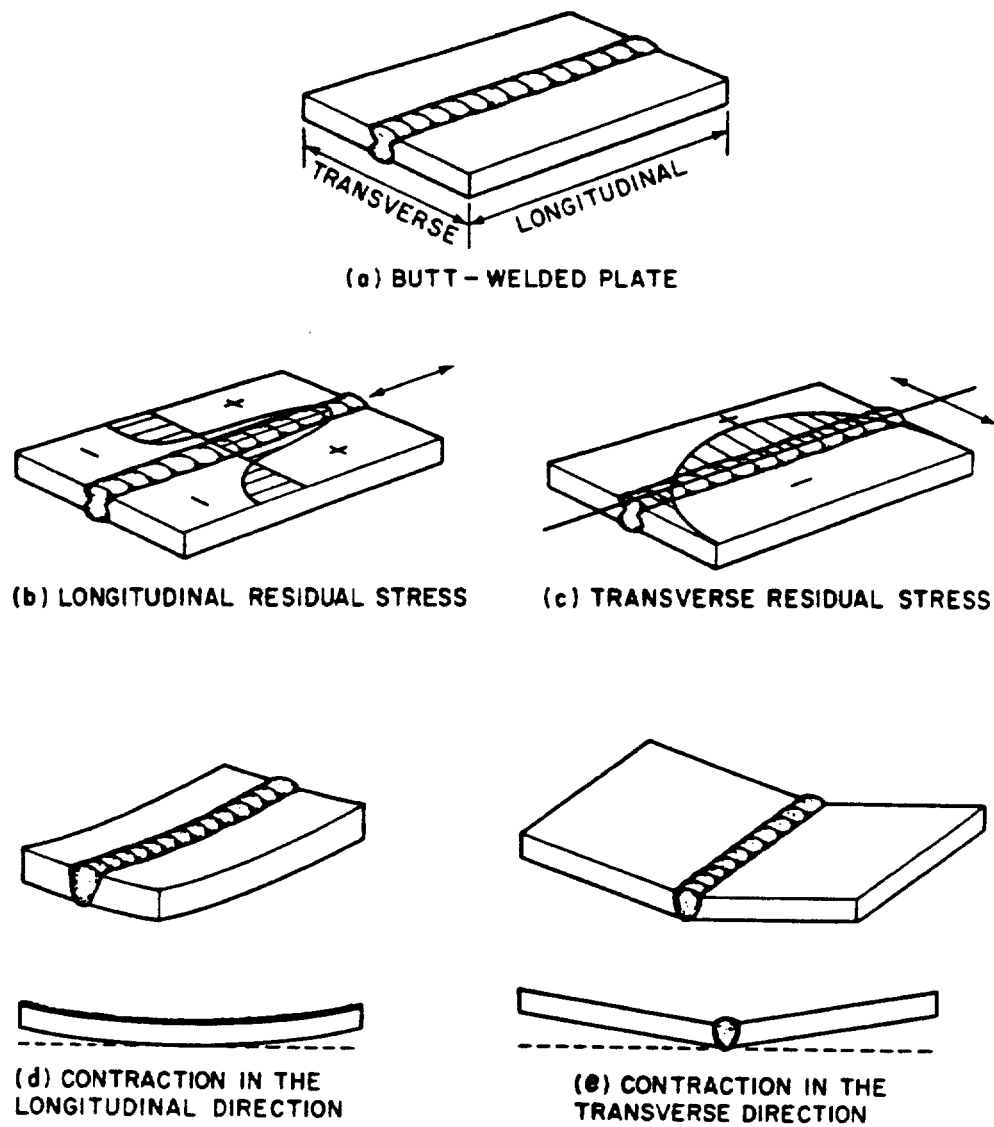


Figure 2.5 Residual Stresses and Welding Distortion in Butt Welded Plate

2.3 Fatigue of welded joints

The fatigue strength of unwelded steel is proportional to its tensile strength; high tensile strength steel has a higher fatigue strength than low tensile strength steel. However, in welded structures, high tensile strength steel usually displays a fatigue strength similar to mild steel [28]. A common explanation of this phenomenon is that weld geometry and/or weld defects cause severe local stress concentrations so that the fatigue crack initiation life is shortened in comparison with the total fatigue life. The difference between the crack initiation life of welded high strength steel and welded low strength steel is therefore not significant. For most steel alloys, crack propagation properties are insensitive to the tensile strength [6]. Therefore, it is weld geometry and/or weld defects that predominantly control the fatigue strength of welded steel structures.

Welded joints can be commonly classified as butt welds, non-load carrying fillet welds, and load carrying fillet welds. They can also be classified as continuous and intermittent welds. Furthermore, under typical laboratory testing conditions, they can be classified as longitudinal and transverse welds, where 'longitudinal' implies the welding direction is parallel to the loading direction and 'transverse' implies the welding direction is perpendicular to the loading direction. When subjected to this classification, the welded joint of concern to the tank car shell belongs in the intermittent, longitudinal, non-load carrying, fillet weld category.

Weld geometry and weld defects are two important factors which are related to the fatigue strength of a welded structure. These factors act as stress

concentrators, so that the local stress is much higher than the nominal external stress. As a result, a crack is likely to form due to one of these factors and potentially develop enough to cause a fracture. Weld geometry, which is always associated with the weld, is of inherent nature and is relatively consistent and stable with respect to the structure properties. Weld defects, which is introduced due to unexpected welding conditions, is relatively inconsistent and unpredictable. For a fatigue problem, the major weld geometry factor is the weld toe notch effect and the major weld defect factors are the effects of undercutting, slag inclusions, porosity and lack of fusion. The role of weld geometry and weld defects in fatigue crack initiation has been studied by a number of investigators [28-38]. By reviewing their results, it was found that different types of weld geometry and weld defects affect fatigue strength of different types of welded joints differently. In transverse welds, the critical factors were found to be slag inclusions and undercutting at the weld toe, and porosity and lack of fusion at the weld root. In longitudinal butt and continuous fillet welds, the critical factors were found to be weld surface imperfections, such as ripples and porosity. In intermittent longitudinal fillet welds, the critical factor was found to be weld end toe notches [29]. Some quantitative results have been reported to correlate the fatigue strength and each type of weld defect to a certain welded structure [30,31]. However, due to the complexity of the system and scatter in reported test data, no generally accepted conclusions have been reached. The microstructure in the heat affected zone (HAZ) can also be an important factor which can affect the fatigue behavior of welded joints. Although it was found that its effect on fatigue crack propagation is of less significance [32,39], since it is related to the mechanical property

of the weld root, it is considered to have a significant effect on fatigue crack initiation.

Most weld defects are randomly distributed around a weld due to the welding conditions. It is, therefore, expected that their effect on fatigue strength would be subjected to a large scatter, and indeed most fatigue test data does show large scatter bands due to the effect of weld defects. By comparing the scatter bands at high test load conditions and at low test load conditions, it was found that the scatter was large under low loads and small under high loads [5]. It is thus believed that the effect of weld defects is dependent on the load conditions as well. At higher loads, the effect of those randomly distributed defects diminishes.

The fatigue strength of welded joints can be significantly improved by properly eliminating the effect of weld geometry and weld defects. Several methods have been reported which increase the fatigue strength of welded joints by either stress conditioning (introducing compressive stress to the crack initiation sites), or by geometry conditioning (completely or partially removing those critical notches and weld defects such that they are lesser stress concentrations). [5,40-43]. The methods for stress conditioning include shot peening, overloading and spot heating while the methods for weld geometry conditioning include grinding, TIG dressing and notch coating.

2.4 Mean stress effect on fatigue of unwelded steel

It is widely accepted that the effect of residual stress on the fatigue strength is equivalent to the effect of the mean stress. Before a detailed review of the effect of welding residual stress on the fatigue behavior of welded steel, it is first necessary to review the effect of mean stress on the fatigue behavior of unwelded steel. In order to make a systematic comparison, a literature review was carried out to compare the effects of mean stress on the fatigue behavior of unwelded steel materials for all the major testing methods used in fatigue studies and for all the major factors which are related to the fatigue strength of structures. The major factors considered were material (mild and high strength), the geometry (thin and thick) and the loading (tension-tension and tension-compression). As discussed in section 2.2, both material and geometry have significant effects on the crack tip plastic zone size and the crack tip residual stress state. So, material and geometry are two important factors related to the toughness of the material. Theoretically, it is not a strict classification to use terms "mild and high strength" and "thin and thick" as measures of toughness since some steel alloys may have high toughness as well as have high strength, and some environmental factors, such as temperature, may cause a "thick" material to have a high ductility or to cause a "thin" material to have a low ductility. However, for most steel alloys under normal conditions, thick or high strength usually implies low toughness; thin or mild usually implies a high toughness. So, under such a classification, it is easy to discuss and compare test results systematically. Table 2.1 shows the results of the literature survey. Some detailed results are discussed as follows:

It is consistent within the literature survey that there is a significant effect of mean stress on the S-N property of unwelded steel. Figure 2.6 shows the generalized test results. Some empirical relationships have been determined, among which the most accurate relationships were appropriately expressed as the Goodman's equation:

$$\frac{\sigma_a}{S_e} + \frac{\sigma_m}{S_u} = 1 \quad (2.4)$$

and Gerber's equation:

$$\frac{\sigma_a}{S_e} + \left(\frac{\sigma_m}{S_u}\right)^2 = 1 \quad (2.5)$$

where S_u is the tensile strength of material. From Figure 2.6, it is evident that the fatigue life for a fixed load or the fatigue strength for a fixed life decreases when tensile mean stress increases.

It is consistent from the literature survey that there is a significant mean stress effect on the strain-life property of unwelded steel specimens. Figure 2.7 shows the mean stress effect on ϵ -N approach. It is seen that the fatigue life decreases when mean stress increases. This effect can be expressed as equation:

$$\frac{\Delta\epsilon}{2} = \frac{\sigma'_f - \sigma_m}{E} (2N_f)^b + \epsilon'_f \left(\frac{\sigma'_f - \sigma_m}{\sigma'_f}\right)^{cb} (2N_f)^c \quad (2.6)$$

From Table 2.1, literature survey results of the effect of mean stress on fatigue crack propagation property seem to be conflicting at first glance. Some results show that there is a mean stress effect and other results show that there is no mean stress effect. When the detailed test conditions of these results

were examined, it was found that a better understanding can be reached by considering the crack propagation property in region I and region II separately. Taylor's report compiled data for fatigue crack propagation in different materials [49]. Figure 2.8 shows the effect of mean stress on crack growth rate of A516 steel, which is a mild steel with similar chemical and mechanical properties as the A515 steel used for constructing tank cars. The differences between A515 steel and A516 steel are that A516 has a slightly higher Mn content and a finer grain size, and A516 is used for lower temperature service conditions. Figure 2.8 shows that mean stress has a significant effect on the crack growth rate in region I crack propagation. Figure 2.9 shows the mean stress effect on the crack growth rate of another mild steel and Figure 2.10 shows the mean stress effect on the crack growth rate of a high strength steel. It was found that no matter whether the stress ratio R is positive or negative, there is a significant effect of stress ratio (mean stress) on fatigue crack propagation when the stress intensity factor range is low; for crack propagation under a high stress intensity factor range, $\frac{da}{dN} - \Delta K$ curves of most steels are merged together when the applied stress ratio, R , is positive, Figures 2.9 and 2.10. This means that the mean stress effect is insignificant for crack propagation under a tension-tension cyclic load with a high stress intensity factor range. Maddox's and Crooker's data [46,53] were obtained from either a deeply notched or a well cracked specimen. The data showed no mean stress effect since they were possibly related with crack propagation at a high stress intensity factor range. So basically, there are no major conflicts from the literature. Some literature reports show that there is a mean stress effect on crack propagation for some steel materials even at a high

stress intensity factor range [52]. Considering that the material itself has some influence on crack propagation, without further evidence, it can be safely stated that in this case, the effect of mean stress on crack propagation at a high stress intensity factor range was perhaps dependent on materials. Figure 2.11 shows the effect of mean stress on the threshold stress intensity factor range. ΔK_{th} will decrease with an increase of mean stress.

For most mild steels, it was found that the stress intensity factor range under which the fatigue crack propagation is subjected to a significant mean stress effect was about $10 \text{ MPa}\sqrt{\text{m}}$. A quantitative concept of this load level can be obtained by calculating the stress intensity factor based on the stress intensity factor of a center cracked infinite plate under constant tension load:

$$K = \sigma \sqrt{\pi a} \quad (2.7)$$

(where 'a' is half crack length)

Calculation results show that a stress intensity factor of $10 \text{ MPa}\sqrt{\text{m}}$ is corresponding to a crack length about 0.5 inch under a tension load of 10 Ksi or a crack length about 0.3 inch under a tension load of 13 Ksi. Referring back to the fatigue problem, this means that under a 0 - 10 Ksi pulsed tension cyclic load, a fatigued specimen will be subjected to the effect of mean stress until the crack length reaches 0.5 inch.

Some empirical equations, such as the Forman equation:

$$\frac{da}{dN} = \frac{C\Delta K^m}{(1-R)K_c - \Delta K} \quad (2.8)$$

(where K_c is the fracture toughness of the material)

were applied to predict the general mean stress effect on fatigue crack propagation properties. However, there is some limitation on the application of these equations and none of them has yet been proven to be accurate for general situations.

Based on the above discussions, the following conclusions can be made:

- a). There is an effect of mean stress on the fatigue strength of materials.
- b). Mean stress has significant effect on fatigue crack initiation, and on fatigue crack propagation when the applied stress intensity factor range is low ($\Delta K \leq 10\text{MPa}\sqrt{\text{m}}$ for mild steel).
- c). When the applied stress intensity factor range is high, the effect of mean stress on fatigue crack propagation is dependent on the material. For most mild steel materials, the mean stress effect is not significant under a tension-tension cyclic load.

Table 2.1 Mean Stress Effect on Fatigue of Unwelded Steel
— A Summary of Literature Review

		mild steel				high strength steel			
		thin ($t < 13\text{mm}$)		thick ($t > 13\text{mm}$)		thin ($t < 13\text{mm}$)		thick ($t > 13\text{mm}$)	
		has effect	no effect	has effect	no effect	has effect	no effect	has effect	no effect
fatigue life (S-N)	R>0	Goodman Gerber Morrow		Yes		Yes		Yes	
	R<0	Yes		Yes		Yes		Yes	
crack initiation (E-N)	R>0	Manson Zheng [44] Lawrance [45] Maddox [46]		Yes		Yes		Yes	
	R<0	Yes		Yes		Yes		Yes	
crack propagation (LEFM)	R>0	Voskovsky [47] Geary [48] Taylor [49] Zhao [50] Itoh [20]	Maddox [46]	Woodfill [51]		Taylor [49] Glinka [52]	Crooker [53]		
	R<0	Taylor [49]				Taylor [49]			

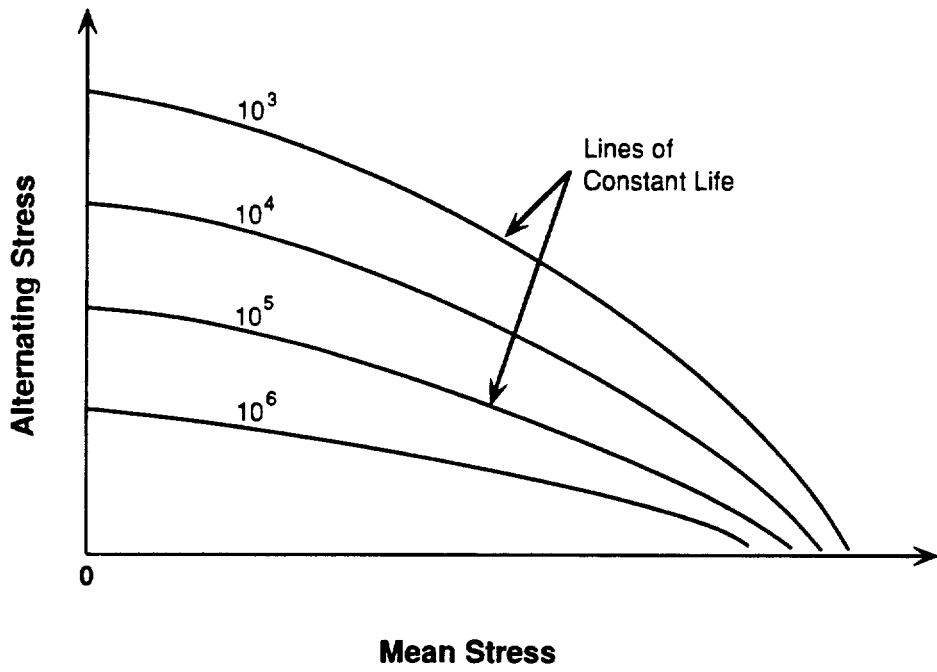


Figure 2.6 Mean Stress Effect on Fatigue Strength

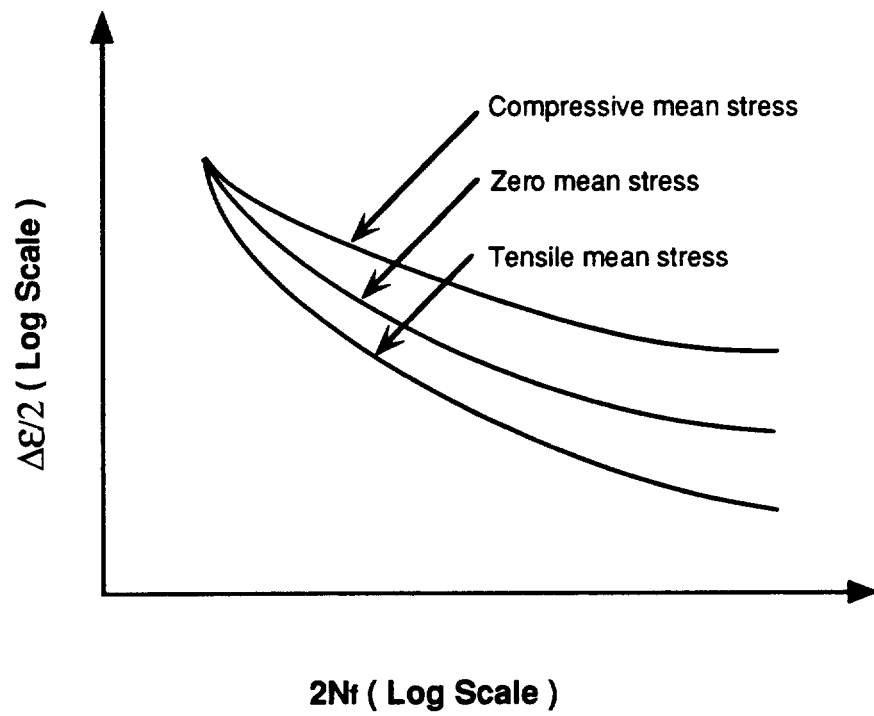


Figure 2.7 Mean Stress Effect on Strain-life Curve

MILD STEELS

MATERIAL: SRS16-70 pipeline steel (0.23C, 0.12Mn, 0.25Si);
normalized. Ferrite and pearlite.

R RATIO: 0.15 0.75

ΔK_{th} (MPa \sqrt{m}): 7.20 4.00

ENVIRONMENT: Air, room temperature.

YIELD STRENGTH (MPa): 327

REFERENCE: (05) (110)

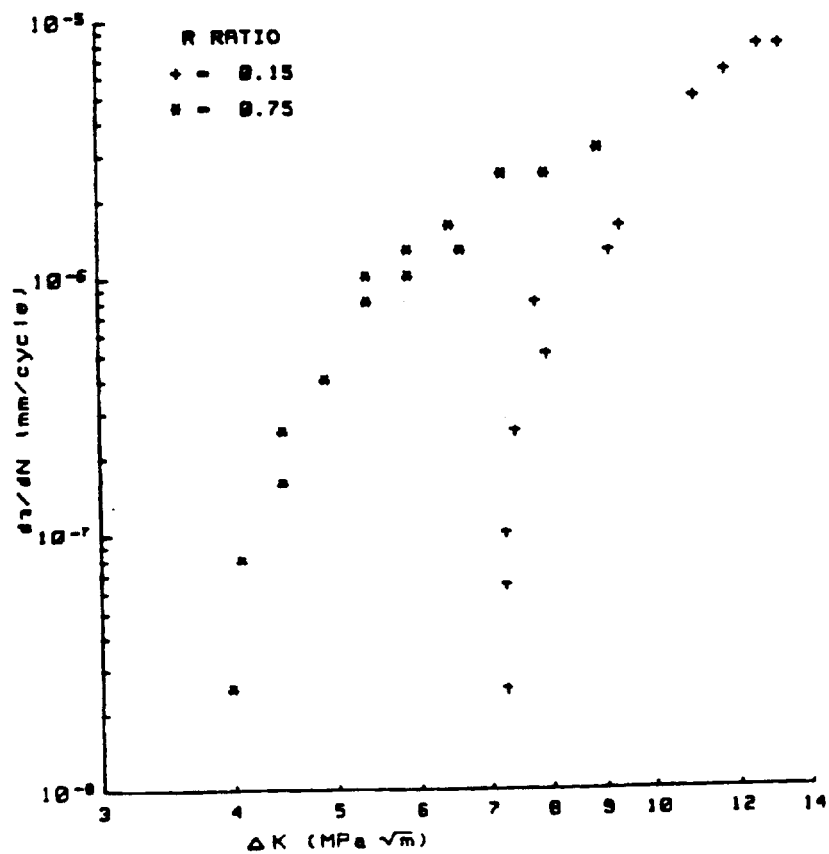


Figure 2.8 Mean Stress Effect on Crack Propagation of A516 Steel [49]

MILD STEELS

MATERIAL: BS4360-50D (0.18C, 1.4Mn, 0.36Si).

Specimens 12mm thick (see comments below).

R RATIO: -0.70 0.00 0.30 0.50 0.70 0.90

ΔK_{th} (MPa \sqrt{m}): 16.00 9.00 7.00 4.20 3.40 3.00

ENVIRONMENT: Air, room temperature.

YIELD STRENGTH (MPa): 385

REFERENCE: (49)

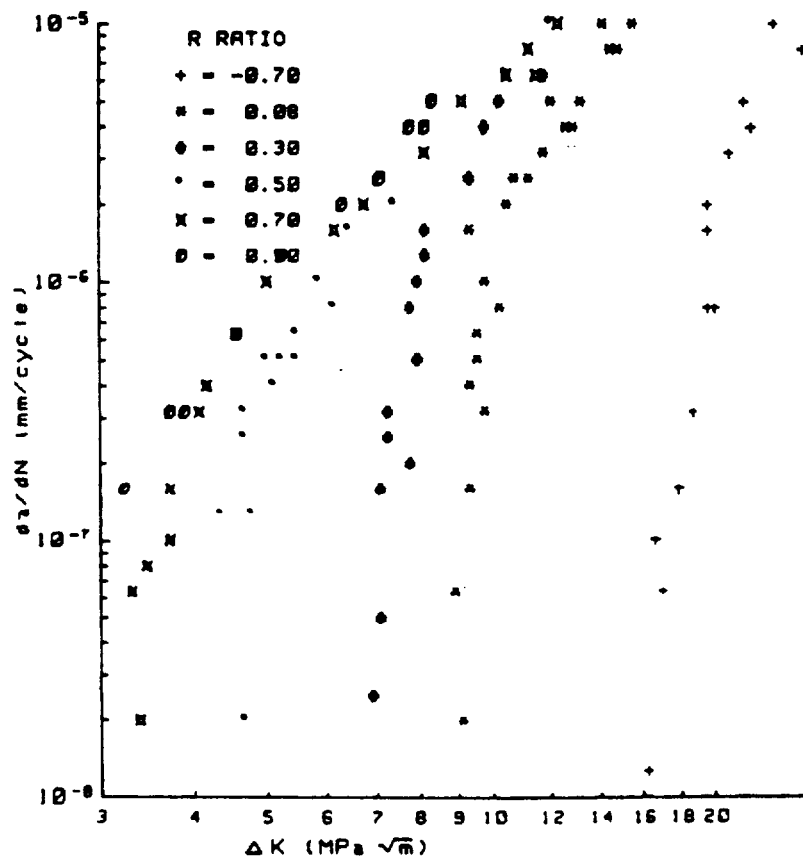


Figure 2.9 Mean Stress Effect on Crack Propagation of Mild Steel [49]

ALLOY STEELS

MATERIAL: HT80 (0.13C, 0.19Si, 0.94Mn, 0.14Mo, 0.46Cr);
quenched and tempered.

R RATIO: -1.00 -0.50 0.00 0.40 0.60 0.80

ΔK_{th} (MPa \sqrt{m}): 13.50 10.50 0.00 5.00 3.80 2.50

ENVIRONMENT: Air, room temperature.

YIELD STRENGTH (MPa): 793

REFERENCE: (12), (160)

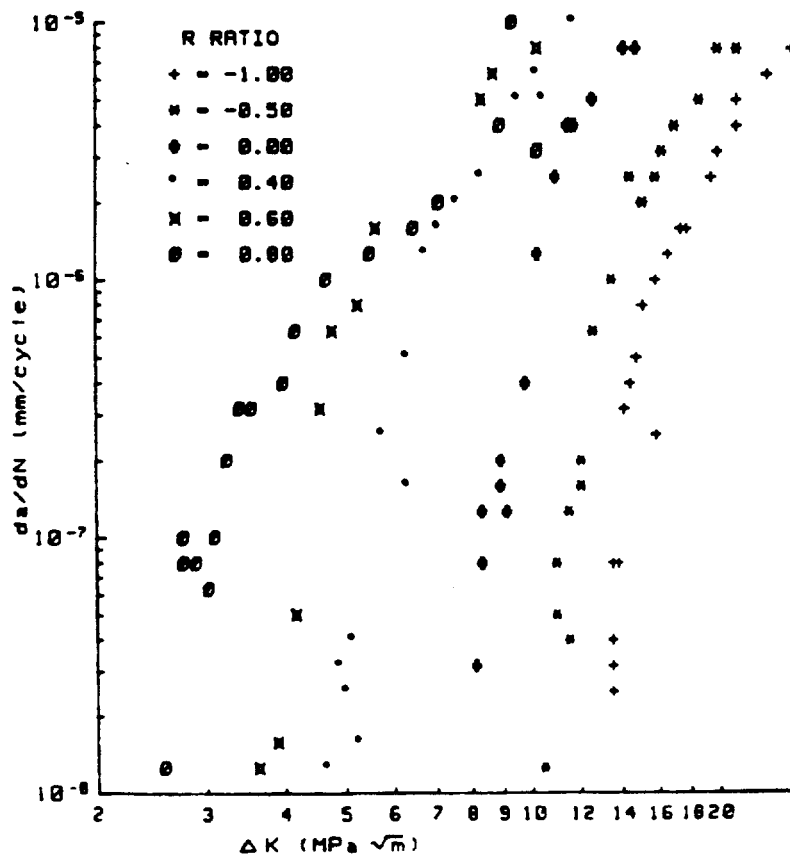


Figure 2.10 Mean Stress Effect on Crack Propagation of High Strength Steel [49]

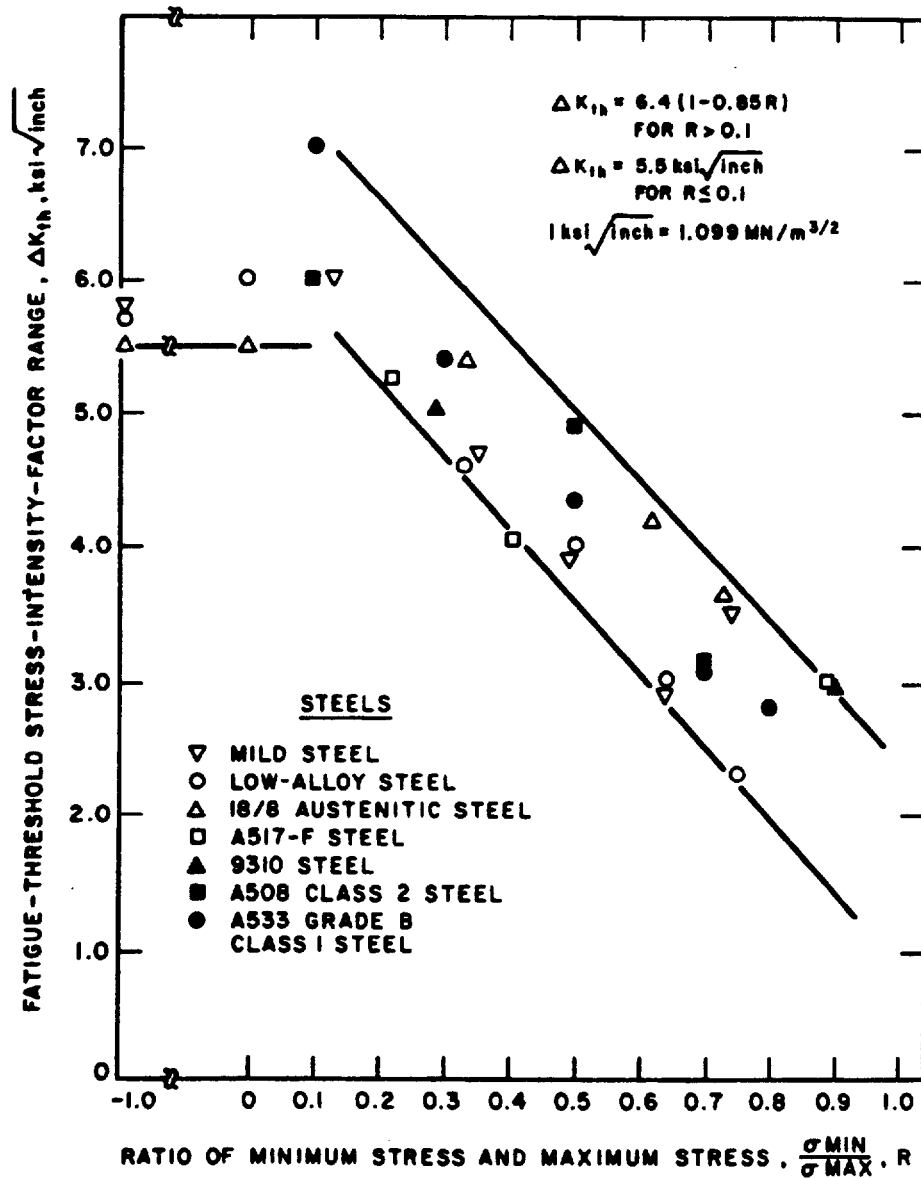


FIG. 7.17. Dependence of fatigue-threshold stress-intensity-factor range on stress ratio.

Figure 2.11 Mean Stress Effect on Threshold Stress Intensity Factor [13]

2.5 Welding residual stress effect on fatigue of welded steel

Most of the investigations on the effect of welding residual stress on the fatigue behavior of welded joints were carried out by comparing fatigue strengths of as-welded and stress-relieved weld specimens. A review of the effect of welding residual stress on the fatigue behavior of welded steel was made based on the same classifications as in the review of the mean stress effect on the fatigue strength of unwelded steel. The results are listed in Table 2.2.

Using the stress-life approach, Gurney and Maddox did a series of tests on fillet welded specimens. Gurney did S-N comparisons of as-welded and stress-relieved mild steel specimens under pulsed tension conditions [54] while Maddox did systematic S-N comparisons of as-welded and stress-relieved specimens for different steels (mild and high strength) under different stress ratios ($R = -1, 0, 0.5$ and 0.67) [6]. Their conclusions were that when the stress ratio R is positive, there is no significant effect of tensile welding residual stress on the S-N property but when R is negative, the existence of tensile welding residual stress will significantly reduce the fatigue strength of welded joints.

In a crack initiation study, Horikawa [57] examined bead-on-plate weld specimens under tension-tension cyclic load conditions with a stress of ratio $R = 0.1$. A crack propagation gage was used to measure crack initiation life and crack propagation life. The crack initiation life was defined as the number of load cycles to cause a 0.1mm increase of the half crack length from the induced center hole defect. Under these conditions, the test results showed that welding residual stress has a significant effect on the fatigue crack initiation life but

has no significant effect on the crack propagation life. Ohta [4] showed that in region I, the fatigue crack propagation rate of stress-relieved specimens was similar to that of the base material and lower than the as-welded specimens. However, with an increase in the crack length (or an increase in stress intensity factor), all the data from as-welded specimens, stress-relieved specimens and the base material emerged together to show that there was no effect of welding residual stress in region II crack propagation.

When Table 2.1 and Table 2.2 were compared, it was found that in the fatigue crack initiation study (ϵ -N approach) and the fatigue crack propagation study (LEFM approach), the effect of welding residual stress on the fatigue behavior of welded steel is equivalent to the effect of mean stress on the fatigue behavior of unwelded steel. Both show that there were effects on crack initiation and region I crack propagation. However, in the stress-life study, there is a substantial difference between the effect of welding residual stress and the effect of mean stress when the stress ratio R is positive. Mean stress has an effect on the fatigue strength of unwelded steel but welding residual stress has no significant effect on the fatigue strength of welded steel. This experimental result raises the question of how to explain this phenomenon. For welded structures, the existence of weld geometry and weld defects is inevitable. Some investigators believe that the fatigue crack initiation life of a welded joint is negligible due to these factors. They, therefore, conclude that crack propagation is the only concern for such structures. Under a tension-tension cyclic load, since there is no significant mean stress effect on crack propagation of the tested materials, there is no significant effect of welding residual stress on the fatigue life of the welded structure [46]. Whether this

explanation is true or not depends on the definition of crack initiation. According to the discussion in section 2.4, even if there is no significant crack initiation life in the fatigue process of a welded joint, it is still possible that the crack propagates under a stress intensity factor range less than $10 \text{ MPa}\sqrt{\text{m}}$ that is subjected to the effect of mean stress. So, theoretically speaking, if there is residual stress, some effect on the fatigue properties is to be expected. For a particular practical application, because of the influence of other factors, the more realistic question that needs to be answered is whether the effect of residual stress is significant in the fatigue process? This can only be answered by a detailed analytical evaluation and on quantitative experimental evidence rather than on the "make sense" discussion.

From Gurney's test results, Figure 2.12, it seems true that there is a significant effect of welding residual stress on fatigue strength at low load levels since there are two well separated lines for the S-N relations of the as-welded and stress-relieved specimens. However, when each data point is examined, it seems that the residual stress effect is not significant because the test scatter is large. This makes it difficult to evaluate the effects of welding residual stress based upon these test data. It is, therefore, believed that for a low load range, such as $\Delta S < 100 \text{ MPa}$ (14Ksi), the test data are not convincing enough to draw any conclusions.

From Maddox's S-N results, Figure 2.13, it seems correct that there is no welding residual stress effect. Considering that the plot in the figure is based on stress ranges with a mixture of different stress ratios, the data at the same load level may represent different stress ratios (or different maximum loads). As discussed in section 2.2, the maximum load will affect the residual stress

state if it causes local yielding. In order to gain a better understanding, a detailed examination of Maddox's test data was made based on the effects of both stress range and maximum stress. Table 2.3 shows a reorganization of Maddox's test results for mild steel. From Table 2.3, it was found that most of the test data were obtained at loads with maximum stress above 14 Ksi (100 MPa). The few test results obtained for loads equal to or less than 14 Ksi are not convincing enough to demonstrate the welding residual stress effect for positive R values. The results from alternating load conditions, $R=-1$, show that sometimes there is a significant effect of welding residual stress and sometimes there is not. The test error scatter is so large that it is hard to draw a definite conclusion.

The efficiency of heat treatment conditions for stress relief is another questionable point in the literature reviewed. Some investigators reported that there were up to 10 Ksi tensile residual stress in the fatigue testing specimens after they had been subjected to stress relief heat treatment [55]. This certainly relates to the fatigue test error scatter and further complicates the analysis.

Based on the above analysis, it is believed that a detailed test is still necessary to study the effect of welding residual stress on the fatigue behavior of welded joints, particularly at low load levels. Also, it is believed that the large scatter in the reported test data may not be merely related to the residual stresses but may also be due to other factors such as weld defects. In conclusion, welding residual stress has a significant effect on fatigue crack initiation and crack propagation at a low stress intensity factor range. However, the effect of welding residual stress on the S-N property of a welded structure is not clearly defined and further detailed examination is necessary.

Table 2.2 Residual Stress Effect on Fatigue of Welded Steel
— A Summary of Literature Review

		mild steel				high strength steel			
		thin ($t < 13\text{mm}$)		thick ($t > 13\text{mm}$)		thin ($t < 13\text{mm}$)		thick ($t > 13\text{mm}$)	
		has effect	no effect	has effect	no effect	has effect	no effect	has effect	no effect
fatigue life (S-N)	R > 0		Maddox [6] Maddox [25] Gurney [54] Reemanyder [29] Harrison [56] Berge [8]	Maddox [25]			Maddox [6]		
	R < 0	Maddox [6] Maddox [55] Gurney [54] Reemanyder [29] Harrison [56] Berge [8]				Maddox [55]			
crack initiation (E-N)	R > 0			Horikawa [57]					
	R < 0								
crack propagation (LEFM)	R > 0	Verreman [58] Itoh [20] Nelson [59] Shi [60] Parker [61]		Kapadia [39] Ohta [4] Wu [62]	Horikawa [57]		Horikawa [63]		
	R < 0	Greasley [23]		Greasley [23]					

Table 2.3 Fatigue Test Result from Maddox [6]

As-welded				Stress-relieved				
R	ΔS MPa (Ksi)	S_{max} MPa (Ksi)	Cycle of failure ($\times 10^6$)	R	ΔS MPa (Ksi)	S_{max} MPa (Ksi)	Cycle of failure ($\times 10^6$)	
0.67	100 (14)	300 (43)	1.00	0.67	100 (14)	300 (43)	0.90	
	75 (11)	220 (31)	2.75		75 (11)	220 (31)	2.60	
	50 (7)	150 (21)	8.34		60 (9)	180 (26)	10.00*	
					50 (7)	150 (21)	10.00*	
0.5	150 (21)	300 (43)	0.27	0.5	150 (14)	300 (43)	0.26	
	100 (14)	200 (29)	0.84		100 (14)	200 (29)	0.94	
	75 (11)	150 (21)	2.29		75 (11)	150 (21)	1.98	
	60 (9)	120 (17)	3.29					
	50 (7)	100 (14)	12.22*					
0.0	150 (21)	150 (21)	0.23	0.0	150 (21)	150 (21)	0.24	
	100 (14)	100 (14)	0.79		100 (14)	100 (14)	1.04	
					75 (11)	75 (11)	11.42*	
	50 (7)	50 (7)	8.01		60 (9)	60 (9)	10.00*	
				50 (7)	50 (7)	12.26*		
-1.0	200 (29)	100 (14)	0.12	-1.0	200 (29)	100 (14)	0.22	
	150 (21)	75 (11)	0.34		150 (21)	75 (11)	1.51	
					150 (21)	75 (11)	0.80	
	100 (14)	50 (7)	1.25		100 (14)	50 (7)	1.33	
					100 (14)	50 (7)	16.65*	
	75 (11)	37.5 (5)	1.97		75 (11)	37.5 (5)	18.33*	
	60 (9)	30 (4)	12.61*					
	50 (7)	25 (3)	10.00*					

Note: '**': unbroken.

Fig. 10.7. Test results for as-welded (●, —) and stress-relieved (▲, - -) specimens with longitudinal non-load-carrying fillet welds subjected to pulsating tension loading(G 67).

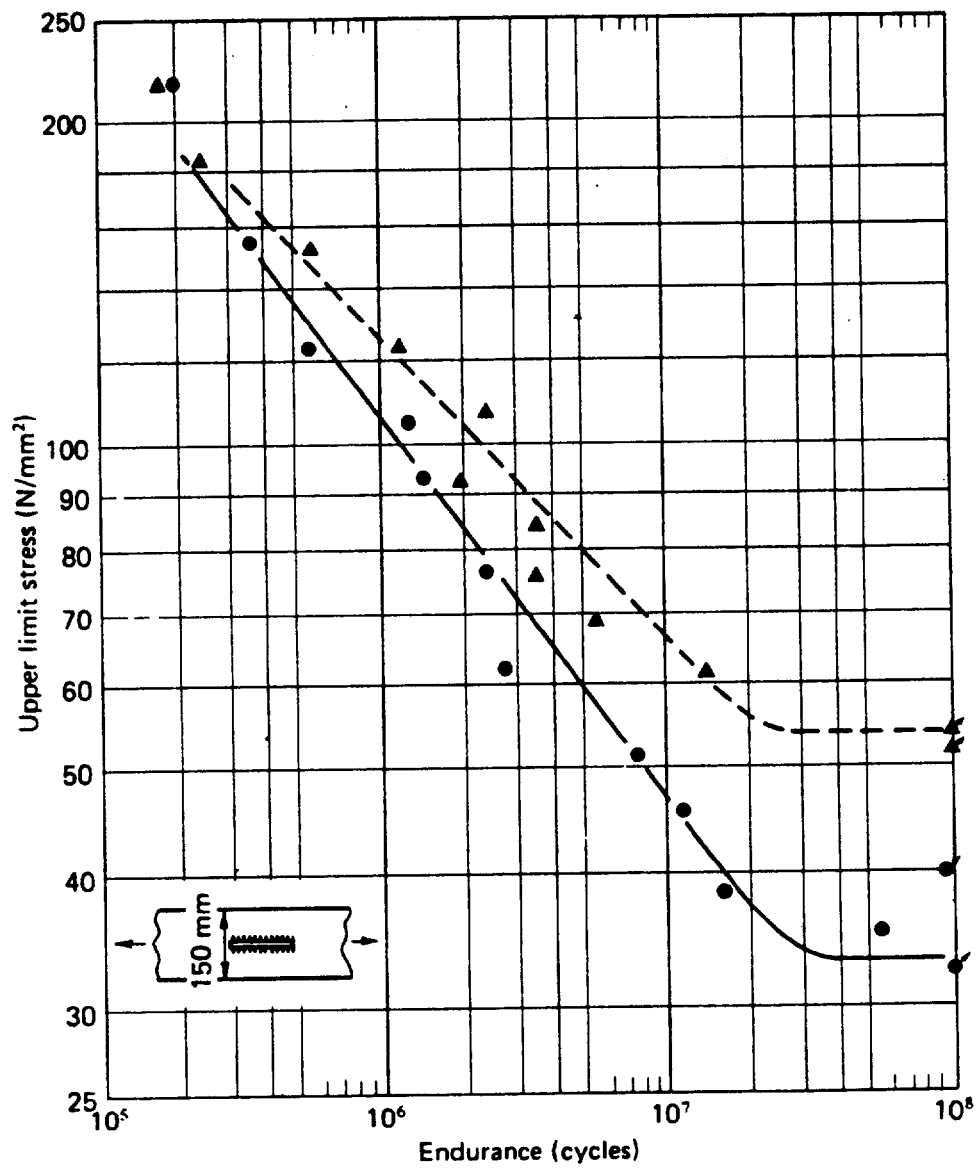


Figure 2.12 Gurney's S-N Results [5]

2.6 Residual stress measurement method

A reliable method for determining residual stress is a key factor in understanding the role of residual stress in the fatigue process. An ideal method would have the following advantages:

- a). High accuracy
- b). High resolution
- c). Least destructive and little impact on the material
- d). Less time consuming and easy to perform
- e). Economical

Residual stress is elastic potential energy locked in the material body in a particular mode. This causes some corresponding changes in the physical properties of the material. The principle of all residual stress measurement methods is to measure the deviation of those physical properties from the stress free state and to determine the residual stress from some theoretical or empirical analysis. This can be done in the following ways.

Mechanical stress relief: The methodology used in this category is to relieve wholly or partially residual stress by mechanical means; to measure the associated deformation (displacement or strain) with electric and optical methods; and to determine the residual stress from the measured deformation based on elastic theories. The methods applied include sectioning, hole-drilling, ring cutting, photoelasticity, moire fringe analysis, brittle coatings, etc [18,64-66]. All of these methods are destructive or semi-destructive. They are commonly used for quantitative or semi-quantitative analysis.

Chemical stress relief: The methodology used in this category is to immerse the stressed material into a corrosive chemical media for a period of time in order to cause stress corrosion cracking and then to analyze the residual stress state from the resulting cracks on the material surface. The methods applied include hydrogen induced cracking and corrosion cracking. These are destructive methods, and are commonly used for semi-quantitative or qualitative analysis.

Physical property measurement: The methodology used in this category is to measure selected physical properties under the effects of residual stress and to determine residual stresses by comparing the measured physical properties with the corresponding stress free states. The methods in this category include x-ray diffraction, ultrasonics, magnetoelasticity and neutron scattering [18,67-69]. These are non-destructive methods, and they are commonly used for quantitative or semi-quantitative analysis.

Among the current available methods, none has all of the ideal advantages. Each method has its own advantages and disadvantages. In practice, one or more should be chosen to achieve the desired result.

Among the above methods, the x-ray diffraction, sectioning and hole-drilling techniques are highly rated, widely accepted and are deemed most accurate for residual stress measurement. They are now the recognized standard for residual stress measurement, and they are used for the evaluation of other residual stress measurement methods. Their advantages and disadvantages are compared below.

X-ray method: A non-destructive method used to measure surface residual stress in a chosen direction. Residual stress is determined from the measured

crystal lattice spacing by employing an x-ray diffraction technique.

Advantages: Its accuracy is based on a solid theoretical background. It is nondestructive, and its resolution is high.

Disadvantages: Its accuracy is sensitive to microstructure and surface conditions. It is not convenient or flexible in operation, and is expensive in both labor and devices.

Sectioning method: A destructive method used to measure both surface and 3 dimensional body residual stresses with strain gages. Residual stress is determined from the measured strain deformation after sectioning provides residual stress relief.

Advantages: Its accuracy for surface stress measurement is based on a solid theoretical background. Its accuracy for body stress measurement is based on semi-solid theoretical background. Its resolution is reasonably high.

Disadvantages: It is completely destructive and the measurements are time consuming. Intensive care is required to protect the strain gage during operation. Its use is limited to performance within a laboratory, and the labor involved is expensive.

Hole-drilling method: A semi-destructive method used to measure surface residual stress with strain gage rosette measurement of the partially relieved residual stress following the drilling of a small hole in the material.

Advantages: It is less destructive with reasonable accuracy and resolution. It is easy to perform, and it is less expensive in both labor and devices.

Disadvantage: Special calibration is required for measurement under high stress and high stress gradient conditions.

Because of the above features and the practicality, the sectioning and hole-drilling methods were selected for this research program to study the effect of welding residual stress on the fatigue of welded joints. The detailed theoretical approach of sectioning and hole-drilling methods are described in sections 2.7 and 2.8.

2.7 Sectioning residual stress measurement

Figure 2.14 shows the principle of sectioning measurement of surface residual stress. A strain gaged square coupon is parted out from parent material that has been subjected to a uniform surface residual stress state: σ_x , σ_y and τ_{xy} . If it is assumed that all the residual stress components in the sectioned coupon are relieved from sectioning and that the material is isotropic and satisfied with linear elastic constitutive conditions, the consequent stress-strain relationships on the coupon surface are then the same as plane stress conditions:

$$\begin{aligned}\sigma_x &= -\frac{E}{1-\nu^2}(\epsilon_x + \nu\epsilon_y) \\ \sigma_y &= -\frac{E}{1-\nu^2}(\epsilon_y + \nu\epsilon_x) \\ \tau_{xy} &= -\frac{E}{1+\nu}\gamma_{xy}\end{aligned}\tag{2.9}$$

where E is the Young's modulus, ν is the Poisson's ratio.

If all strain components, ϵ_x , ϵ_y and γ_{xy} , which correspond to strain changes due to residual stress relaxation from sectioning can be accurately measured, the residual stress can be determined from equation (2.9). The strain gage is the preferred technique to measure these strain components. Since there are three unknown strain components, three strain gages need to be arranged in three different directions to determine the strain state. A convenient way to measure the strain components is to use the commercially available three element strain gage rosette. The use of a strain gage requires that the gage be aligned along the direction of interest, that the resistance change of the strain gage then be measured by a bridge circuit and that the resistance

change value be converted to its corresponding strain value by the use of a strain indicator.

The way a strain indicator converts the resistance change to a strain value is based on a simplified linear strain gage equation:

$$\frac{\Delta R}{R} = K_o \epsilon \quad (2.10)$$

This equation, which neglects the effect of transverse sensitivity of the strain gage for the convenience of strain calculation from a linear measurement bridge, suffers from a measurement error of: [70,71]

$$n_\epsilon = \frac{\frac{K_t}{K_l} \frac{\epsilon_t}{\epsilon_l} (\frac{K_t}{K_l} + \nu_o)}{1 - \nu_o \frac{K_t}{K_l}} \times 100 \approx \frac{K_t}{K_l} \left(\frac{\epsilon_t}{\epsilon_l} \right) \times 100 \quad (\text{when } \frac{\epsilon_t}{\epsilon_l} \gg \nu_o) \quad (2.11)$$

where R is the resistance of the strain gage, ΔR is the change of the resistance, K_o is the manufacturers' gage factor, ϵ is the supposed strain change in gage axis direction (which is true when the gage is mounted in the loading direction of a uniaxial stress condition), n_ϵ is the measurement error as a percentage of the real strain along the gage axis, K_l is the axial gage factor, K_t is the transverse gage factor, ν_o is Poisson's ratio of the material on which K_o is measured, ϵ_l and ϵ_t are respectively the actual strains parallel to and perpendicular to the gage axis.

The ratio of $\frac{K_t}{K_l}$ is called the transverse sensitivity coefficient. It is the measure of the transverse sensitivity of the gage. Its value is about 1% for a foil bonded strain gage. Equation (2.11) shows that the error owing to

transverse sensitivity is significant when the ratio of $\frac{\epsilon_t}{\epsilon_l}$ is large.

To eliminate the error due to transverse sensitivity of the gage, the generalized strain gage equation:

$$\frac{\Delta R}{R} = K_l \epsilon_l + K_t \epsilon_t \quad (2.12)$$

was used for this study. Where $\Delta R/R$ is the relative resistance change of strain gage, K_l and K_t are longitudinal and transverse sensitivity coefficients, respectively, and ϵ_l and ϵ_t are the longitudinal and transverse strains occurring under the gage.

For the strain gage rosette in Figure 2.14, we have:

$$\begin{aligned} \frac{\Delta R_x}{R_x} &= K_l \epsilon_x + K_t \epsilon_y \\ \frac{\Delta R_y}{R_y} &= K_l \epsilon_y + K_t \epsilon_x \\ \frac{\Delta R_{45}}{R_{45}} &= K_l \epsilon_{45} + K_t \epsilon_{135} \end{aligned} \quad (2.13)$$

Under plane stress condition, the strain relations become:

$$\begin{aligned} \epsilon_{45} &= \frac{1}{2}(\epsilon_x + \epsilon_y) + \gamma_{xy} \\ \epsilon_{135} &= \frac{1}{2}(\epsilon_x + \epsilon_y) - \gamma_{xy} \end{aligned} \quad (2.14)$$

So

$$\epsilon_x + \epsilon_y = \frac{1}{K_l + K_t} \left(\frac{\Delta R_x}{R_x} + \frac{\Delta R_y}{R_y} \right) = \frac{(1-\nu)}{E} (\sigma_x + \sigma_y)$$

$$\begin{aligned}\epsilon_x - \epsilon_y &= \frac{1}{K_l - K_t} \left(\frac{\Delta R_x}{R_x} - \frac{\Delta R_y}{R_y} \right) = \frac{(1+\nu)}{E} (\sigma_x - \sigma_y) \\ \gamma_{xy} &= \frac{1}{K_l - K_t} \left[\frac{\Delta R_{45}}{R_{45}} - \frac{1}{2} \left(\frac{\Delta R_x}{R_x} + \frac{\Delta R_y}{R_y} \right) \right] = \frac{2(1+\nu)}{E} \tau_{xy}\end{aligned}\quad (2.15)$$

If we let

$$A = \frac{2}{E} (1-\nu)(K_l + K_t), \quad B = \frac{2}{E} (1+\nu)(K_l - K_t) \quad (2.16)$$

The final equations for sectioning measurement of surface residual stress become:

$$\begin{aligned}\sigma_x &= \left[\frac{1}{A} \left(\frac{\Delta R_x}{R_x} + \frac{\Delta R_y}{R_y} \right) + \frac{1}{B} \left(\frac{\Delta R_x}{R_x} - \frac{\Delta R_y}{R_y} \right) \right] \\ \sigma_y &= \left[\frac{1}{A} \left(\frac{\Delta R_x}{R_x} + \frac{\Delta R_y}{R_y} \right) - \frac{1}{B} \left(\frac{\Delta R_x}{R_x} - \frac{\Delta R_y}{R_y} \right) \right] \\ \tau_{xy} &= \frac{1}{B} \left[\frac{\Delta R_{45}}{R_{45}} - \frac{1}{2} \left(\frac{\Delta R_x}{R_x} + \frac{\Delta R_y}{R_y} \right) \right]\end{aligned}\quad (2.17)$$

where $\frac{\Delta R_x}{R_x}$, $\frac{\Delta R_y}{R_y}$, $\frac{\Delta R_{45}}{R_{45}}$ are the relative resistance changes of the gage in the

x, y, and 45-degree directions respectively. Each needs to be measured experimentally to determine the residual stresses. A and B are calibration constants that depend on both material and strain gage parameters. They can be determined experimentally from a tensile bar test as discussed in section 3.5.

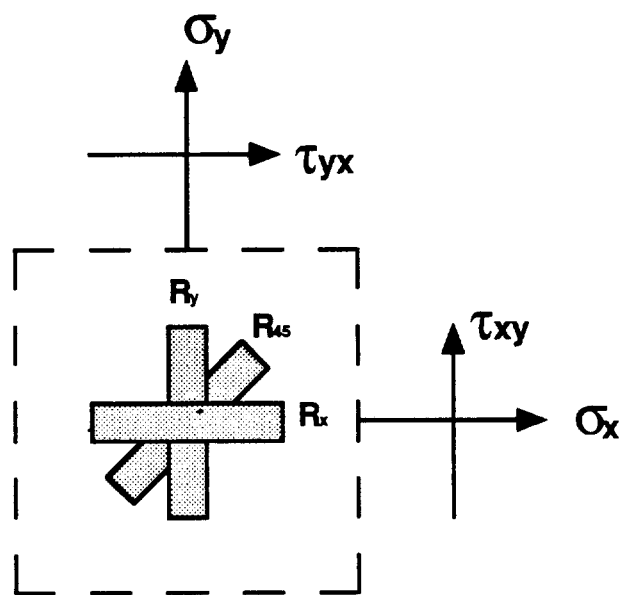


Figure 2.14 Sectioning Configuration

2.8 Hole-drilling residual stress measurement

The hole-drilling residual stress measurement method is used to measure residual stress on a material surface. Its measurement processes include mounting a strain gage rosette, Figure 2.15, on the measured surface, drilling a hole of appropriate dimension at the center of the rosette and measuring the strain change of each gage due to hole-drilling. The residual stress state is then calculated. The premise conditions for the application of this technique are a uniform plane stress state and complete linear elastic behavior of the material.

The strain gage rosette used for the hole drilling technique is usually composed of three single gage elements in 0° - 45° - 90° or 0° - 90° - 225° orientations. The equations used for the hole-drilling technique are [72]:

$$\begin{aligned}\sigma_1 &= \frac{\epsilon_x + \epsilon_y}{4A'} - \frac{1}{4B'} [(\epsilon_x - \epsilon_y)^2 + (\epsilon_x + \epsilon_y - 2\epsilon_{45})^2]^{1/2} \\ \sigma_2 &= \frac{\epsilon_x + \epsilon_y}{4A'} + \frac{1}{4B'} [(\epsilon_x - \epsilon_y)^2 + (\epsilon_x + \epsilon_y - 2\epsilon_{45})^2]^{1/2} \\ \operatorname{tg}2\theta_0 &= \frac{\epsilon_x + \epsilon_y - 2\epsilon_{45}}{\epsilon_y - \epsilon_x}\end{aligned}\quad (2.18)$$

where σ_1, σ_2 are principle stresses and θ_0 is the angle between σ_1 and the longitudinal direction of gage x as shown in Figure 2.15. $\epsilon_x, \epsilon_{45}$ and ϵ_y are the strain changes due to the relaxation of residual stress after hole-drilling. A' and B' are calibration constants. Although this method is well accepted and widely used, it is subject to a variety of measurement errors during the measurement processes. Special calibration is required for some applications.

The residual stress state on a material surface is usually biaxial and unknown. Since there are three strain gages involved in the hole drilling measurement, the error due to the transverse sensitivity of the strain gage might significantly affect some of the gages. To correct this error, as mentioned in section 2.7, the general strain gage equation:

$$\frac{dR}{R} = K_t \epsilon_1 + K_t \epsilon_t \quad (2.12)$$

is used in the stress analysis. The gage in 0 degrees, in 90 degrees and in 45 degrees are defined as gage x, y and 45 respectively in the following analysis. An equation for hole drilling residual stress measurement is derived as follows. Its purpose is to eliminate the effect of transverse sensitivity of the strain gage.

Consider an infinite plate with negligible thickness which is subjected to a fixed uniform plane stress load σ_1 and σ_2 (where σ_1 and σ_2 are principle stresses and $\sigma_1 \geq \sigma_2$), and a through hole with radius 'a' is drilled with its center at point o, a polar coordinate system is established with point o as the origin and with the direction of σ_1 as the polar axis, Figure 2.15. If the constitutive relation of materials is satisfied with a complete linear elastic condition, according to Kirsch's theory, the components of stress change at any point p(r, θ) due to the hole drilling can be expressed in polar coordinates as:

$$\begin{aligned} \sigma_r &= -\frac{1}{2}(\sigma_1 + \sigma_2) \frac{a^2}{r^2} - \frac{1}{2}(\sigma_1 - \sigma_2) \left(\frac{4a^2}{r^2} - \frac{3a^4}{r^4} \right) \cos 2\theta \\ \sigma_\theta &= \frac{1}{2}(\sigma_1 + \sigma_2) \frac{a^2}{r^2} - \frac{1}{2}(\sigma_1 - \sigma_2) \frac{3a^4}{r^4} \cos 2\theta \\ \tau_{r\theta} &= -\frac{1}{2}(\sigma_1 - \sigma_2) \left(\frac{2a^2}{r^2} - \frac{3a^4}{r^4} \right) \sin 2\theta \end{aligned} \quad (2.19)$$

From Hooke's law and equation (2.12), if a strain gage with negligible size is mounted at point $p(r, \theta)$ with its gage axis parallel to the r axis, the ratio of the resistance change becomes:

$$\frac{dR}{R} = K_t \epsilon_r + K_t \epsilon_\theta = \frac{1}{E} [(K_t - \nu K_t) \sigma_r + (K_t - \nu K_t) \sigma_\theta] \quad (2.20)$$

where E and ν are the Young's modulus and Poisson's ratio of the material on which the residual stress is to be determined. Putting equation (2.19) into (2.20), we get the following equation, (2.21):

$$\frac{dR}{R} = -\frac{1}{2E} \left\{ [(1+\nu)(K_t - K_t) \frac{a^2}{r^2}] (\sigma_1 + \sigma_2) + [(K_t - \nu K_t) \frac{4a^2}{r^2} - (1+\nu)(K_t - K_t) \frac{3a^4}{r^4}] (\sigma_1 - \sigma_2) \cos 2\theta \right\}$$

If we let:

$$L_1 = -\frac{1}{2E} [(1+\nu)(K_t - K_t) \frac{a^2}{r_o^2}] \quad (2.22)$$

$$L_2 = -\frac{1}{2E} [(K_t - \nu K_t) \frac{4a^2}{r_o^2} - (1+\nu)(K_t - K_t) \frac{3a^4}{r_o^4}]$$

Then (2.21) becomes:

$$\frac{dR}{R} = L_1 (\sigma_1 + \sigma_2) + L_2 (\sigma_1 - \sigma_2) \cos 2\theta \quad (2.23)$$

This gives the resistance change ratio of the gage at location (r, θ) due to the hole drilling.

In the strain gage rosette shown in Figure 2.15, the gages x , 45 and y are located at coordinates (r_o, θ_o) , $(r_o, \theta_o + 45)$ and $(r_o, \theta_o + 90)$ respectively. Since

$$\cos 2(\theta_o + 45) = -\sin 2\theta_o, \quad \cos 2(\theta_o + 90) = -\cos 2\theta_o \quad (2.24)$$

from equation (2.23), the resistance changes of these gages are

$$\begin{aligned}\frac{dR_x}{R_x} &= L_1(\sigma_1 + \sigma_2) + L_2(\sigma_1 - \sigma_2)\cos 2\theta_o \\ \frac{dR_{45}}{R_{45}} &= L_1(\sigma_1 + \sigma_2) - L_2(\sigma_1 - \sigma_2)\cos 2\theta_o \\ \frac{dR_y}{R_y} &= L_1(\sigma_1 + \sigma_2) - L_2(\sigma_1 - \sigma_2)\sin 2\theta_o\end{aligned}\quad (2.25)$$

By solving these equations, the values of σ_1 , σ_2 and θ_o can be determined. If the gage is considered to be of a length within coordinates r_1 and r_2 and if the effect of gage width is eliminated, then let

$$A = \int_{r_1}^{r_2} L_1 dr \quad B = \int_{r_1}^{r_2} L_2 dr \quad (2.26)$$

the equation (2.25) becomes:

$$\begin{aligned}\frac{\Delta R_x}{R_x} &= A(\sigma_1 + \sigma_2) + B(\sigma_1 - \sigma_2)\cos 2\theta_o \\ \frac{\Delta R_{45}}{R_{45}} &= A(\sigma_1 + \sigma_2) - B(\sigma_1 - \sigma_2)\cos 2\theta_o \\ \frac{\Delta R_y}{R_y} &= A(\sigma_1 + \sigma_2) - B(\sigma_1 - \sigma_2)\sin 2\theta_o\end{aligned}\quad (2.27)$$

So we can finally get:

$$\sigma_1 = \frac{\left(\frac{\Delta R_x}{R_x} + \frac{\Delta R_y}{R_y}\right)}{4A} - \frac{1}{4B} \left[\left(\frac{\Delta R_x}{R_x} - \frac{\Delta R_y}{R_y}\right)^2 + \left(\frac{\Delta R_x}{R_x} + \frac{\Delta R_y}{R_y} - 2\frac{\Delta R_{45}}{R_{45}}\right)^2 \right]^{1/2}$$

$$\sigma_2 = \frac{\left(\frac{\Delta R_x}{R_x} + \frac{\Delta R_y}{R_y}\right)}{4A} + \frac{1}{4B} \left[\left(\frac{\Delta R_x}{R_x} - \frac{\Delta R_y}{R_y}\right)^2 + \left(\frac{\Delta R_x}{R_x} + \frac{\Delta R_y}{R_y} - 2\frac{\Delta R_{45}}{R_{45}}\right)^2 \right]^{1/2} \quad (2.28)$$

$$\theta_o = \frac{1}{2} \operatorname{tg}^{-1} \left[\frac{\left(\frac{\Delta R_x}{R_x} + \frac{\Delta R_y}{R_y} - 2\frac{\Delta R_{45}}{R_{45}}\right)}{\left(\frac{\Delta R_y}{R_y} - \frac{\Delta R_x}{R_x}\right)} \right]$$

The constants A and B depend on both the strain gage parameters and the material, and they can be theoretically calculated from equation (2.26). In reality, the specimen is usually of a considerable thickness and a blind hole is usually drilled instead of a through hole. Also, the strain gage is not the ideal line type (without width). So, the above equations are only assumed to be correct for practical situations, and the required constants A and B must be calibrated from an appropriate experimental test.

If high residual stress or non-uniform stress distributions (stress gradient) are involved in the application, local plastic deformation or non-uniform elastic deformation may take place and the above premise conditions will not be satisfied. To apply the hole-drilling technique under such conditions, the coefficients A and B are no longer constants but variables that depend on the stress level and stress gradient. Special calibration is then required to account for the conditions.

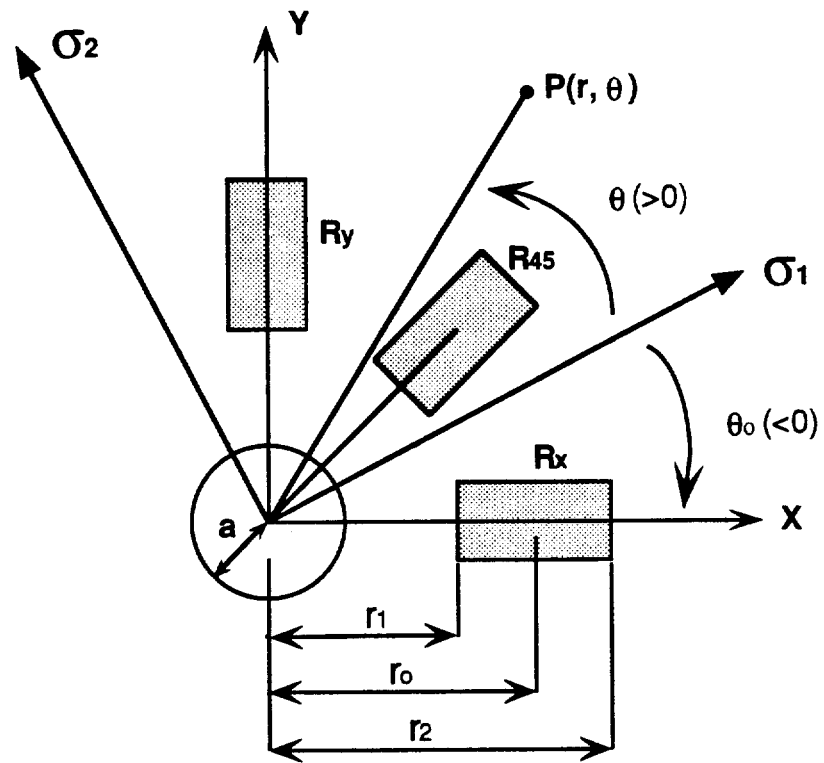


Figure 2.15 Hole-drilling Configuration

CHAPTER 3

EXPERIMENTAL

3.1 General test program

The purpose of this research program was to determine the effects of welding residual stress, weld toe notch and weld defects on the fatigue behavior of welded joints. With the tank car problem as the basis for this study, the major test design focused on the fatigue behavior of the fillet welded tank car shell structures. The detailed test program included:

- 1). To establish reliable blind hole drilling and sectioning techniques for experimental residual stress measurement.
- 2). To design a pad weld specimen to simulate the fillet welded tank car shell structure and to determine the welding residual stress distribution pattern associated with the welds.
- 3). To design a simple weld specimen with similar welding residual stress and weld defect features as in the pad weld specimen but which is as compact as possible for fatigue testing.
- 4). To determine the effect of cyclic stress on the welding residual stress of simple specimens so that the appropriate fatigue load conditions can be determined for the study of the effects of welding residual stress on fatigue properties.

- 5). To determine the effective heat treatment conditions for thermal residual stress relaxation and to determine the effect of heat treatment on microstructures.
- 6). To determine stress-life relationships and fatigue crack propagation properties of as-welded and stress relieved simple specimens under pulsed tension and alternating cyclic load conditions.
- 7). To determine the stress concentration factor at the weld end toe of simple fatigue testing specimens.
- 8). To determine the features of microstructure, weld defects, crack initiation site and fracture surface of simple fatigue testing specimens.
- 9). To establish quantitative or semi-quantitative correlations between fatigue life, welding residual stresses, weld toe notch and weld defects.
- 10). To provide practical principles for fatigue design and fatigue life prediction of welded structures.

3.2 Material

To solve the question of the fatigue performance of tank car shells, the laboratory test conditions were selected to be as close as possible to the field conditions. The materials used in this study are 1/2 inch thick hot-rolled ASTM A515 grade 70 steel plate and 1/2 inch thick A283 grade C steel. They are the same materials used in the tank car structure except that the 1/2 inch thick A515 steel plate used in the test differs slightly in thickness from the 7/16 inch thick A515 grade 70 steel plate used in real tank car shell structures. Table 3.1 gives the chemical compositions and tensile properties of as-received A515 steel and A283 steel. Table 3.2 gives the tensile properties of these steels.

Both materials are low carbon mild steels. A515 steel plate is commonly used for pressure vessel structures in intermediate and high temperature service applications. A283 is a general purpose structure steel with low tensile strength and good weldability.

Table 3.1 Chemical Compositions of A515 and A283 Steel

	C	Mn	P	S	Si
A515-70	0.18	1.08	0.006	0.01	0.20
A283-C	0.13	0.65	0.007	0.008	0.21

Table 3.2 Tensile Properties of A515 Steel and A283 Steel

	yield strength	tensile strength	elongation	reduction in area
A515-70	45 (Ksi)	70 (Ksi)	37.5%	60.0%
A283-C	44 (Ksi)	67 (Ksi)	31.0%	Not available

3.3 Specimen preparation

3.3.1 Pad-on-plate weld specimen

The pad-on-plate specimen, Figure 3.1, was designed to simulate the real tank car shell structure so that it could be used to determine the typical welding residual stress of the tank car shell under laboratory conditions. It was fabricated by skip fillet welding a $19 \times 2.5 \times 0.5$ inch A283 steel pad onto a $27 \times 10.5 \times 0.5$ inch A515 steel plate. It was assumed that the selected specimen dimensions were big enough to model the real tank car structure. The welding was carried out by the shielded metal arc welding (SMAW) process. The welding procedures followed were the same as those used to manufacture the tank car. E7018 electrodes, 3/16" in diameter, were used at an arc current of 200 amps. Two such specimens were prepared for welding residual stress measurements. The sequence of welding passes for the first specimen were randomly chosen by the welder. The sequence of welding passes for the second specimen were taken by welding the four corner welds first in order to increase restraint on the following passes and to create higher welding residual stresses.

3.3.2 Simple weld specimen

Simple specimens were designed for the fatigue test. On the one hand, they needed to be as simple and as compact as possible in order to be suitable for the fatigue test; but on the other hand, they had to be big enough to maintain the same welding residual stress and weld defects features as that of the larger pad-on-plate specimens. Two types of simple specimens were designed. One was made with skip, bead-on-plate welding, and the other was made with skip, gusset fillet welding. They were both fabricated using the same welding

conditions as those for the pad-on-plate weld specimens except that the welding travel speed of the bead-on-plate weld was slower than that of the fillet weld in order to accommodate a single welding pass. The longitudinal direction of the specimen was chosen to be parallel to the rolling direction of the as-received A515 plate. These simple specimens were made with different widths, and the associated welding residual stresses were measured to determine the effect of specimen width on the residual stress (see section 3.7.3). The optimum specimen width was then determined to be the one which is sufficient to maintain the same tensile residual stress level at the weld end toe as in the pad-on-plate weld specimen, and which is also satisfied with the load capacity of the testing machine. The length of the specimen was chosen at approximately three times the width in order to create a center test region with a sensible uniform nominal stress distribution according to an empirical tension test design standard [15]. Figure 3.2 shows the configurations of bead-on-plate and gusset fillet simple specimens.

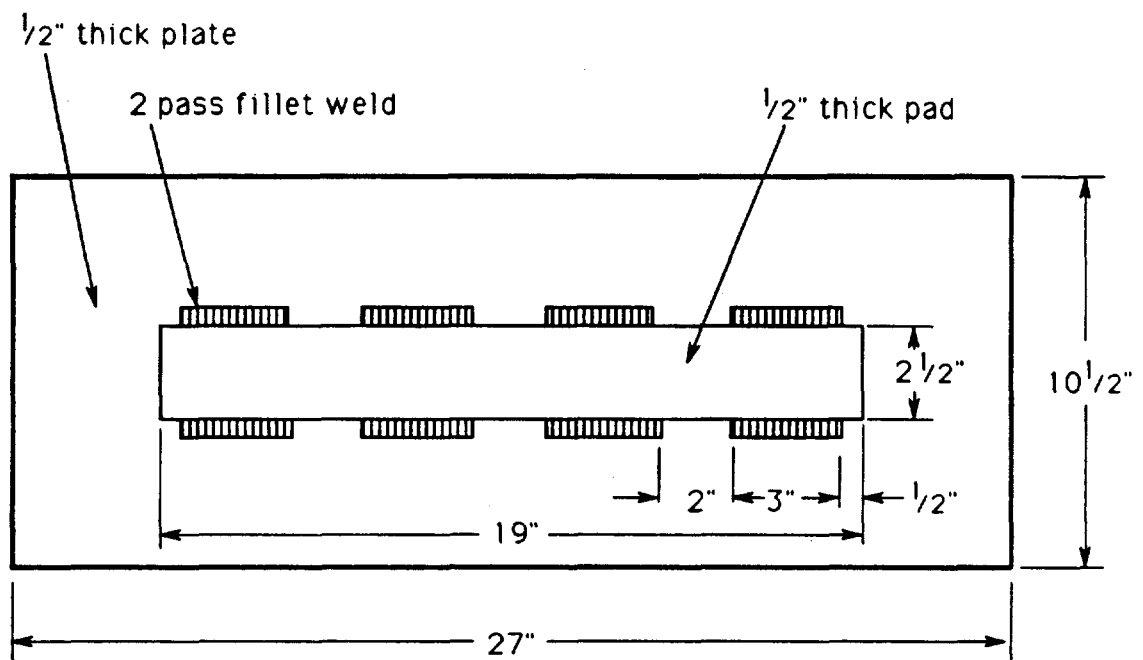


Figure 3.1 Pad-on-plate weld specimen

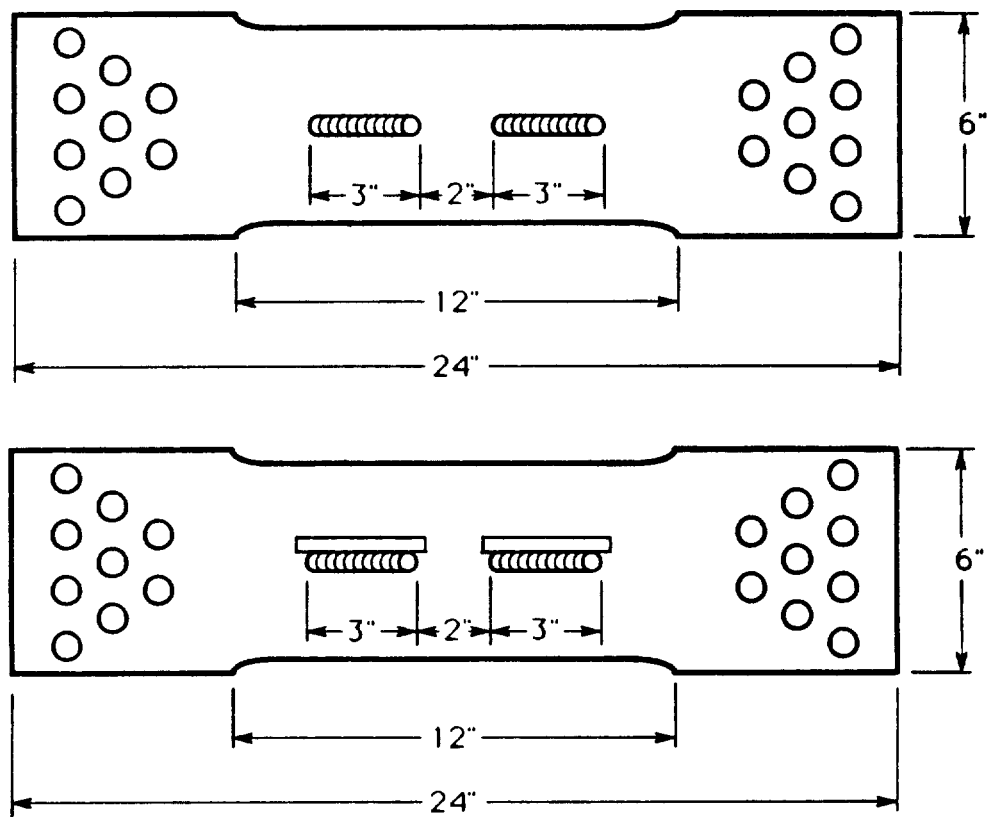


Figure 3.2 Bead-on-plate and Fillet Simple Weld Specimens

3.4 Fatigue test design

3.4.1 Testing machine

The fatigue test was carried out in an Instron series 1335 loading frame equipped with an Instron series 2150 servohydraulic control and a computer interface. The actuator has a load capacity of $\pm 120,000$ lbs. The servohydraulic control is capable of load, position and strain control and is equipped with a function generator to create cyclic sine, sawtooth and square loading forms. When the load range, mean load, load form and frequency are chosen, the test program can be precisely controlled by the computer. Information on load, position and strain can be read out from the control panel during the test, or they can be stored in the computer for later analysis. The number of load cycles is automatically recorded by a counter. Figure 3.3 shows the fatigue testing arrangement.

3.4.2 Grip system

To carry out a fatigue test under cyclic load conditions, a rigid constraint system is required to hold the specimen so that the load will be properly transferred into the specimen body. Also, the system should be able to undertake any cyclic load within the maximum test load range. With several options having been tried, the final design was a multibolt clamping grip system, Figure 3.4. Each bolt needs to be tightened with a torque of approximate 150 ftlb so as to create a clamping force great enough to avoid any relative movement between the specimen and the grips. To avoid the buckling effects under alternating load conditions, a rigid frame with multiple side rollers was used to clamp onto the specimen's surface across its entire length. This limits the

bending deformation of the specimen without restricting its axial deformation.

3.4.3 Fatigue test condition

Fatigue tests were carried out under pulsed tension and alternating sinusoidal cyclic load conditions in order to obtain stress-life and crack propagation properties. The applied loads were chosen at 0 to 7 Ksi, 0 to 10 Ksi, 0 to 13 Ksi, -7 to 7 Ksi and -10 to 10 Ksi. Under these conditions the maximum tensile stress is below 14 Ksi, which was determined to be the upper limit of applied stress to avoid significant residual stress relaxation at the weld end toe (see the test detail in section 3.7.5 and the result in section 4.3.5). The test frequency was chosen between 5 to 12 Hz. Since some of the welded specimens had slight bending distortion due to welding, some additional bending stresses had to be induced into the specimen when the specimens were clamped into the grips. Strain gages were used to measure the bending stresses.

3.4.4 Crack propagation measurement

To obtain the fatigue crack propagation information a crack propagation gage was used to measure the crack length during the fatigue process. Figure 3.5 shows the principle for the measurement. The gage used was a type CPA01 made by Measurement Group, Inc. for automatic crack propagation detection. The accuracy of this method was examined by applying one cycle of overload when the fatigue crack was within the gage recording range. This method left a clearly defined crack profile on the fracture surface, and, after the specimen was fractured, the relative location of the crack and the gage could then be determined and compared with the strip chart plot of the gage recorded location. It was found that the gage had an accuracy of ± 0.005 inch.

The application of an overload during the fatigue process was also used as a method of obtaining detailed crack profile features of the tested specimens. The applied overload was chosen to be twice the maximum tensile stress of the applied constant cyclic load. The application of an overload will inevitably cause some additional plastic deformation as well as some compressive residual stress at the crack tip so that the crack propagation will be retarded and the fatigue life modified. However, for a high cycle fatigue test, this effect is usually insignificant. The advantage of doing this, is that the crack profile is well defined, and it can be accurately determined.

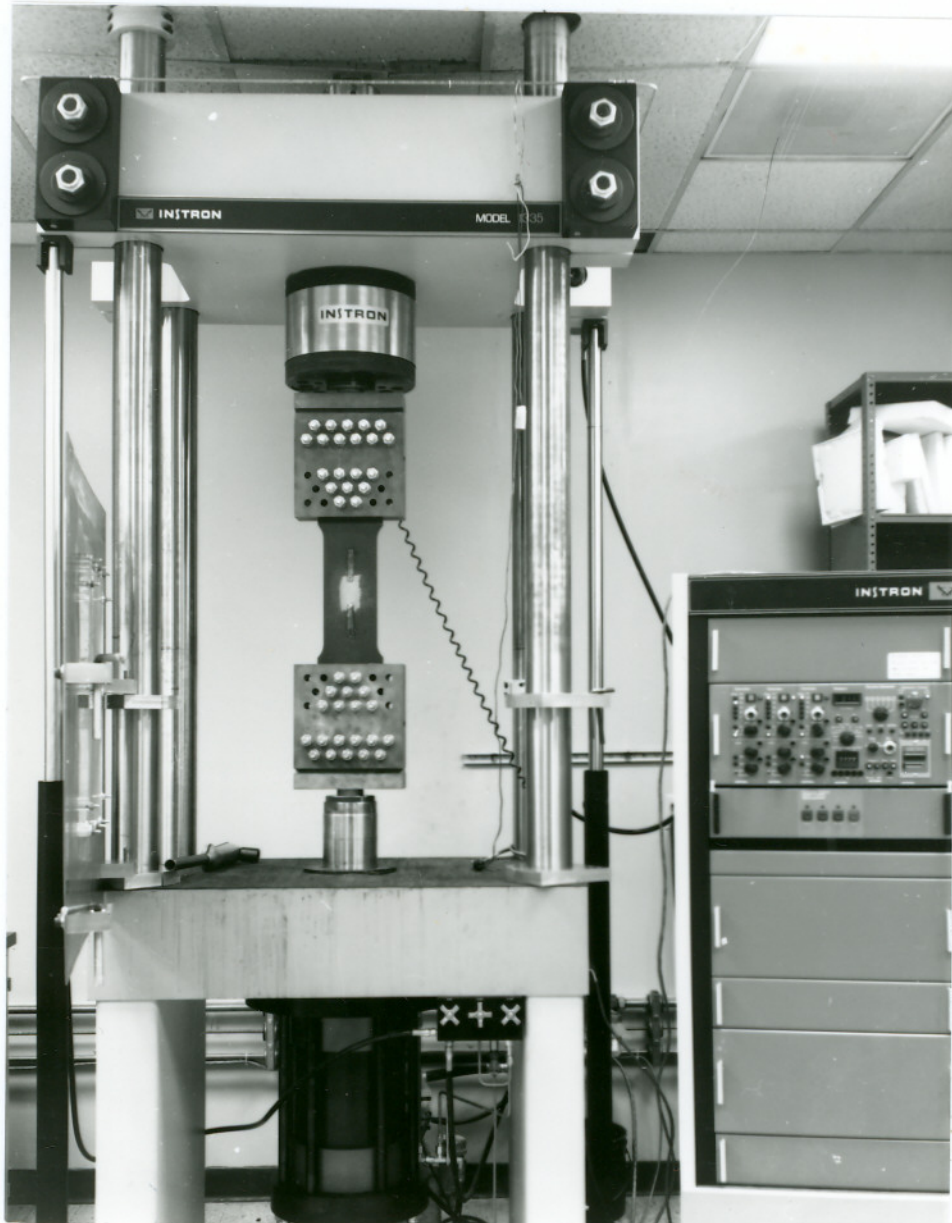


Figure 3.3 Fatigue Testing Arrangement

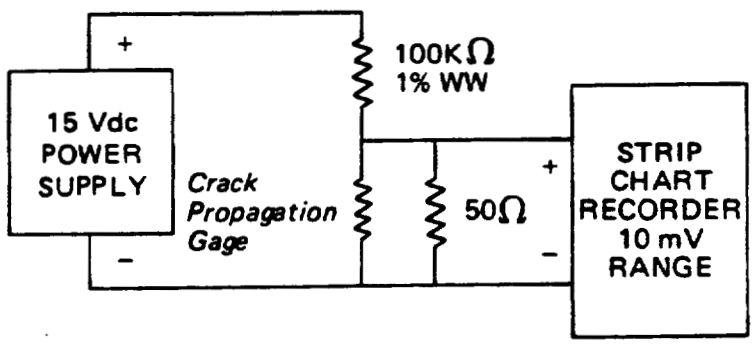
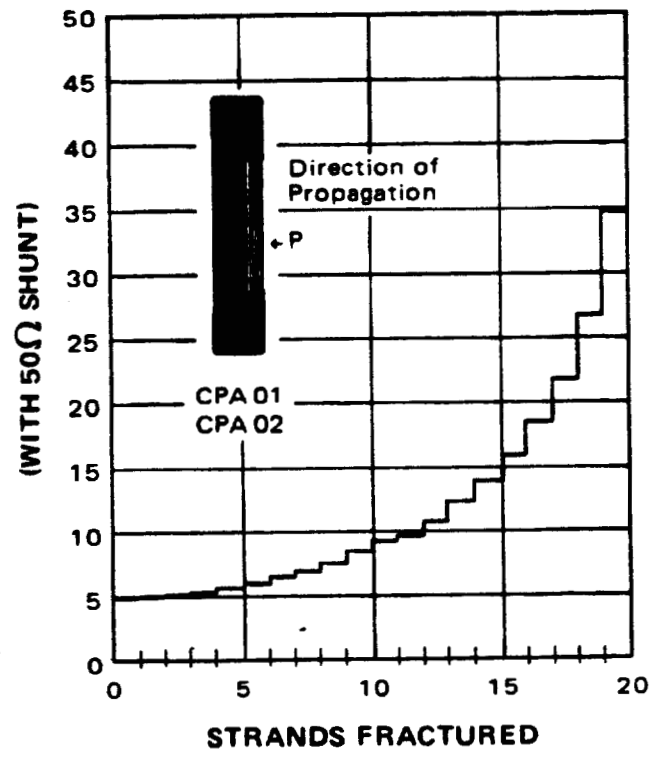


Figure 3.5 Crack Propagation Gage and Its Principle

3.5 Application of Sectioning method

3.5.1 Sectioning operation

The strain gage rosette used for the sectioning method is type WA-06-030WR-120, Figure 3.6, provided by Measurement Group, Inc. The matrix of the gage is 0.19×0.17 inch (4.8×4.3 mm) in size. The sectioning process involves parting out the strain gaged material from the main body by mechanical means. It was required that no significant machining stress be introduced into the material and that the strain gage bonding conditions remain undisturbed during the operation. A special coating, M-coat A, was used to protect the gage rosette from humidity and from mechanical damage. A cutting wheel, with a precise position control, was used for the sectioning operation. The thickness of the blade used is approximately 0.5mm, and the cutting gap is approximately 1mm. To avoid any contact between the blade and the gage matrix, a 2 to 3 mm separation is actually required between the matrices of two neighboring gages. A liquid coolant was used and each cutting increment was limited to less than 15 microinch so as to eliminate heat and machining stress during the process. In order to examine the machining stress, a stress-free specimen was tested first, the results of which showed that the machining stress was negligible if the operation was performed carefully.

3.5.2 Calibration test

Under uniaxial tension conditions with the x axis in the loading direction, the equation (2.9) becomes:

$$\sigma_y = \tau_{xy} = 0, \quad \epsilon_y = -\nu\epsilon_x, \quad \sigma_x = E\epsilon_x \quad (3.1)$$

From equation (2.17), we have

$$A = \frac{2}{\sigma_x} \left(\frac{\Delta R_x}{R_x} + \frac{\Delta R_y}{R_y} \right) \quad B = \frac{2}{\sigma_x} \left(\frac{\Delta R_x}{R_x} - \frac{\Delta R_y}{R_y} \right) \quad (3.2)$$

These are the simplified equations to determine constants A and B. A stress-relieved tensile bar specimen of A515 steel was used to determine the constants. With the loading direction defined as x, the strain gage rosette was aligned with one gage in the x direction and another in the y direction. The constants A and B were then determined by measuring relative resistance changes of the strain gages under a determined nominal loading σ_x .

During strain measurement, it was found that the strain reading on an available strain indicator was inconsistent and there was a measurement error of approximately $\pm 40\mu\epsilon$. A Keithley 191 digital multimeter was then used to measure the resistance change of the strain gage instead of measuring the strain. The multimeter has a built-in 4 terminal resistance measurement bridge that allows the measurement accuracy to be approximately $\pm 0.001\Omega$. This accuracy, which corresponds to a strain value of $\pm 4\mu\epsilon$, is acceptable in practice.

To eliminate any possible effects of temperature variation on the accuracy of the resistance measurement, another strain gage was bonded onto a small A515 steel sample for temperature compensation. Its resistance was measured simultaneously with the stress-measurement gage. If there was a temperature variation that caused its resistance to change from R to R', a coefficient $\frac{R'}{R}$ was then determined to modify the measured resistance value of the stress-measurement gage.

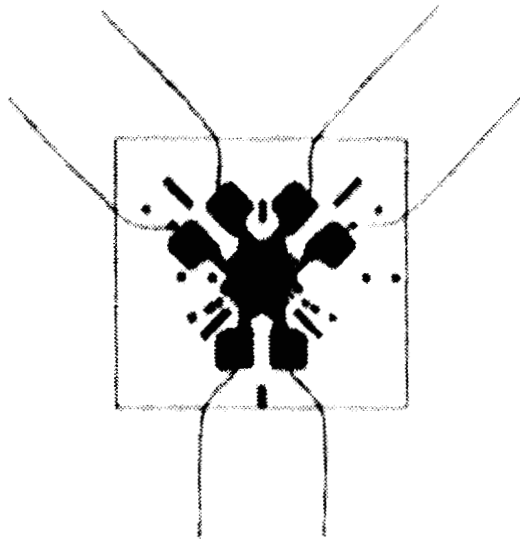


Figure 3.6 Strain Gage Rosette for Sectioning Measurement (8×)

3.6 Application of Hole-drilling method

3.6.1 Hole drilling operation

The strain gage rosette used for hole-drilling residual stress measurement was of type CEA-06-062UM-120, Figure 3.7, supplied by Measurement Group, Inc.. For the hole drilling process, it is required to drill a hole, 1.5 mm in diameter and 2 mm in depth, at the strain gage rosette center so as to relieve part of the residual stresses. The hole drilling process should be free of machining stress and should be accurate in both hole drilling location and dimensions. A high speed carbide cutter driven by an air turbine device was used to drill the hole. The drilling speed used was approximately 300,000 rpm, and at this speed, the machining stress introduced by the hole drilling process is negligible [73]. A milling guide with microscope aided position control was used to align the hole center. A vertical position control with scale adjustment was used to set the increment of hole drilling depth. Compressed dry nitrogen (with a pressure of approximately 40 psi) was used to drive the air turbine device. Figure 3.8 illustrates the system used for the hole drilling operation.

3.6.2 Calibration constants

The calibration of the hole-drilling method was carried out by applying the hole-drilling technique to a specimen with a determined stress loading according to ASTM standard E837 [72].

A tensile bar specimen was uniaxially loaded to a known load before and after drilling the hole, Figure 3.9. With the longitudinal direction of gage x parallel to the loading direction, the stress condition in the specimen becomes: $\sigma_1 = \sigma_x$, $\sigma_2 = \sigma_y = 0$, $\theta = 0$. From equation (2.28), we have:

$$\operatorname{tg}2\theta=0 \text{ and } \frac{\Delta R_x}{R_x} + \frac{\Delta R_y}{R_y} - 2\frac{\Delta R_{45}}{R_{45}} = 0$$

So we can get:

$$4A = \frac{2}{\sigma_x} \left(\frac{\Delta R_x}{R_x} + \frac{\Delta R_y}{R_y} \right) \quad (3.3)$$

$$4B = \frac{2}{\sigma_x} \left(\frac{\Delta R_x}{R_x} - \frac{\Delta R_y}{R_y} \right)$$

When a known stress σ_x is applied, we can directly measure the resistance change ratios, $\frac{\Delta R_x}{R_x}$ and $\frac{\Delta R_y}{R_y}$ before and after drilling the hole. To determine the coefficients A and B, the load σ_x was limited to less than one third of the yield strength of the material so that there was no plastic deformation involved in the calibration process. A multichannel strain meter with a computer aided stress-strain recording program was used. Since the strain measured by a strain meter is not exactly the strain value but is instead the resistance change value divided by the gage factor K_0 (equation (2.10)), the measured 'strain' value can be transformed into the resistance value by rewriting equation (3.3) as:

$$4A = \frac{2K_0}{\sigma_x} (\Delta\epsilon_x^m + \Delta\epsilon_y^m) \quad (3.3^*)$$

$$4B = \frac{2K_0}{\sigma_x} (\Delta\epsilon_x^m - \Delta\epsilon_y^m)$$

where $\Delta\epsilon_x^m$, $\Delta\epsilon_y^m$ are differences of the measured strains (not the true strain) for gage x and gage y before and after drilling the hole. With this expression, the calibration results are consistent with the application of the multimeter. So

the convenient multimeter can to be used for hole-drilling residual stress measurement.

Several tensile bar specimens were prepared and each was loaded several times to obtain the statistical A and B values.

3.6.3 Hole drilling machining stress

To examine the effect of hole drilling machining stress, a small sample, 1.5×1×0.5 inches in dimension, was made from an as-received A515 specimen, and was annealed at 650°C in an evacuated glass tube for two hours and furnace cooled to ensure that it was residual stress and oxidation free. Then, the hole drilling machining stress was determined by applying the normal hole-drilling technique to this stress free sample.

3.6.4 High stress application

When the load σ_x in a tensile bar test is greater than 1/3 of the yield strength of the material, local yielding will occur around the hole due to stress concentration. As a result, A and B are no longer constants but become functions of the nominal load. This effect was considered in the calibration processes so as to improve the overall accuracy of the hole-drilling method. This calibration test was carried out in a similar way as the calibration test in the elastic region except that a higher stress load level was applied. Under such conditions, the stress-strain relationship is no longer a straight line but a non-linear curve. From the calibration curve obtained, different calibration constants were determined corresponding to different stress levels. A numerical iteration method was established to choose the right calibration constants for

the corresponding residual stress levels.

3.6.5 Accuracy of hole-drilling method

Tests were carried out to examine the accuracy of the determined calibration constants for hole-drilling application in both the complete elastic region and the elastic-plastic regions. Stress-relieved A515 tensile specimens were used for the test. Two specimens were uniaxially loaded to about 44% of yield strength and two other specimens were uniaxially loaded to about 90% of yield strength. While the load was maintained on the specimens, the hole drilling process was applied to determine the stress state with the calibrated constants. By comparing the results with the nominal stress states, the accuracy of the calibration constants was determined.

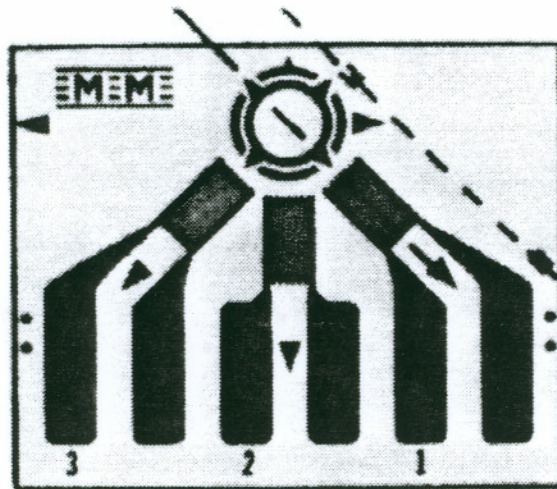


Figure 3.7 Strain Gage Rosette for Hole-drilling Measurement (6×)

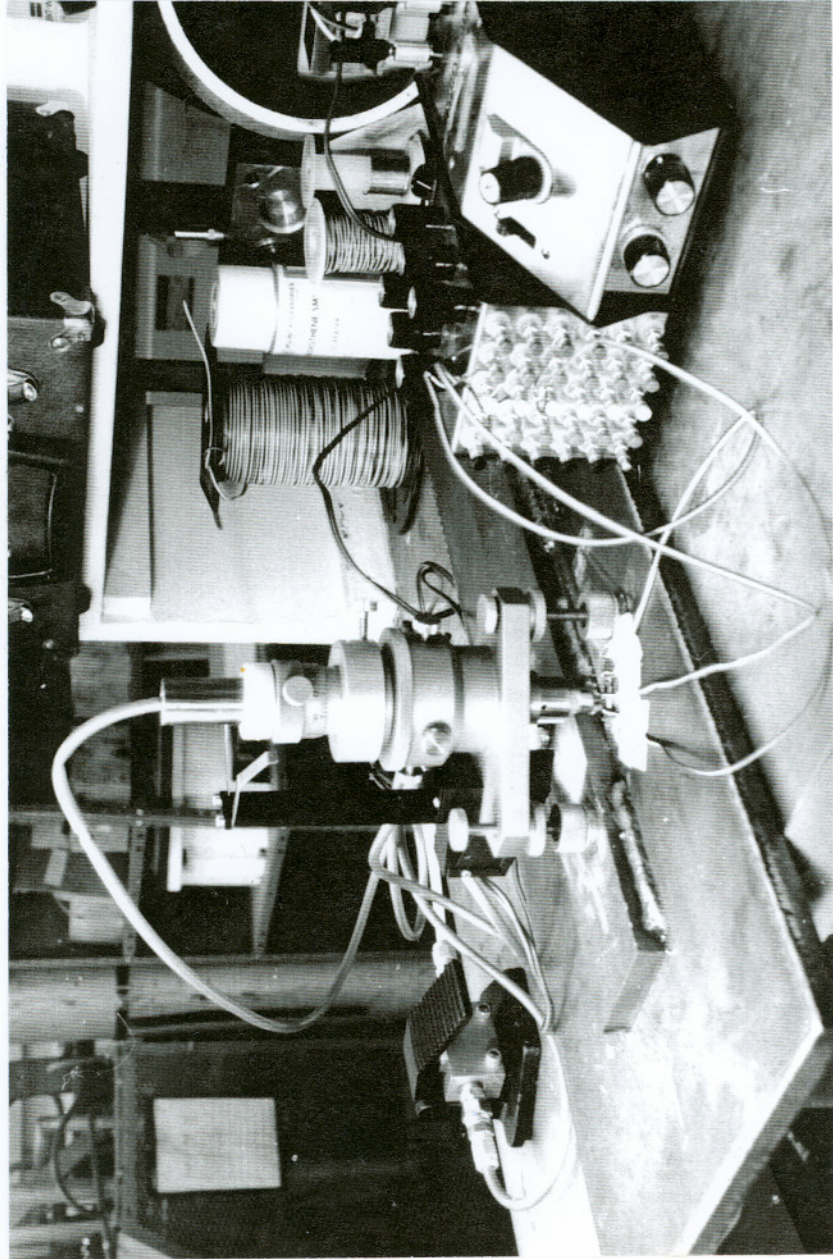


Figure 3.8 Hole-drilling Fixture

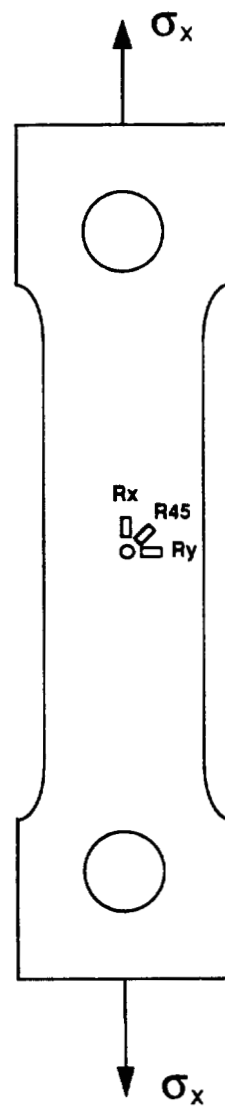


Figure 3.9 Tensile Bar Configuration

3.7 Residual stress measurement

3.7.1 Residual stress in as-received A515 steel plate

The hole-drilling method was used to determine the residual stresses in as-received A515 steel plate.

3.7.2 Residual stress in as-welded pad-on-plate specimen

Both hole-drilling and sectioning methods were used to determine residual stresses in pad-on-plate weld specimens. Since a certain separation was required between two neighboring measurement points, it is impossible to use one single weld to determine the overall residual stress pattern. Based on the assumption that all the welds were identical, a local coordinate system, Figure 3.10, was established. The residual stress measurement results from different welds can then be brought together to form a composite stress pattern based on the same local coordinate system. The origin of the coordinate system was chosen to be the intersection of the extensions of the side fusion line and end fusion line of the weld. The X axis was chosen to be parallel to the welding direction with positive values being into the weld, and the Y axis was chosen to be perpendicular to the welding direction with positive values being away from the weld. Most measurements were carried out in the vicinity of the weld ends and the weld center along lines parallel to the weld with y coordinates equal to 0, 3 and 6mm. Figure 3.11 shows the distribution of all the measurement points.

For sectioning measurements, a 3mm gap was left between the matrices of two neighboring gage rosettes in order to protect the gage from damage during

the cutting process. As a result, the measured residual stress was the averaged stress over an approximate 9mm×9mm area. The coordinates of the center of the rosette were taken to be the coordinates of the sectioning measurement point. For the hole-drilling measurement, the coordinates at the center of the hole were taken to be the coordinates of the measurement point.

3.7.3 Residual stress in as-welded simple specimen

An 8 inch wide bead-on-plate simple weld specimen was first constructed and tested. The welding residual stresses at both the weld end and weld center were determined by the hole-drilling method in order to confirm that it had similar residual stress features as the pad-on-plate weld specimens. The effect of the specimen width on the residual stress was further explored by performing hole-drilling measurements of the residual stresses at the weld end of other bead-on-plate simple specimens with widths equal to 2, 4, and 5 inches respectively. Additional 5 inch wide fillet welded specimens were also used to collect information about residual stress at the weld end toes.

3.7.4 Residual stress in stress-relieved simple specimen

The thermal stress relief method was used to relieve welding residual stress in simple weld specimens. Two heat treatment conditions were used and compared. One was to anneal the specimen at 600°C for two hours and then furnace cool, the other was to anneal the specimen at 650°C for one hour and then furnace cool. The hole-drilling method was used to measure residual stress at the weld toes and to examine the results of stress relief.

3.7.5 Residual stress in cyclic loaded simple specimen

As discussed in section 2.2, the welding residual stress is variable and dependent on the external load. To determine the effect of residual stress on fatigue properties, it is necessary to limit the level of the test load conditions so that no significant residual stress relaxation occurs at the critical weld toe area. Only under such conditions can the effect of residual stress on the fatigue of the weld joint be determined, by comparing the fatigue strength of as-welded and stress-relieved simple weld specimens under the same test load conditions.

To determine the appropriate fatigue test load conditions, the tests were designed to study the effect of external cyclic load on welding residual stress. The hole drilling method was used to measure residual stresses at the weld end and the weld center of simple weld specimens after they were loaded under a particular pulsed-tension cyclic stress. Different load conditions were used to determine the upper limit of the applied tensile stress that would not cause residual stress relaxation at the weld toe. Several 5 inch (125mm) wide simple weld specimens, both bead-on-plate and gusset fillet, were tested for this purpose. The loads used in the test were 0 to 6 Ksi (0 to 40 MPa), 0 to 14 Ksi (0 to 100 MPa), 0 to 22 Ksi (0 to 150 MPa) and 0 to 30 Ksi (0 to 210 MPa). The number of load cycles used in the test were chosen to be 150, 2000 and 115,000 so that the effect of load cycles on residual stress relaxation could be simultaneously determined.

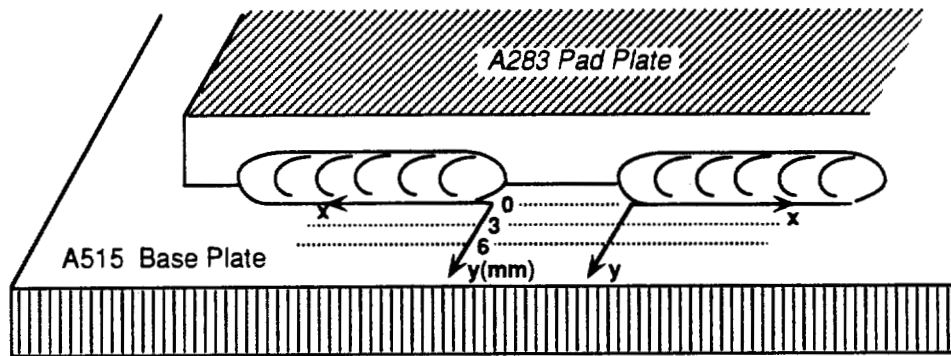
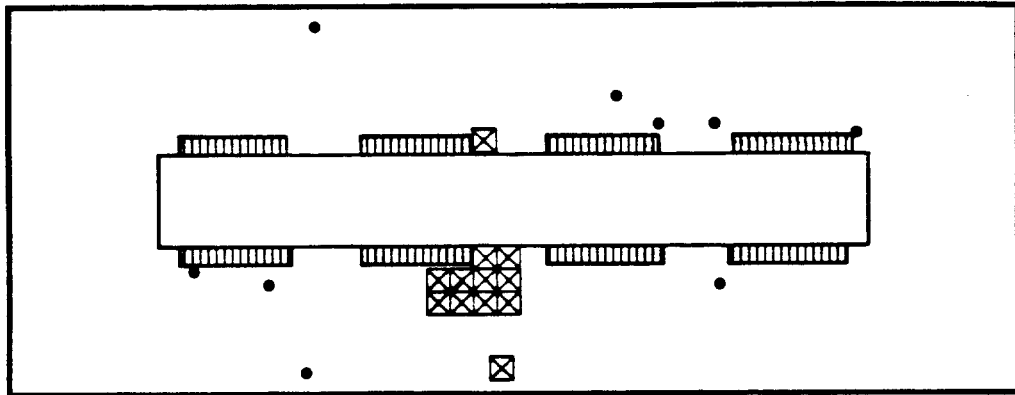


Figure 3.10 Local Coordinate System for Residual Stress Measurement



☒ = Sectioning measurement
• = Hole drilling measurement

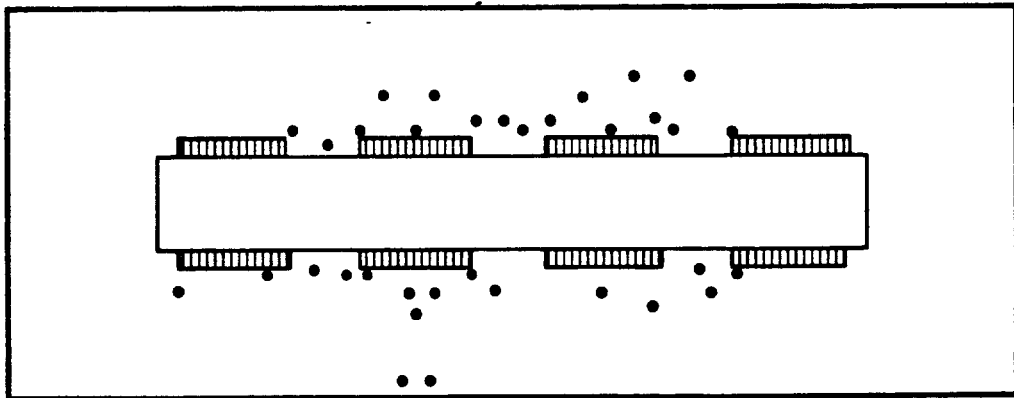


Figure 3.11 Measurement Points Distribution

3.8 Weld toe stress concentration

For a welded structure, the weld toe is always the critical site for fatigue crack initiation due to the effect of stress concentration at that location. As such, it was of interest to determine the stress concentration factor at the weld toe and to study its effect on the fatigue life of a welded joint. The stress concentration factor, SCF, is the ratio of the local maximum stress to the remote nominal stress. It is a measure of the stress concentration effect. Methods for determining SCF include analytical methods (elasticity theory, finite element and finite difference) and experimental methods (photoelasticity, strain gage etc). Photoelasticity is a widely accepted experimental method for SCF measurement. Because it is just a simulation method, its application is limited for structures with complex geometry, such as welded structures. Theoretically speaking, a numerical method, such as the finite element method, can be used to analyze the stress concentration problem for any complex structure; however, it is usually time consuming and inconvenient to use for particular applications. The strain gage method, as a traditional way to measure strain, has direct physical meaning for stress measurement. The only disadvantage for the use of the strain gage method in stress concentration analysis is its limited size. It can only be used to measure the average strain over an area that is usually much larger than the zone affected by the stress concentration, so its application for the direct measurement of SCF is rarely reported in the literature. However, with some improvement in the measurement process, the strain gage method could be effectively used to obtain reliable stress concentration information.

There have been several numerical analysis results reported about the SCF at the weld toes of different welded structures [74]. Unfortunately, none of these results are directly related to the SCF at the end toe of a skip fillet weld. To analyze the SCF for the tested simple weld specimens, the strain gage method was used in this research program. A fillet welded plate specimen was made and further machined into a tensile specimen, to explore the maximum stress concentration area on the side surface, Figure 3.12. The specimen was thermal stress relieved and then strain gaged, Figure 3.13, to measure the average stress concentration factor in the area of gage width. Strain gages of different widths were used alternately to measure the average stress concentrations of different width areas. A numerical extrapolation approach was then used to determine the SCF at the weld toe.

It was assumed that the SCF value at the weld toe was f_t . A coordinate system was defined with the origin located at the weld toe and with the positive x axis oriented toward the specimen, Figure 3.13. The average stress concentration factor value within the width defined by coordinates 0 to x is given by a function of $K(x)$ which is satisfied with boundary conditions of:

$$K(x) = f_t \text{ when } x=0, \text{ and } K(x) = 1 \text{ when } x \rightarrow \infty \text{ (} x \gg 0 \text{)}$$

$K(x)$ can be assumed to have a form:

$$K(x) = \frac{f_t - 1}{f(x) + 1} + 1 \quad (3.4)$$

where $f(x)=0$ when $x=0$, $f(x)=\infty$ when $x \rightarrow \infty$ ($x \gg 0$)

Function $f(x)$ can be simply expressed as a Taylor series:

$$f(x) = \sum_{i=1}^{\infty} a_i x^i \approx \sum_{i=1}^N a_i x^i \quad (3.5)$$

$K(x)$ can be measured by a strain gage with width x as shown in Figure 3.13. By using strain gages with $N+1$ different widths $x_1, x_2, \dots, x_N, x_{N+1}$, we can obtain $N+1$ linear equations. By solving these equations, the SCF value at the weld toe, f_t , and all the coefficients a_1, a_2, \dots, a_N can be determined. This gives a N th order approximation for the SCF value at the weld toe.

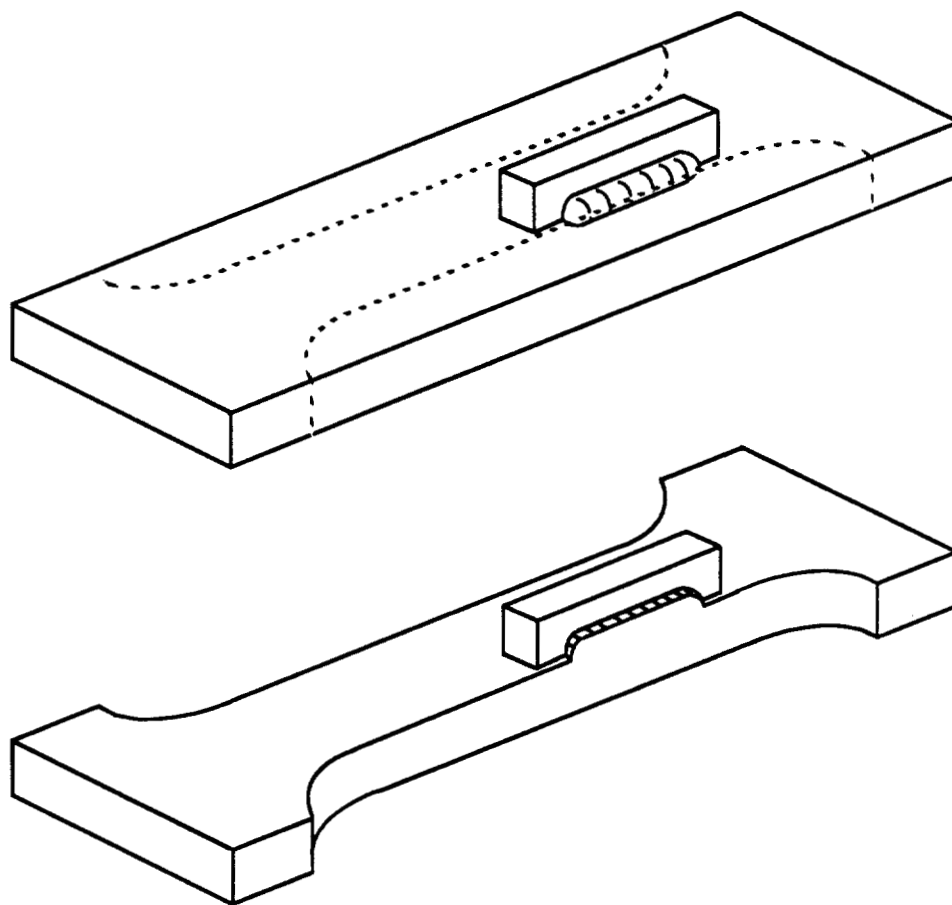


Figure 3.12 Specimen for SCF Measurement

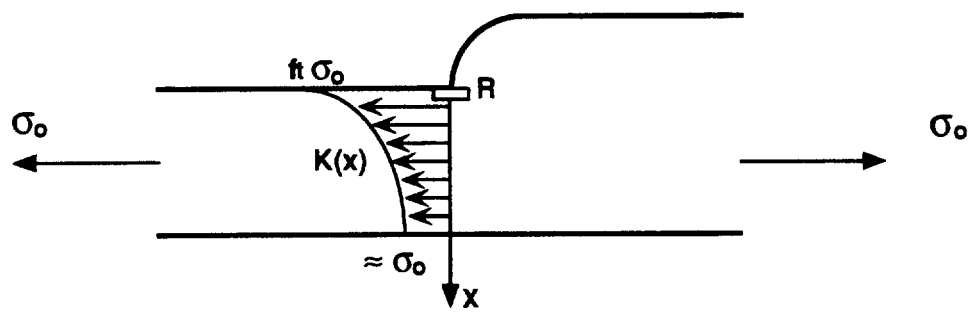


Figure 3.13 Principle of SCF Measurement

3.9 Metallurgical analysis

3.9.1 Microstructure and microhardness

Both as-welded and stress-relieved specimens were sectioned to examine the microstructure and the effect of stress relief heat treatment on the microstructure. The sectioning was made with a cold band saw. The sectioned surface was further ground to 14 μ m with abrasive paper, polished to 1 μ m with a diamond polishing disk and etched with 2% Nital. The microstructure analysis was performed by optical microscopy.

Microhardness was measured on the sectioned surfaces of both as-welded and stress-relieved specimens to determine the effect of the stress relief heat treatment on the mechanical properties of the specimens. Considering that the grain orientation can also affect the hardness, both longitudinally and transverse sectioned samples were used in the measurements. The test was carried out with a LECO DM-400 Hardness Tester, and the load used was 500 grams. The surfaces of the tested samples were lightly etched, to enable measurements to be made in the weld, heat affected zone and parent material respectively. The test results were obtained as Knoop Hardness which could be converted into other hardness units with a conversion chart.

3.9.2 Welding defects

To examine the internal weld defect features, the simple weld specimens were sectioned. The sections were taken in both the longitudinal and transverse directions near the weld end toe. The sectioned surfaces were further ground, polished and etched as was accomplished in the process of microstructure analysis. An optical microscope was used to obtain defect

information.

3.9.3 Fracture surface analysis

After fatigue fracture, a spray plastic coating was used to protect the fracture surface details. This type of coating can be removed by acetone cleaning. The crack profile caused by an overload was measured with a ruler with an accuracy of 0.01 inch, The examinations of the fracture surface feature and crack initiation site were made by visual and SEM observations. The fracture surface was then further sectioned in the longitudinal direction for detailed crack initiation analysis by optical microscope.

CHAPTER 4

RESULTS

4.1 Sectioning calibration

From a tensile bar test, it was found that the relationship between the resistance changes of gage x and gage y is $\frac{\Delta R_y}{R_y} \approx -0.29 \frac{\Delta R_x}{R_x}$. Considering that

$\frac{\Delta R_x}{R_x} = K_o \epsilon_x$, where K_o is the manufacturer gage factor which is equal to 2.08

for the strain gage rosette used for the sectioning measurement. From equation (3.2), with the Young's modulus E taken to be 30,000 Ksi, the constants A and B for sectioning residual stress measurement were determined to be:

$$A = \frac{2}{\sigma_x} (1-0.29)K_o \epsilon_x = \frac{2}{E} (1-0.29)K_o \approx 98.45 \times 10^{-6} \text{ (Ksi}^{-1}\text{)}$$

$$B = \frac{2}{\sigma_x} (1+0.29)K_o \epsilon_x = \frac{2}{E} (1+0.29)K_o \approx 178.88 \times 10^{-6} \text{ (Ksi}^{-1}\text{)}$$

To calculate the residual stresses from the measured resistance values, a computer program was developed based on equation (2.17). This program is capable of calculating residual stress components for any desired direction as well as the principle stresses. A listing of the program is in Appendix 1.

4.2 Hole-drilling calibration

4.2.1 Calibration constant

Figure 4.1 shows the measured stress-strain relationships in the elastic region of a tensile bar test. The lines $R_x(n)$ and $R_x(w)$ are the measured stress-strain relations from gage R_x before and after hole drilling. And, the lines $R_y(n)$ and $R_y(w)$ are the measured stress-strain relations from gage R_y before and after hole drilling. All these relations are in linear mode. Thus, the slope of each stress strain line $\frac{\sigma}{\epsilon}$ for strain gages R_x , R_y before and after drilling the hole can be determined. Table 4.1 gives the test results from several test runs with different specimens. The mean values of these measured stress strain slopes, which were subjected to an error of less than 5%, were used to determine the hole-drilling calibration constants.

The manufacturer gage factor for the strain gage rosette used for the hole drilling measurement is $K_o=2.06$. From equation (3.3*), the hole-drilling calibration constants in the linear elastic region were determined as:

$$4A=2K_o \left\{ \left(\frac{1}{43556} - \frac{1}{29106} \right) + \left(\frac{1}{106250} - \frac{1}{189584} \right) \right\} = -29.9 \times 10^{-6} \text{ (Ksi}^{-1}\text{)}$$

$$4B=2K_o \left\{ \left(\frac{1}{43556} - \frac{1}{29106} \right) - \left(\frac{1}{106250} - \frac{1}{189584} \right) \right\} = -64.0 \times 10^{-6} \text{ (Ksi}^{-1}\text{)}$$

4.2.2 Hole drilling machining stress

The measurement results in Table 4.2 show that the machining stress from the applied high speed hole drilling process is small enough to be negligible in

application. This is in agreement with the results obtained by other investigators [73].

In Table 4.2, the Von Mises equivalent stress, σ_{EQ} , is also presented. The definition of equivalent stress is:

$$\sigma_{EQ} = \frac{\sqrt{2}}{2} \sqrt{\sigma_x^2 + \sigma_y^2 + (\sigma_x - \sigma_y)^2 + 6\tau_{xy}^2} = \frac{\sqrt{2}}{2} \sqrt{\sigma_1^2 + \sigma_2^2 + (\sigma_1 - \sigma_2)^2} \quad (4.1)$$

The yield criteria for plane stress is usually expressed as:

$$\sigma_{EQ} = \sigma_{ys} \quad (4.2)$$

where σ_{ys} is the yield strength. As a measure of the stress level under plane stress conditions, the equivalent stress is an important parameter in the plane stress analysis. It will be presented along with all residual stress measurement results in the following sections.

4.2.3 High stress correction

Figure 4.2 shows the elastic-plastic stress strain relationships from the hole drilling tensile bar test. The definitions of curves $R_x(n)$, $R_x(w)$, $R_y(n)$ and $R_y(w)$ are the same as in section 4.2.1. It is clear that the stress strain relationships are no longer linear when the stress load level is greater than 50% of the yield strength. The higher the load, the larger the deviation from the linear relation. This means that the plastic deformation around the hole, due to stress concentration, will significantly affect the hole drilling measurement accuracy at high stress levels if the proper correction isn't taken into account. This also means that the coefficients A and B will no longer be constants at high stress levels but become variables that depend on the load.

By applying equation (3.3*) at each stress level, the values of A and B, as a function of the stress level, were determined. Since the equivalent stress in equation (4.1) is the same as the applied tensile stress for the tensile bar test, the so obtained calibration coefficients 4A and 4B, as functions of the tensile stress level, were plotted as functions of equivalent stress in Figure 4.3. Since at different stress levels, different calibration coefficients should be used in the calculation of residual stresses, a numerical iteration method was used to select the most appropriate calibration coefficients. A computer program, shown in Appendix 2, was developed to quickly process data from the measured resistance changes.

4.2.4 Accuracy of Hole-drilling method

The tensile bar test results listed in Table 4.3 show that even at a stress close to the yield strength of the material an accuracy of about 2 Ksi, or a relative error of about 5%, for the hole-drilling residual stress measurement technique is satisfied under uniaxially loaded conditions. Without the use of the calibration constants at the higher stress levels, the so obtained residual stress values for specimen 3 and 4 would be 48.3 Ksi and 53.3 Ksi. This corresponds to a measurement error about 20% attributable to plastic deformation.

Table 4.1 Hole-drilling Calibration

Before hole drilling			After hole drilling		
#	$\frac{\sigma_x}{\epsilon_x}$	$\frac{\sigma_x}{\epsilon_y}$	#	$\frac{\sigma_x}{\epsilon_x}$	$\frac{\sigma_x}{\epsilon_y}$
A1R1N	27950	-104250	A2R2W	42900	-181667
A1R2N	29270	-108650	A2R3W	43167	-191000
A2R1N	29667	-107500	A2R4W	42967	-187667
A2R3N	29867	-108250	A2R5W	42633	-193000
A2R4N	29120	-103750	B1R1W	45100	-192667
A2R5N	28759	-105105	B1R2W	44567	-191500
Mean value	29106	-106250		43556	-189584
Relative error	4%	2.5%		3.5%	4.1%

Table 4.2 Hole-drilling Machining Stress

Test #	σ_x (Ksi)	σ_y (Ksi)	τ_{xy} (Ksi)	σ_{EQ} (Ksi)
1	-0.9	-1.4	0.3	1.3
2	0.0	0.0	0.0	0.0
Mean Value	-0.45	-0.7	0.15	0.65

*Note: σ_{EQ} is the Von Mises equivalent stress

Table 4.3 Accuracy of Hole-drilling Technique

Specimen #	Nominal Stress (Ksi)	Measured Stress (Ksi)	Relative Error
1	19.8	20.4	3.0%
2	21.2	22.3	5.2%
3	40.0	37.6	-6.0%
4	41.1	41.2	0.2%

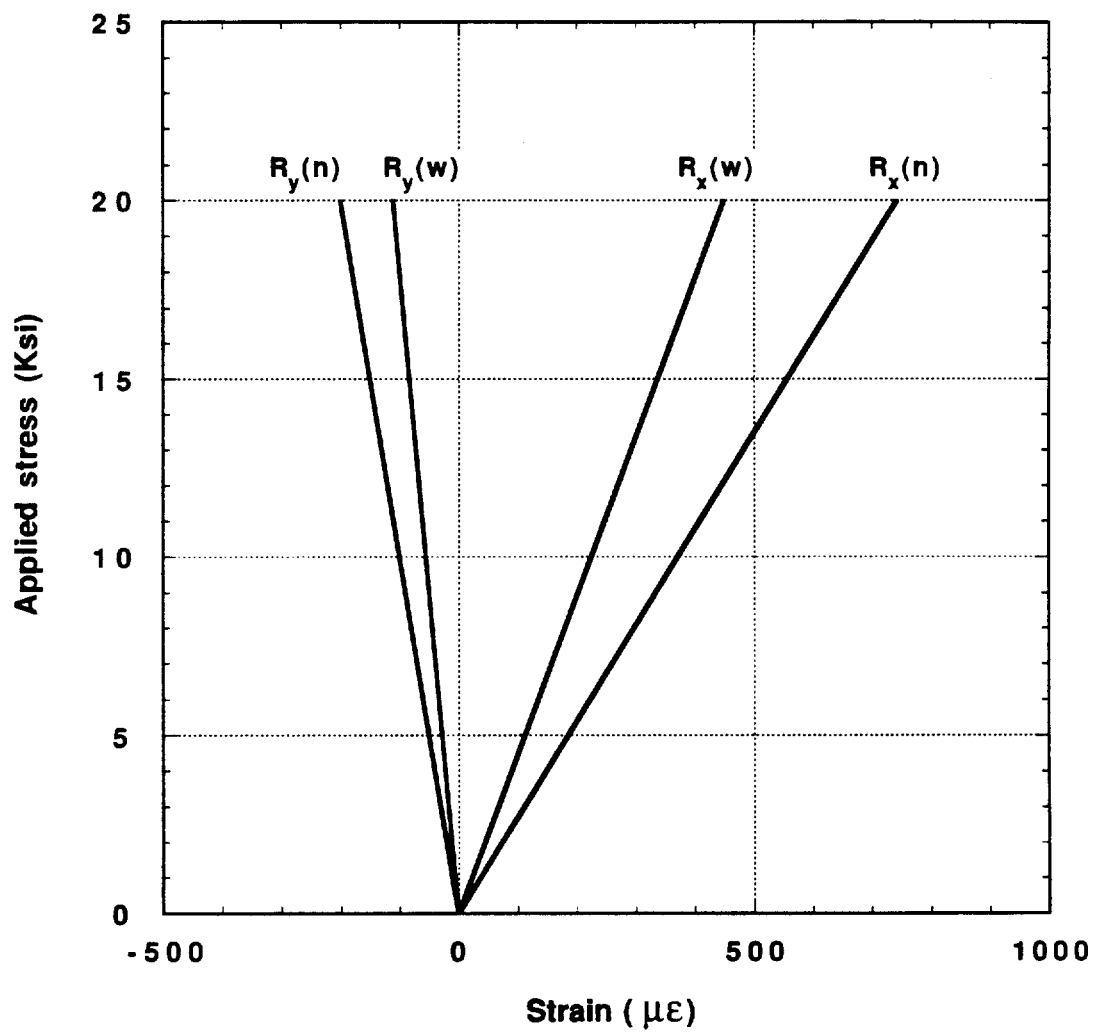


Figure 4.1 Stress-strain Curve for Hole-drilling Calibration

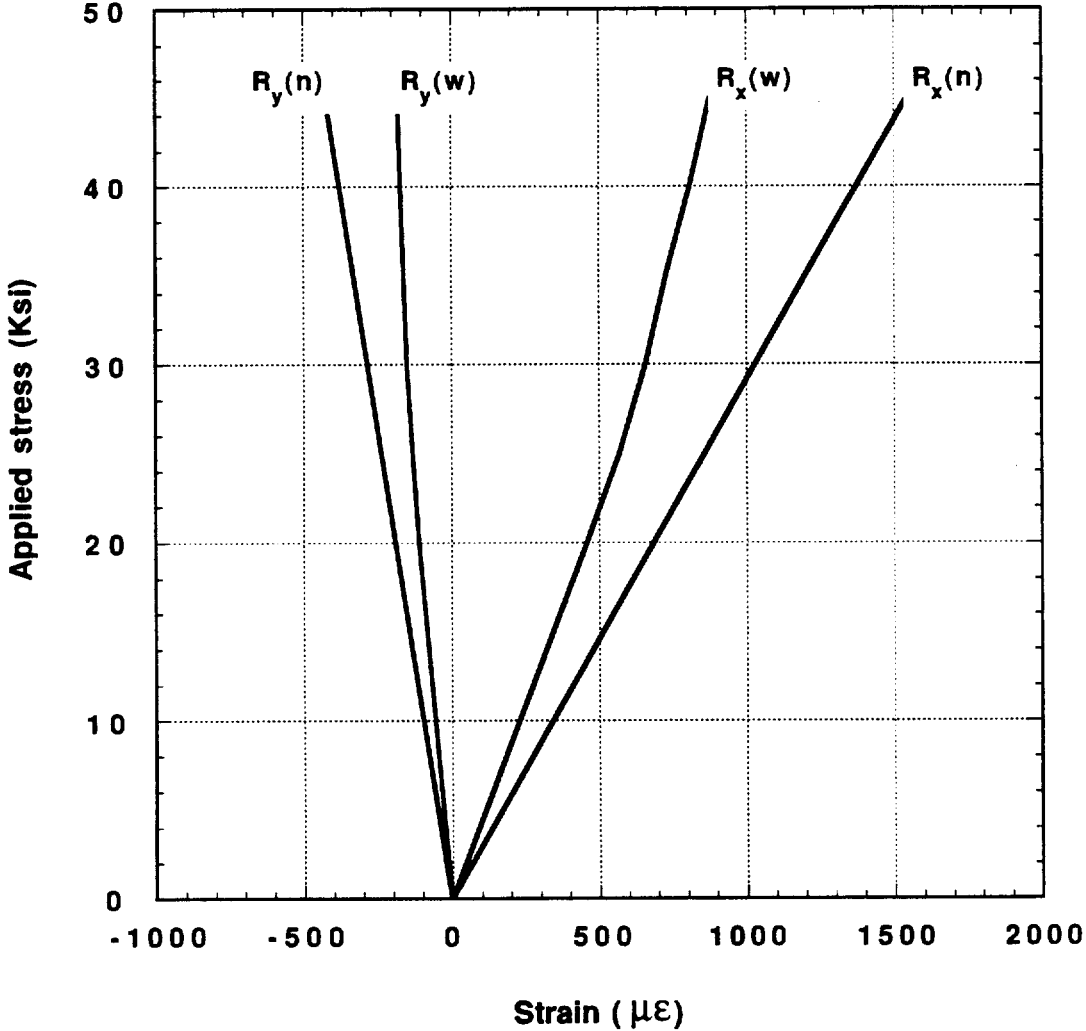


Figure 4.2 Stress-strain Curve for High Stress Hole-drilling Calibration

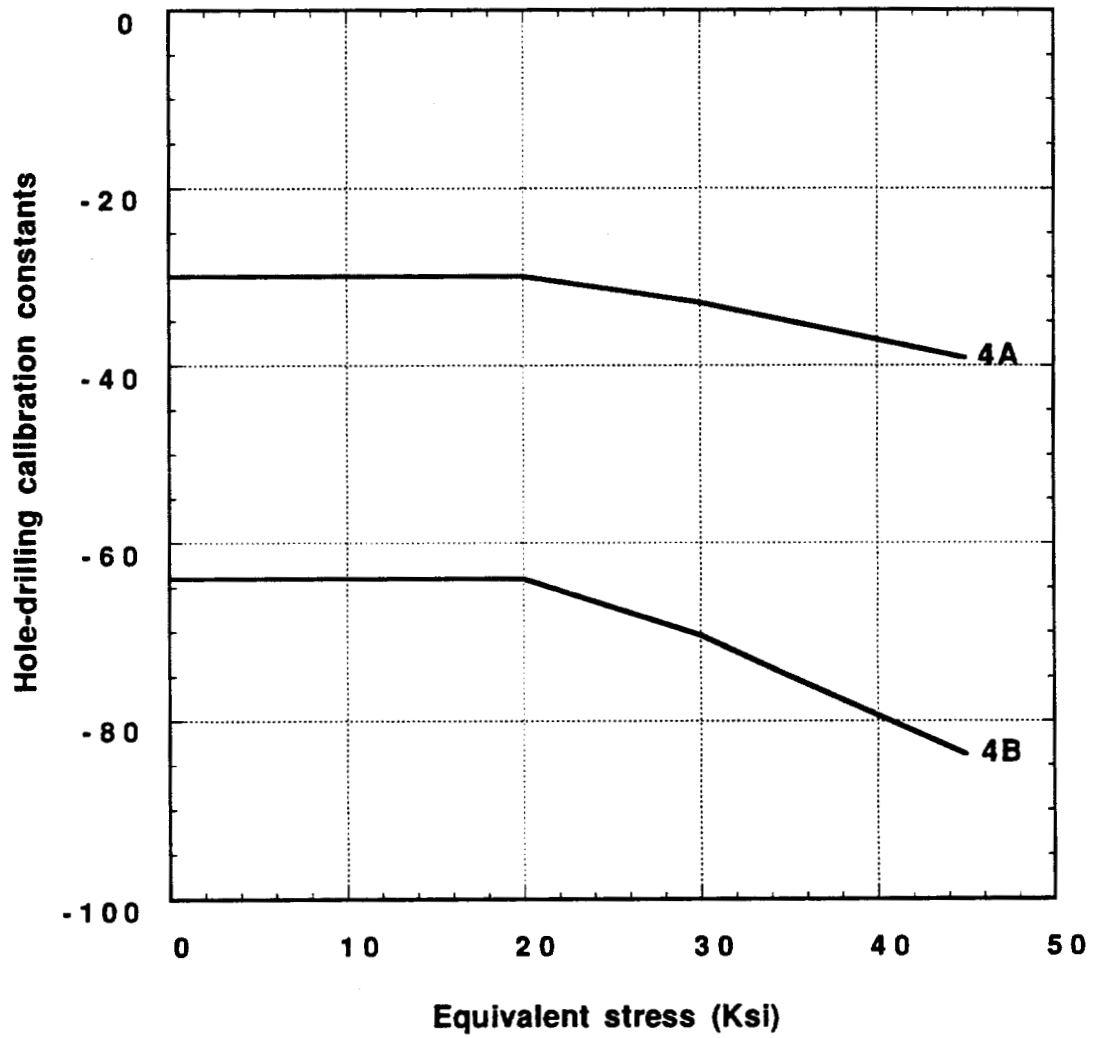


Figure 4.3 Calibration Constants as A Function of Stress Level

4.3 Residual stress measurement

4.3.1 *As-received plate*

Table 4.4 shows the residual stress measurement results from an as-received A515 plate. The y direction was chosen to be the rolling direction. It was found that there is a consistent compressive residual stress of about 4 Ksi in the rolling direction of the as-received A515 plate.

4.3.2 *As-welded pad-on-plate specimen*

Table 4.5 shows the residual stress measurement results from as-welded pad-on-plate specimens. Figure 4.4 shows the resultant residual stress state when all of the test data were combined around a single weld. In Figure 4.4, an outward arrow represents a tensile residual stress in that direction while an inward arrow represents a compressive residual stress in that direction, and the length of the arrow represents the magnitude of the stress. A cursory glance fails to turn up any clear stress distribution feature around the weld in Figure 4.4. However, the welding residual stresses can be qualitatively separated into four different zones around the weld. Zone A is at the front of the weld end toe, and the residual stress is biaxial tension-compression. Zone B is in the neighborhood of the weld center toe, and the residual stress is biaxial tension-tension. Zone C is in the remote part of the weld center, and the residual stress is biaxial compression-tension. Zone D is a remote area with residual stress in biaxial compression-compression.

Figure 4.5 gives a better quantitative view of the welding residual stress distribution patterns around the weld. The patterns represent the residual stresses measured along lines at y coordinates 0, 3 and 6mm. From these

patterns, it was found that residual stress patterns are symmetric with respect to the start and finish ends of the weld bead. In the near weld area, σ_x has its maximum tensile stress value at both the weld end ($x=0$) and the weld center ($x=C$). For a fixed y coordinate, the transverse residual stress σ_y changes from tensile stress to compressive stress at a location near the weld end when the x coordinate changes from $x>0$ to $x<0$.

In Table 4.5, the measurement results from the sectioning method show some quantitative differences with the measurement results from the hole-drilling method. However, when both results were plotted together, as Figure 4.5 shows, they followed the same stress pattern. It is therefore believed that the results from both residual stress measurement methods are consistent and that both methods are reliable.

4.3.3 As-welded simple specimen

Figure 4.6 shows the effect of specimen width on the welding residual stress at the weld end toe. It was found that in order to maintain the same residual stress pattern as the big pad-on-plate weld specimen, the width of the simple weld specimen had to be greater than 4 inches.

Table 4.6 shows the measurement results from simple specimens with widths 5 inches and above. Figure 4.7 shows the comparison between measurement results from pad-on-plate weld specimens and simple weld specimens. There are similar stress states at the weld end toes for both pad-on-plate and simple weld specimens. This proves that the designed simple specimen is suitable for the fatigue tests to determine the effect of welding residual stress on fatigue life.

4.3.4 Stress-relieved simple specimen

Table 4.7 shows the thermal stress relief results. About 85% of the residual stress was relieved under heat treatment conditions of 600°C for two hours, and the complete relief of residual stress was achieved under heat treatment conditions of 650°C for one hour. So, an effective stress relief for this type of weld specimen is to heat treat at 650°C for 1 hour. The measured slight compressive residual stresses after heat treatment at 650°C may not have any significant physical meaning. Although these residual stresses are principally in the rolling direction and quantitatively compatible to those in the as-received A515 plate (see Table 4.4), they must be due to some other reasons since they were not detected from stress-relieved, unwelded specimens.

4.3.5 Effect of cyclic load

Table 4.8 shows all the test results for the effect of cyclic load on residual stress. The results are also plotted in three dimensions, Figure 4.8, and two dimensions, Figure 4.9, to show how the general cyclic load affects residual stress. It is seen that when the applied tensile stress is greater than 14 Ksi, the longitudinal residual stress near the weld end toe will be significantly reduced due to the weld toe stress concentration effect. The results also show that the major residual stress relaxation effect takes place during the first few hundred cycles. Figure 4.10 shows the test results for the effect of cyclic load conditions on transverse residual stress levels. It is seen that the transverse residual stress is insensitive to the longitudinal tensile cyclic load.

Table 4.4 Residual Stress in As-received A515 Plate

Test #	σ_x (Ksi)	σ_y (Ksi)	τ_{xy} (Ksi)	σ_{EQ} (Ksi)
1	-0.9	-3.5	0.5	3.3
2	-2.6	-5.2	-0.3	4.5
3	-0.4	-4.0	-1.3	4.5
Mean Value	-1.3	-4.2	-0.4	4.1

* Note: y is parallel to the rolling direction of the plate.

Table 4.5 Residual Stress in As-welded Pad-on-plate Specimens

#	x(mm)	y(mm)	σ_x (Ksi)	σ_y (Ksi)	τ_{xy} (Ksi)
S1-f	-5.3	-2.5	N/A	N/A	N/A
S2-f	-13.8	-2.5	N/A	N/A	N/A
S3-f	-5.3	-2.5	6.7	-20.6	4.4
S4-f	-13.8	6.0	-8.5	-26.5	-3.8
S5-f	-5.3	6.0	-5.4	-15.8	-15.2
S6-f	3.3	6.0	5.4	0.4	-15.3
S7-f	11.8	6.0	-5.2	-5.0	-18.4
S8-f	-13.8	16.0	-23.4	-42.4	-15.2
S9-f	-5.3	16.0	-16.2	-24.8	-15.6
S10-f	3.3	16.0	-11.6	-8.4	-20.3
S11-f	11.8	16.0	-11.8	3.2	-14.2
S12-f	-13.8	62.0	-14.1	-7.9	-19.5
H1	-20.0	0.0	3.3	-37.2	-8.9
H2-f	-12.0	0.0	5.6	-33.5	-4.1
H3-s	-10.0	0.0	1.4	-32.5	7.0
H4-s	-5.0	0.0	5.6	-31.5	5.0
H5-f	-5.0	0.0	14.9	-17.7	13.2
H6-f	0.0	0.0	16.4	-9.8	11.5
H7-s	0.0	0.0	19.5	-18.0	-3.3
H8-s	-21.0	3.0	-6.1	-47.8	-3.7
H9-s	-6.0	3.0	2.4	-28.1	13.3
H10-f	-3.0	3.0	3.5	-25.7	2.8
H11-s	-3.0	3.0	6.9	-16.2	14.5
H12-f	-0.5	3.0	20.3	-15.8	12.7
H13-s	0.5	3.0	17.7	11.6	17.4
H14-s	1.0	2.0	3.0	-7.4	17.8
H15-f	1.5	3.0	10.6	0.5	12.5
H16-s	2.5	2.0	11.2	-16.5	5.5
H17-f	7.0	2.5	8.0	-14.9	-9.9
H18-c	C	2.0	27.0	22.5	-8.7
H19-c	C	3.0	11.8	20.2	-14.5
H20-c	C	3.0	12.9	23.1	5.8
H21-f	-11.8	6.0	-1.9	-34.0	-12.2
H22-s	-7.0	6.0	10.2	-27.9	-4.8
H23-f	-5.3	6.0	1.5	-11.4	14.5
H24-s	-3.0	5.0	3.9	-11.6	14.9
H25-s	0.0	6.0	16.3	5.9	17.5
H26-f	2.5	6.0	10.4	2.6	-22.7
H27-s	5.0	6.0	-7.1	-1.1	-19.2
H28-f	12.0	6.0	4.2	3.6	-8.3
H29-f	13.5	6.0	8.3	22.9	-11.2
H30-c	C	6.0	7.3	21.9	-9.0
H31-f	10.0	9.0	-4.3	-0.6	18.4
H32-c	C	9.0	-6.2	16.8	-3.8
H33-c	C	9.0	3.1	19.2	-6.3
H34-c	C	11.0	-17.5	17.6	-6.7
H35-c	C	11.0	-24.0	10.3	-0.1
H36-c	C	12.0	-15.8	18.4	-2.3
H37-f	-11.8	16.0	0.1	-21.9	11.5
H38-f	15.0	16.0	-11.7	9.1	13.5
H39-f	-9.0	65.0	-16.2	-8.4	-7.8
H40	C	66.0	-20.4	-3.5	0.9
H41-f	-8.0	67.0	-18.2	3.7	2.3
H42	C	67.0	-20.7	-11.1	-0.4

*Note: S: sectioning measurement result, H: hole drilling measurement result, -s: at start weld end, -f: at finish weld end, -c: at weld center, C: x coordinate at weld center, N/A: not available.

Table 4.6 Residual Stress in As-welded Simple Specimen

#	x(mm)	y(mm)	σ_x (Ksi)	σ_y (Ksi)	τ_{xy} (Ksi)
hb1-f	-3.0	-7.0	23.3	-26.3	4.7
hb2-f	-3.0	-4.0	16.5	-26.2	1.0
hb3-s	0.0	0.0	22.1	-18.6	12.5
hb4-s	0.0	0.5	21.1	-13.6	12.6
hb5-s	0.0	0.5	18.6	-10.8	10.6
hb6-f	0.0	0.5	16.6	-18.5	10.5
hb7-s	5.0	3.0	26.5	-5.1	13.9
hb8-c	C	3.0	37.8	6.9	3.2
hb9-c	C	3.0	44.2	2.3	0.2
hg10-f	0.0	0.0	19.9	1.7	18.4
hg11-c	C	3.0	25.0	6.3	0.8
hg12-f	0.0	0.0	11.8	-13.6	17.2
hg13-s	0.0	0.0	8.2	-14.2	13.8

*Note: hb: hole drilling measurement in bead-on-plate simple weld specimen, hg: hole drilling measurement in gusset fillet simple weld specimen, -s: at start weld end, -f: at finish weld end, -c: at weld center, C: x coordinate at weld center.

Table 4.7 Residual Stress in Stress-relieved Specimen

a). stress relieved at 600°C for 2 hours

Location	x(mm)	y(mm)	σ_x (Ksi)	σ_y (Ksi)	τ_{xy} (Ksi)	σ_{EQ} (Ksi)
Weld end	0.0	0.0	6.6	3.5	-1.0	6.0
Weld center	C	3.0	2.5	-3.0	3.3	7.4

b). Stress relieved at 650°C for 1 hour

Location	x(mm)	y(mm)	σ_x (Ksi)	σ_y (Ksi)	τ_{xy} (Ksi)	σ_{EQ} (Ksi)
Weld end	0.0	0.0	-2.0	-3.6	0.3	3.1
Weld end	0.0	0.0	-3.1	-0.8	-0.1	2.8
Weld center	C	3.0	-3.3	-1.2	0.5	3.0

Table 4.8 Effect of Cyclic Load on Residual Stress

<i>condition</i>	#	x(mm)	y(mm)	σ_x (Ksi)	σ_y (Ksi)	τ_{xy} (Ksi)	σ_{EQ} (Ksi)
0-6 Ksi 115,000 cycles	1s*	0.0	0.0	20.6	-7.7	15.4	36.8
	2f	0.0	0.0	15.8	-13.8	12.1	33.1
	3c	C	3.0	23.5	8.9	-9.1	25.9
0-14 Ksi 2,000 cycles	4s	0.0	0.0	10.9	-4.5	16.7	32.1
	5f	0.0	0.0	12.6	0.1	16.0	30.4
	6c	C	3.0	14.1	7.6	1.2	12.4
0-14 Ksi 115,000 cycles	7s	0.0	0.0	21.2	-5.5	10.5	30.5
	8f	0.0	0.0	15.2	-9.3	13.4	31.6
	9c	C	3.0	23.5	11.0	-2.9	21.0
0-22 Ksi 150 cycles	10s	0.0	0.0	1.9	-8.9	12.4	23.7
	11f	0.0	0.0	2.8	-20.5	5.1	23.7
	12c	C	3.0	22.1	13.0	2.5	19.7
0-22 Ksi 2,000 cycles	13s	0.0	0.0	2.2	-14.5	7.8	20.7
	14f	0.0	0.0	6.2	-13.6	10.9	25.8
	15c	C	3.0	13.9	11.8	-3.4	14.2
	16s	0.0	0.0	3.3	-2.2	13.6	24.1
	17f	0.0	0.0	1.3	-6.6	13.6	24.7
	18c	C	3.0	22.3	11.7	-1.2	19.5
0-22 Ksi 115,000 cycles	19s	0.0	0.0	7.8	-14.6	9.9	26.1
	20f	0.0	0.0	8.2	-23.1	4.2	29.0
	21c	C	3.0	17.5	7.1	0.8	15.3
	22s	0.0	0.0	3.8	-14.3	11.5	26.0
	23f	0.0	0.0	5.8	-16.8	10.8	27.7
	24c	C	3.0	19.3	9.1	2.5	17.3
0-30 Ksi 150 cycles	25s	0.0	0.0	-0.3	-7.5	10.7	19.9
	26f	0.0	0.0	3.7	-9.2	10.6	21.6
	27c	C	3.0	13.4	10.6	-0.4	12.3
0-30 Ksi 115,000 cycles	28s	0.0	0.0	-4.2	-9.7	9.2	18.1
	29s	0.0	0.0	2.6	-3.7	8.9	16.3
	30f	0.0	0.0	-4.3	-11.7	10.4	20.8
	31c	C	3.0	12.7	24.5	-3.1	21.8

*Note: s: at start weld end, f: at finish weld end, c: at weld center.

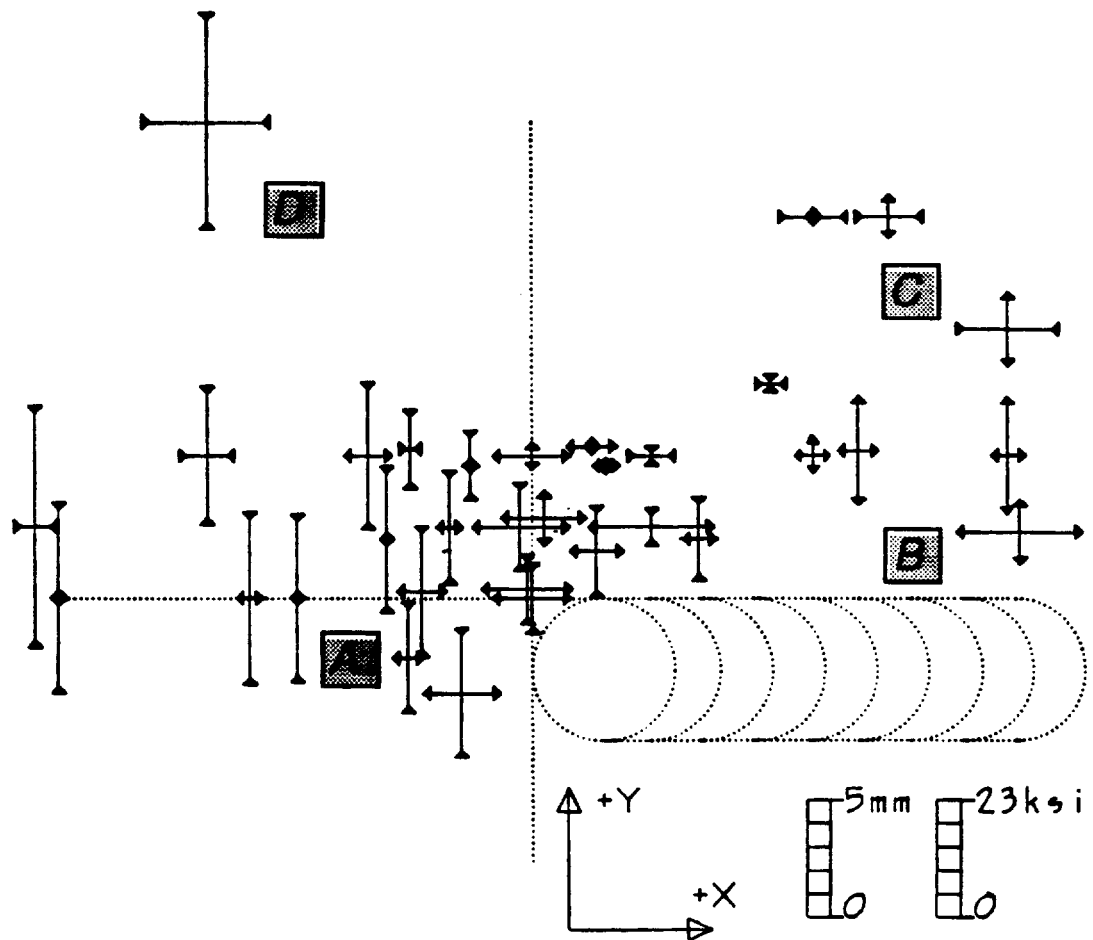


Figure 4.4 Residual Stress in Pad-on-plate Weld Specimen

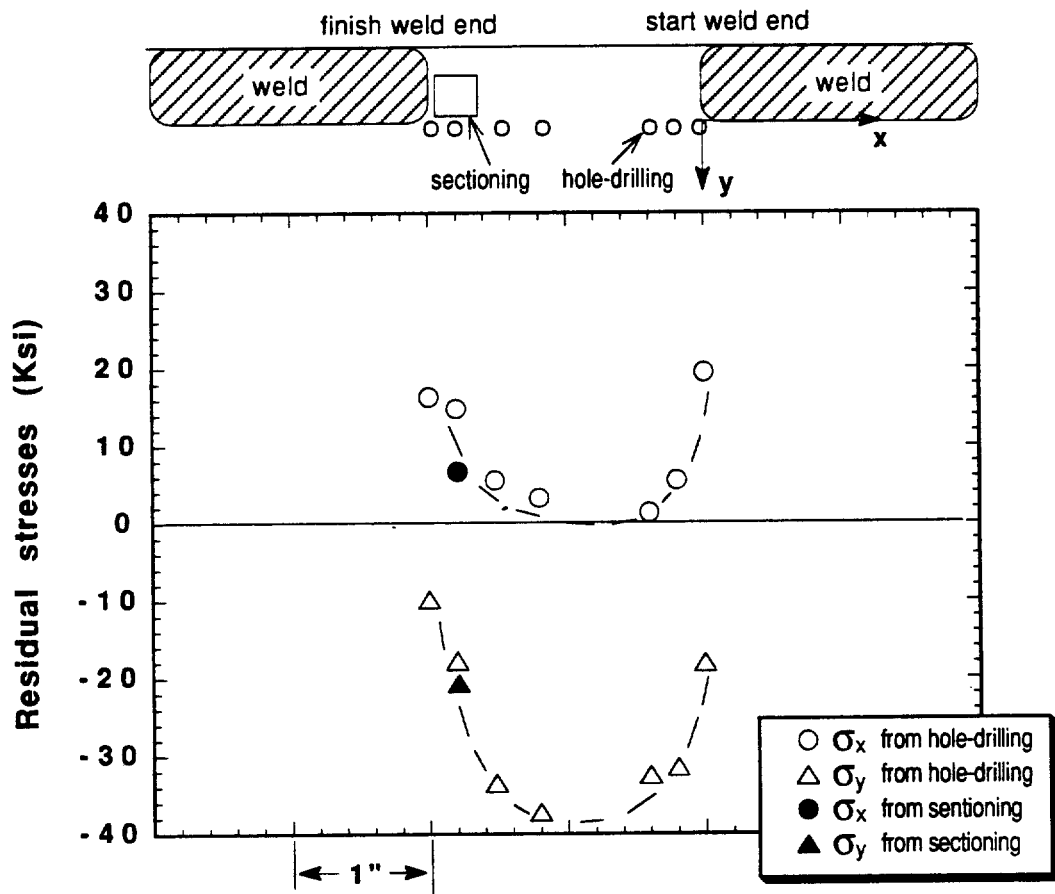


Figure 4.5 Residual Stress Pattern in Pad-on-plate Weld Specimens
(Measurements along line $y=0\text{mm}$)

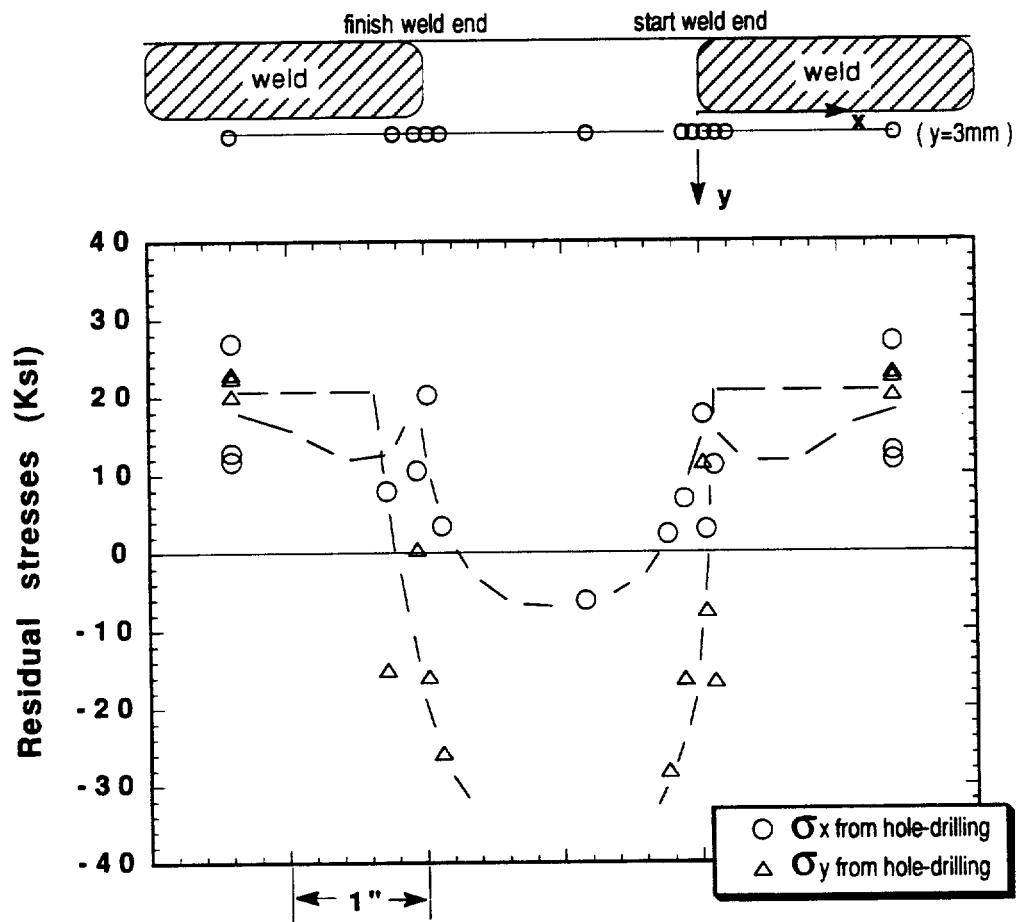


Figure 4.5 Continued (Measurements along line y=3mm)

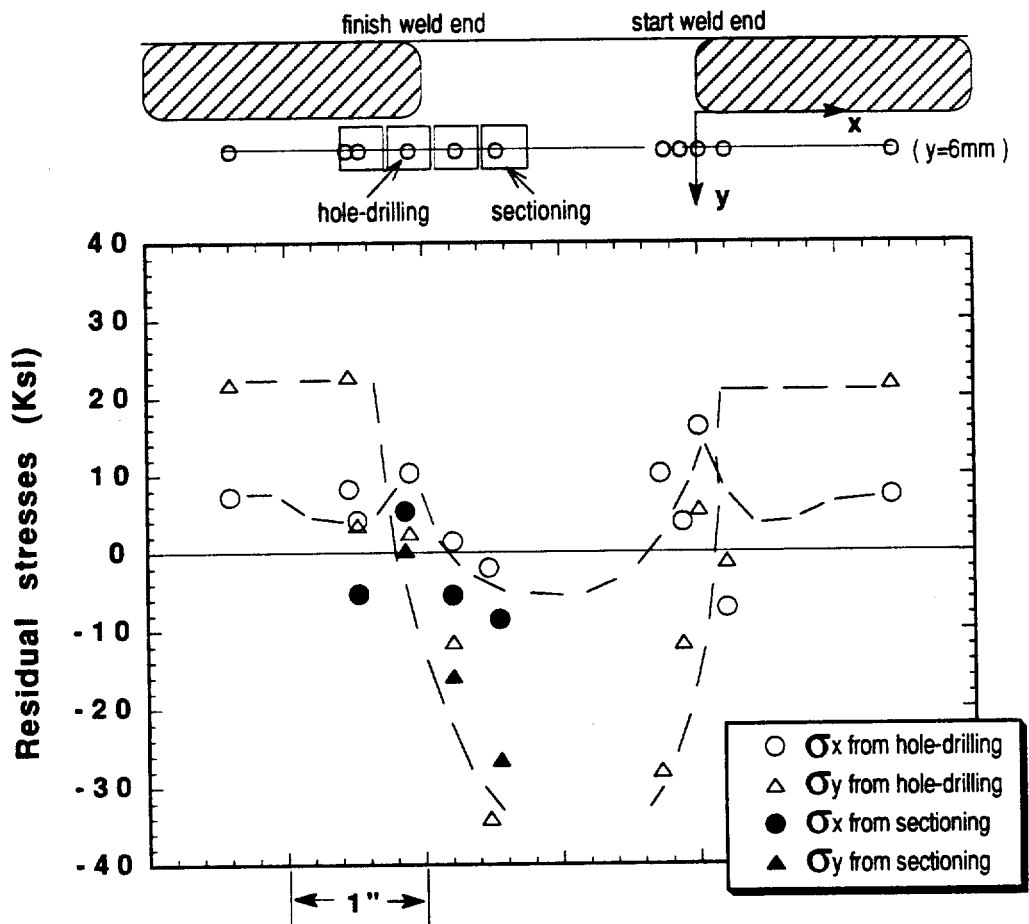


Figure 4.5 Continued (Measurements along line y=6mm)

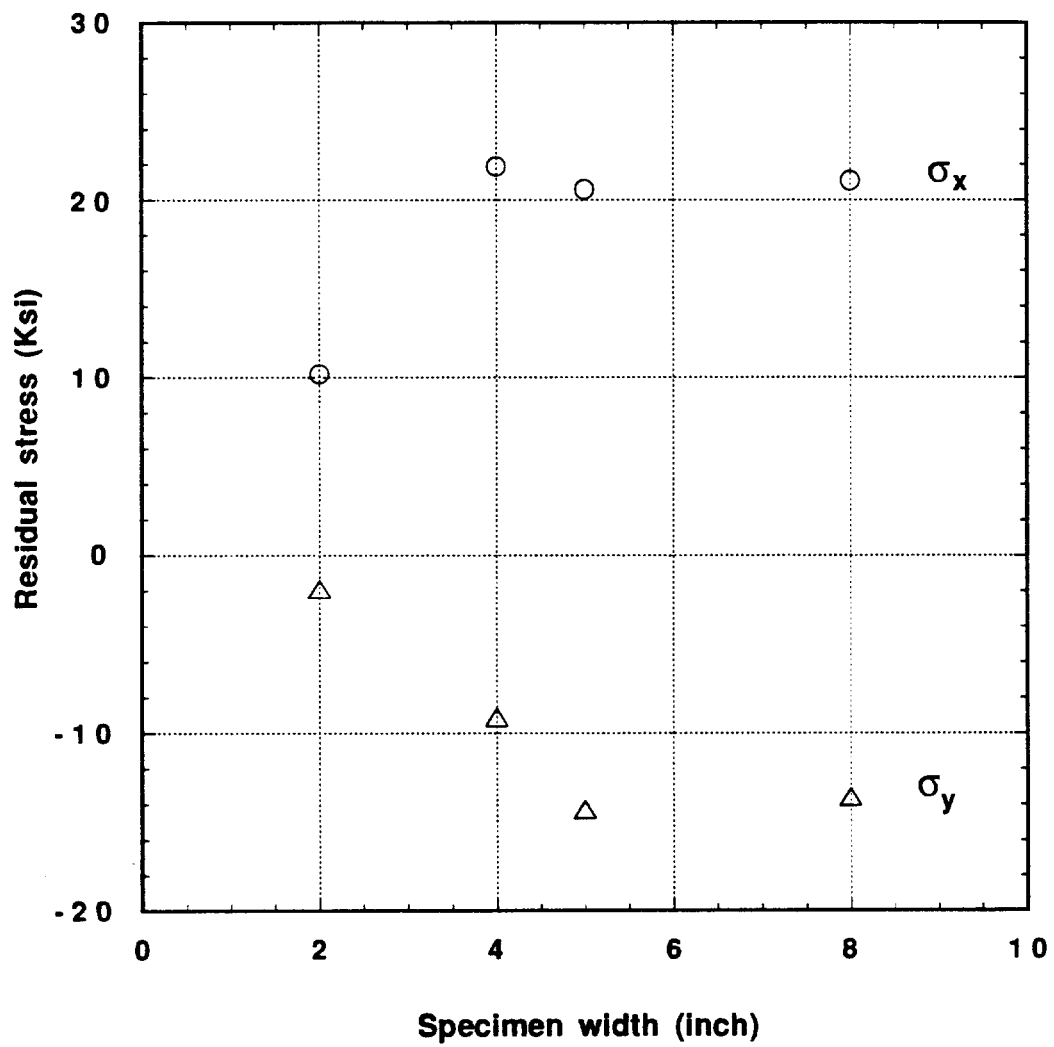


Figure 4.6 Effect of Specimen Width on Residual Stress

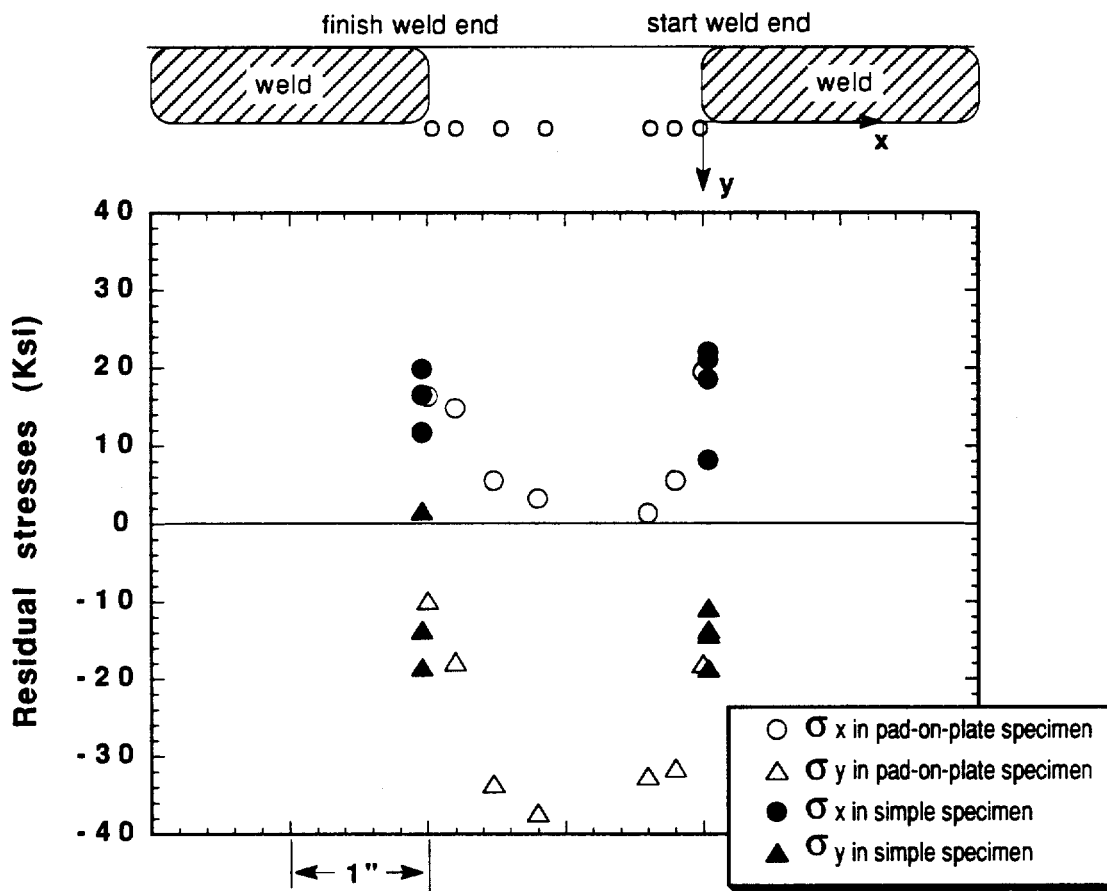


Figure 4.7 Residual Stress in Simple Weld Specimens

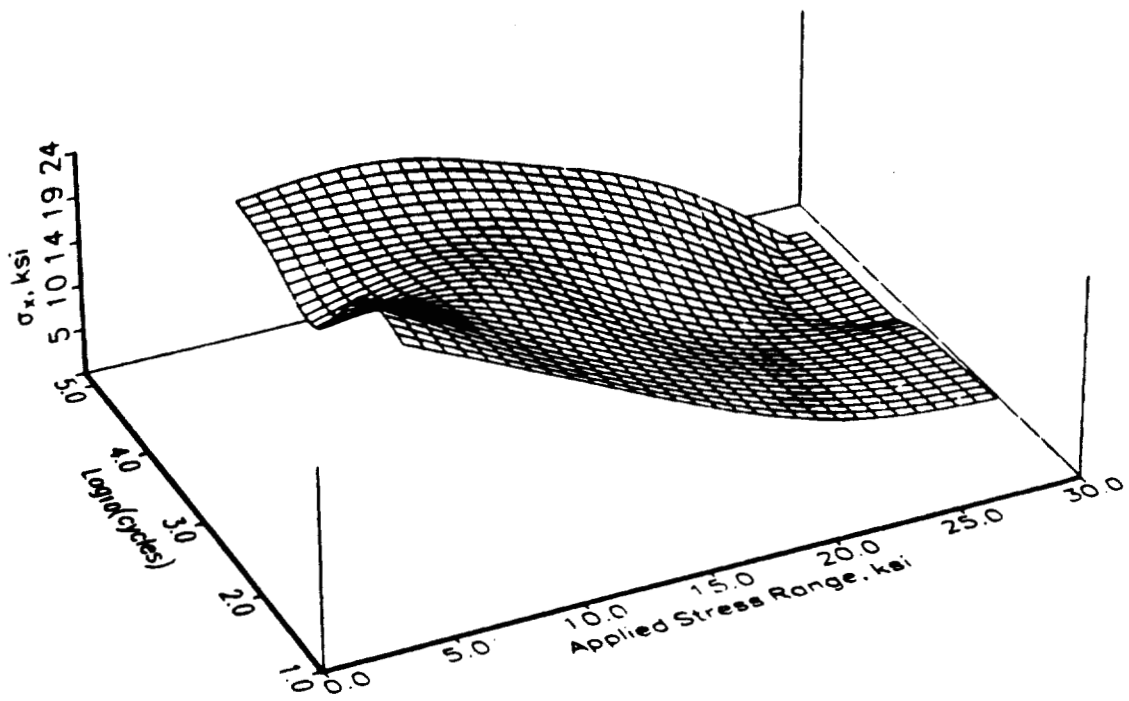


Figure 4.8 Cyclic Load Effect on Longitudinal Residual Stress (3D plotting)

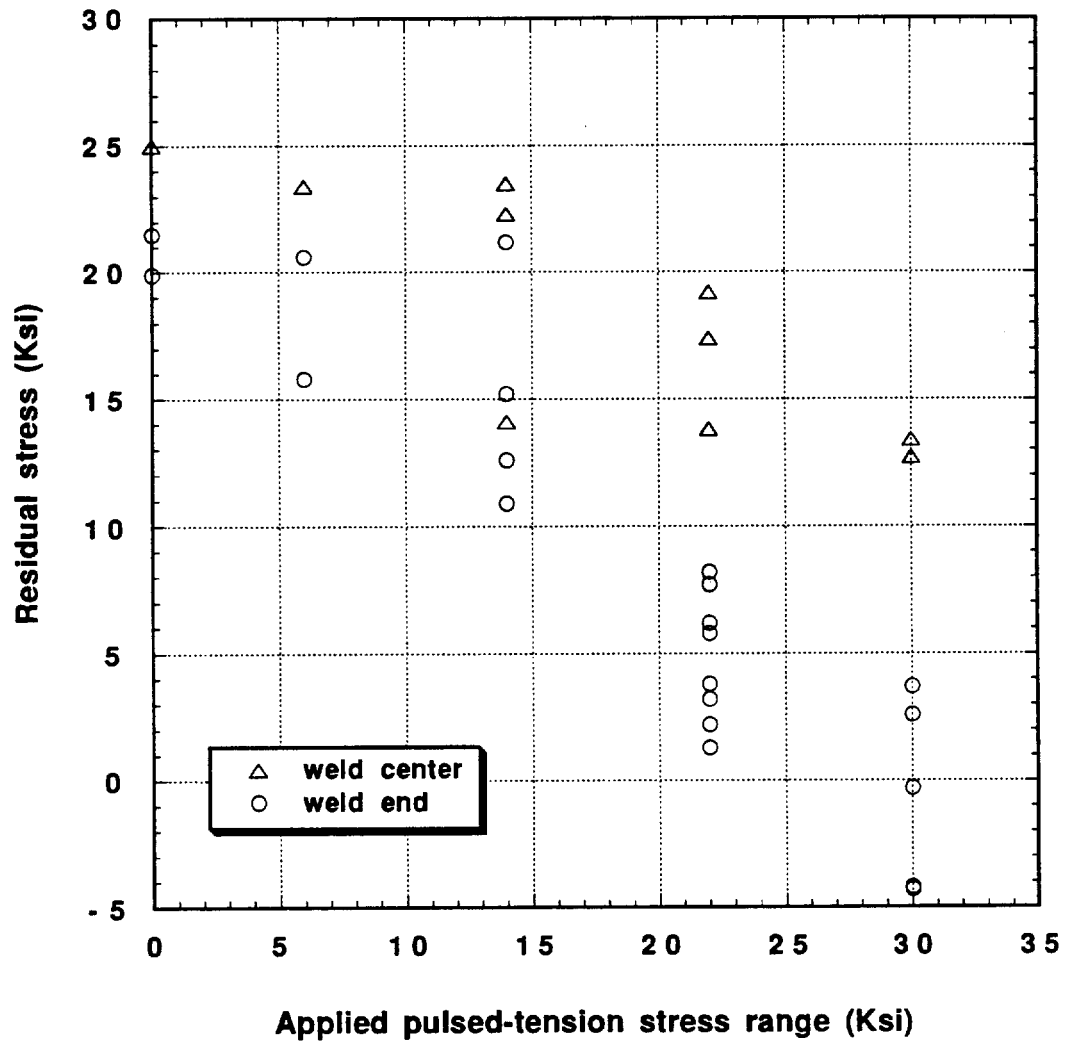


Figure 4.9 Cyclic Load Effect on Longitudinal Residual Stress (2D plotting)

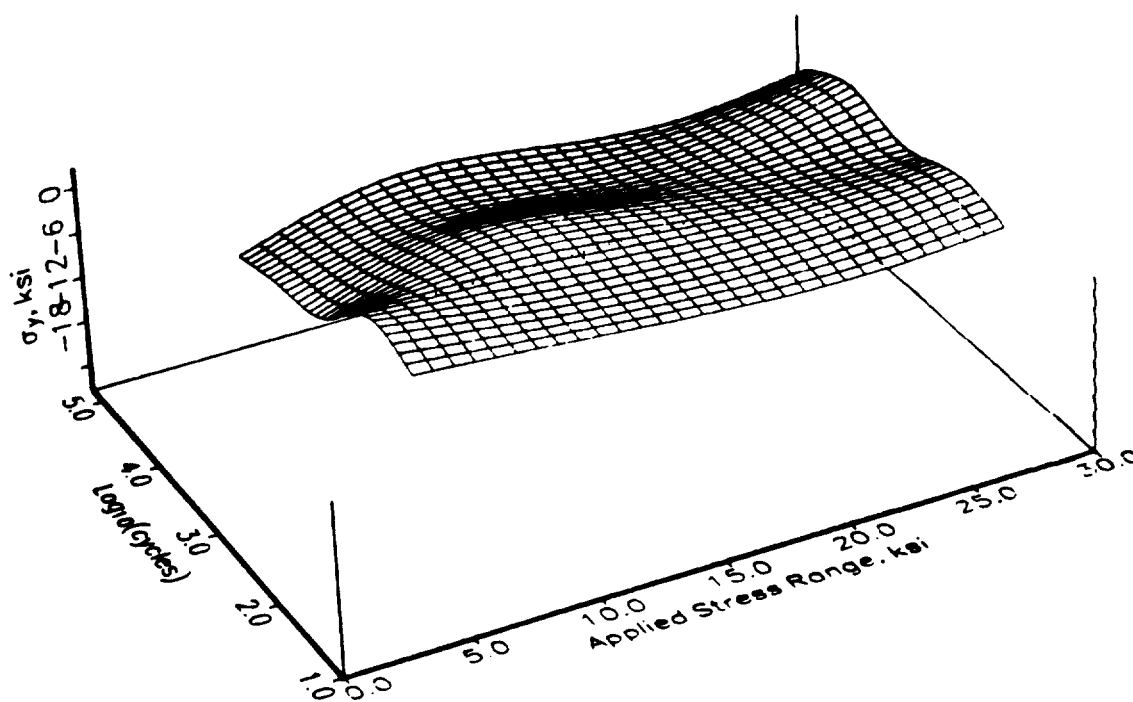


Figure 4.10 Cyclic Load Effect on Transverse Residual Stress

4.4 Fatigue test

4.4.1 *S-N relationship*

Table 4.9 shows the fatigue test results. All the fatigue cracks originated from weld end toes. Most cracks originated at the start weld end toes but some of the cracks were found at the finish weld end toes.

Under pulsed-tension cyclic load conditions, no consistent test results were found to show residual stress as having a significant effect on the fatigue strength. However, under tension-compression cyclic load conditions, stress relieved specimens revealed a significant increase in the fatigue strength (or fatigue life).

The clamping induced bending stress didn't reveal a consistent effect on the overall fatigue life. It is believed that its effect is the same as welding residual stress and it will be relieved after a particular crack length has developed.

4.4.2 *Crack propagation property*

Figure 4.11 shows the measured fatigue crack propagation diagram. All the as-measured crack propagation data are listed in Table 4.10. Theoretically, the crack growth rate should increase when the crack length increases. By examining each individual crack growth step in Figure 4.11, it was found that this is not always true. The error from the applied measurement techniques and the specimen surface conditions are believed to be responsible for this phenomenon. To eliminate the effect of these random measurement errors, the average crack propagation rate in 3 to 5 growth steps were used to determine the crack propagation property.

Figure 4.12 shows the relationship of surface crack length as a function of load cycles under loads: 0 to 13 Ksi, 0 to 10 Ksi and 0 to 7 Ksi. Figure 4.13 shows the relationship of crack growth rate as a function of crack length from test results under load 0 to 13 Ksi. It was found that the applied overload has a significant effect on crack growth rate. A crack growth rate reduction of about 90% was identified due to the applied overload. However, the effect of applying one or two overloads was found to cause only about a 10% increase in the total fatigue life. So the effect of applying one or two cycles of overloads is insignificant relative to the scatter in the fatigue test data.

Table 4.9. Fatigue Test of Fillet-welded A515 Steel Specimen

test #	specimen	load	bending stress	fatigue life
5	as-welded	0 - 13 Ksi	1.5 Ksi	2.48×10^6
6	as-welded	0 - 13 Ksi	0.0 Ksi	2.51×10^6
8	stress-relieved	0 - 13 Ksi	1.4 Ksi	2.41×10^6
9	stress-relieved	0 - 13 Ksi	7.0 Ksi	2.55×10^6
1	as-welded	0 - 10 Ksi	...	6.30×10^6
2	as-welded	0 - 10 Ksi	...	5.08×10^6
13*	as-welded	0 - 10 Ksi	3.0 Ksi	5.06×10^6
3	stress-relieved	0 - 10 Ksi	...	10.00×10^6 †
4	stress-relieved	0 - 10 Ksi	...	6.35×10^6
11	stress-relieved	0 - 10 Ksi	9.0 Ksi	4.28×10^6
12*	stress-relieved	0 - 10 Ksi	6.6 Ksi	7.68×10^6
7	as-welded	0 - 7 Ksi	3.0 Ksi	8.94×10^6
10	as-welded	0 - 7 Ksi	6.0 Ksi	11.00×10^6 †
15	as-welded	-10 - 10 Ksi	...	1.02×10^6
16*	as-welded	-10 - 10 Ksi	...	0.58×10^6
14	stress-relieved	-10 - 10 Ksi	...	5.44×10^6
18	stress-relieved	-10 - 10 Ksi	...	2.05×10^6
17*	as-welded	-7 - 7 Ksi	...	2.21×10^6

NOTE: ' * ': Crack initiated at finish weld end, ' † ': No crack is detected.

Table 4.10 Fatigue Crack Propagation Measurement

Specimen #2 (As-welded under 0-10ksi)			
# of cycle ($\times 10^6$)	crack length a (inch)	$\frac{da}{dN}$ ($\times 10^{-6}$) (inch/cycle)	average crack length a (inch)
3.5000*	0.453	0.3333	0.578
4.2500	0.703	0.4400	0.758
4.5000*	0.813	0.5000	0.876
4.7500	0.938	1.5000	1.126
5.0000	1.313	8.5875	1.657
5.0800	2.000		

Note: 'a' is half crack length, '**': overload applied.

Specimen #4 (Stress-relieved under 0-10ksi)			
# of cycle ($\times 10^6$)	crack length a (inch)	$\frac{da}{dN}$ ($\times 10^{-6}$) (inch/cycle)	average crack length a (inch)
5.0000*	0.656	0.3560	0.701
5.2500	0.745	0.3960	0.795
5.5000	0.844	0.5000	0.907
5.7500	0.969	0.7480	1.063
6.0000*	1.156	0.7520	1.250
6.2500	1.344	6.5600	1.672
6.3500	2.000		

Note: 'a' is half crack length, '**': overload applied.

Table 4.10 (continued)

Specimen #5 (As-welded under 0-13ksi)			
# of cycle ($\times 10^6$)	crack length a (inch)	$\frac{da}{dN}$ ($\times 10^{-6}$) (inch/cycle)	average crack length a (inch)
2.0000*	0.555	0.5600	0.583
2.0980	0.610	0.6897	0.615
2.1125	0.620	0.7634	0.625
2.1256	0.630	1.0638	0.635
2.1350	0.640	0.9259	0.645
2.1458	0.650	1.1111	0.655
2.1548	0.660	0.9615	0.665
2.1652	0.670	1.2048	0.675
2.1735	0.680	1.0638	0.685
2.1829	0.690	1.2658	0.695
2.1908	0.700	1.1111	0.705
2.1998	0.710	1.1111	0.715
2.2088	0.720	1.2346	0.725
2.2169	0.730	1.1364	0.735
2.2257	0.740	1.5385	0.745
2.2322	0.750	6.2500	0.753
2.2330*	0.755	0.7353	0.758
2.2398	0.760	0.8197	0.765
2.2520	0.770	0.9259	0.775
2.2628	0.780	1.3889	0.785
2.2700	0.790	1.2658	0.795
2.2779	0.800	1.8724	0.868
2.3500	0.935	8.4524	1.468
2.4760	2.000		

Note: 'a' is half crack length, '**': overload applied.

Table 4.10 (continued)

Specimen #6 (As-welded under 0-13ksi)			
# of cycle ($\times 10^6$)	crack length a (inch)	$\frac{da}{dN}$ ($\times 10^{-6}$) (inch/cycle)	average crack length a (inch)
1.3360	0.290	0.3546	0.295
1.3642	0.300	0.3021	0.305
1.3973	0.310	0.3367	0.315
1.4270	0.320	0.3344	0.325
1.4569	0.330	0.3610	0.335
1.4846	0.340	0.3704	0.345
1.5116	0.350	0.3968	0.355
1.5368	0.360	0.3817	0.365
1.5630	0.370	0.6579	0.375
1.5782	0.380	0.4587	0.385
1.6000*	0.390	0.0562	0.392
1.7780	0.400	0.1792	0.405
1.8338	0.410	0.2119	0.415
1.8810	0.420	0.6173	0.425
1.8972	0.430	0.3861	0.435
1.9231	0.440	0.7299	0.445
1.9368	0.450	0.3968	0.455
1.9620	0.460	0.8621	0.575
2.2288	0.690	1.1905	0.695
2.2372	0.700	1.1111	0.705
2.2462	0.710	1.0870	0.715
2.2554	0.720	1.1364	0.725
2.2642	0.730	1.5152	0.735
2.2708	0.740	1.0870	0.745
2.2800	0.750	1.3158	0.755
2.2876	0.760	1.6667	0.765
2.2936	0.770	1.5152	0.775
2.3002	0.780	1.2821	0.785
2.3080	0.790	2.2727	0.795
2.3124	0.800	1.4706	0.805
2.3192	0.810	1.6129	0.815
2.3254	0.820	1.6667	0.825
2.3314	0.830	6.7396	1.415
2.5050	2.000		

Note: 'a' is half crack length, '**': overload applied.

Table 4.10 (continued)

Specimen #7 (As-welded under 0-7ksi)			
# of cycle ($\times 10^6$)	crack length a (inch)	$\frac{da}{dN}$ ($\times 10^{-6}$) (inch/cycle)	average crack length a (inch)
4.8200	0.350	0.0896	0.355
4.9316	0.360	0.0751	0.365
5.0648	0.370	0.0926	0.375
5.1728	0.380	0.0731	0.385
5.3096	0.390	0.1085	0.395
5.4018	0.400	0.1094	0.405
5.4932	0.410	0.0902	0.415
5.6041	0.420	0.1060	0.425
5.6984	0.430	0.1167	0.435
5.7841	0.440	0.1198	0.445
5.8676	0.450	0.1263	0.455
5.9468	0.460	0.1157	0.465
6.0332	0.470	0.1634	0.475
6.0944	0.480	0.1285	0.485
6.1722	0.490	0.1433	0.495
6.2420	0.500	0.1263	0.505
6.3212	0.510	0.1634	0.515
6.3824	0.520	0.1779	0.525
6.4386	0.530	0.1462	0.535
6.5070	0.540	0.2059	0.635
7.4300	0.730	0.3086	0.735
7.4624	0.740	0.2439	0.745
7.5034	0.750	0.2890	0.755
7.5380	0.760	0.3472	0.765
7.5668	0.770	0.2315	0.775
7.6100	0.780	0.2778	0.785
7.6460	0.790	0.2778	0.795
7.6820	0.800	0.2674	0.805
7.7194	0.810	0.3472	0.815
7.7482	0.820	0.3012	0.825
7.7814	0.830	0.4348	0.835
7.8044	0.840	0.3086	0.845
7.8368	0.850	0.3759	0.855
7.8634	0.860	0.3472	0.865
7.8922	0.870	0.3086	0.875
7.9246	0.880	0.4202	0.885
7.9484	0.890	0.3650	0.895
7.9758	0.900	0.3968	0.905
8.0010	0.910	0.4348	0.915
8.0240	0.920	1.1790	1.460
8.9400	2.000		

Note: 'a' is half crack length.

Table 4.10 (continued)

Specimen #8 (stress-relieved under 0-13 Ksi)			
# of cycle ($\times 10^6$)	crack length a (inch)	$\frac{da}{dN}$ ($\times 10^{-6}$) (inch/cycle)	average crack length a (inch)
1.5135	0.320	0.2532	0.325
1.5530	0.330	0.3788	0.335
1.5794	0.340	0.3610	0.345
1.6071	0.350	0.3401	0.355
1.6365	0.360	0.3802	0.365
1.6628	0.370	0.3788	0.375
1.6892	0.380	0.3257	0.385
1.7199	0.390	0.4292	0.395
1.7432	0.400	0.3984	0.405
1.7683	0.410	0.5319	0.415
1.7871	0.420	0.4202	0.425
1.8109	0.430	0.4950	0.435
1.8311	0.440	0.4854	0.445
1.8517	0.450	0.5051	0.455
1.8715	0.460	0.5291	0.465
1.8904	0.470	0.6024	0.475
1.9070	0.480	0.5988	0.485
1.9237	0.490	0.5814	0.495
1.9409	0.500	0.7143	0.505
1.9549	0.510	0.9207	0.600
2.1504	0.690	1.1494	0.695
2.1591	0.700	1.3333	0.705
2.1666	0.710	1.5152	0.715
2.1732	0.720	1.2658	0.725
2.1811	0.730	1.5152	0.735
2.1877	0.740	1.5152	0.745
2.1943	0.750	1.5152	0.755
2.2009	0.760	1.5152	0.765
2.2075	0.770	1.5385	0.775
2.2140	0.780	2.2727	0.785
2.2184	0.790	1.7544	0.795
2.2241	0.800	1.8868	0.805
2.2294	0.810	1.8868	0.815
2.2347	0.820	1.5152	0.825
2.2413	0.830	2.2727	0.835
2.2457	0.840	2.0833	0.845
2.2505	0.850	1.8868	0.855
2.2558	0.860	2.2727	0.865
2.2602	0.870	7.5434	1.435
2.4100	2.000		

Note: 'a' is half crack length.

Specimen: #5
Load: 0~13 Ksi
Frequency: 10 Hz

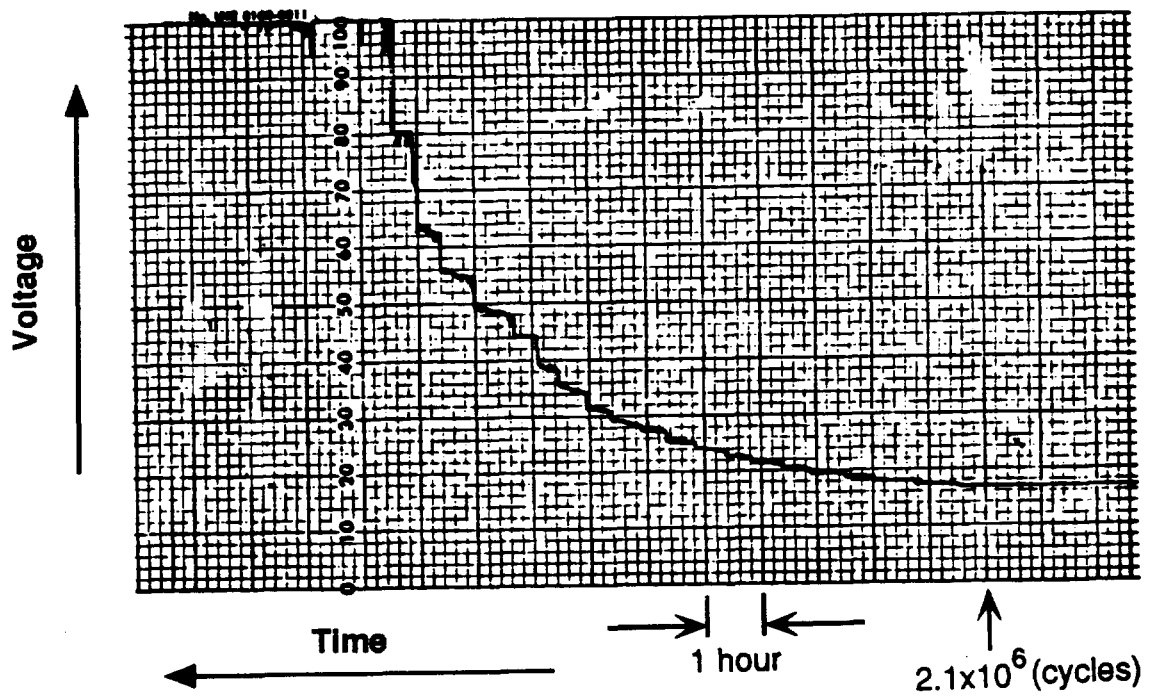


Figure 4.11 Crack Propagation Measurement

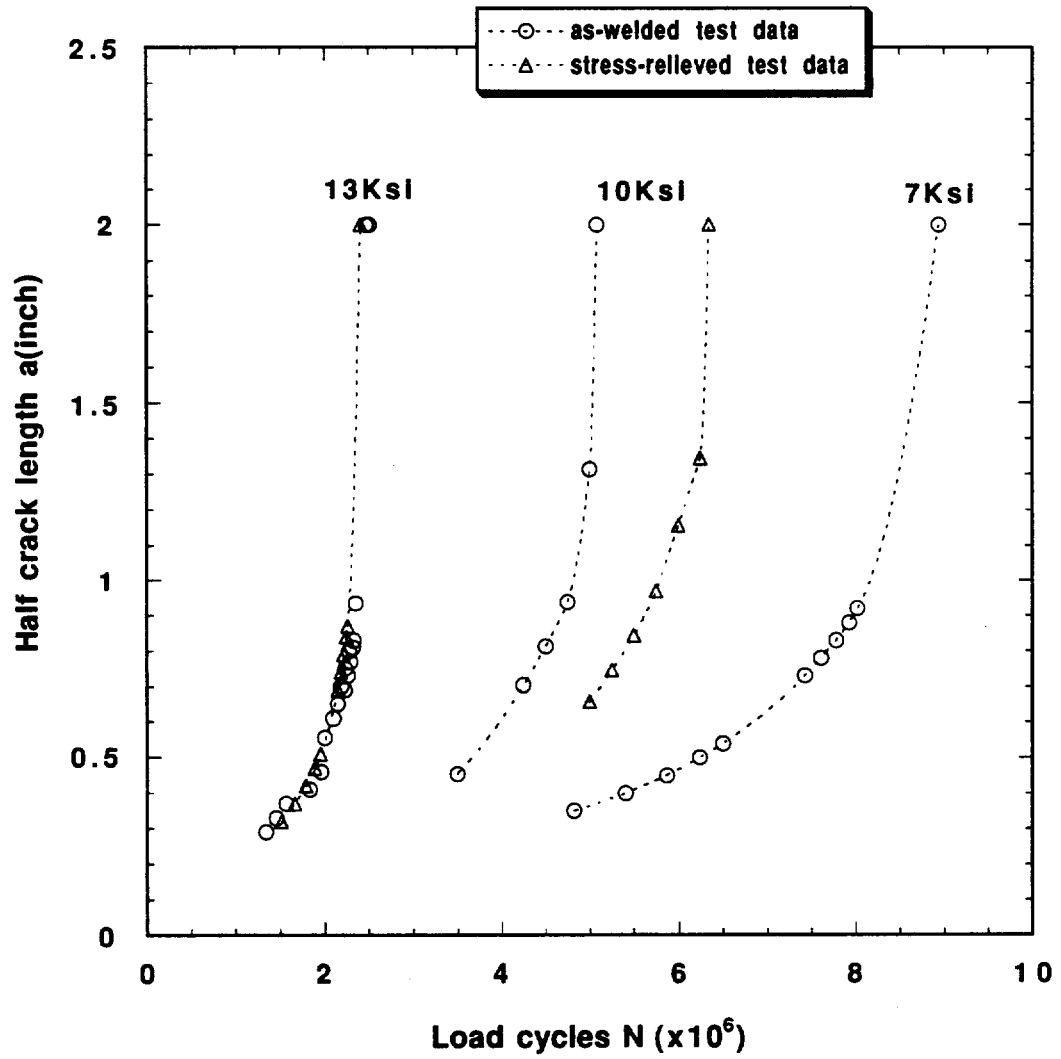


Figure 4.12 Crack Length as a Function of Load Cycles

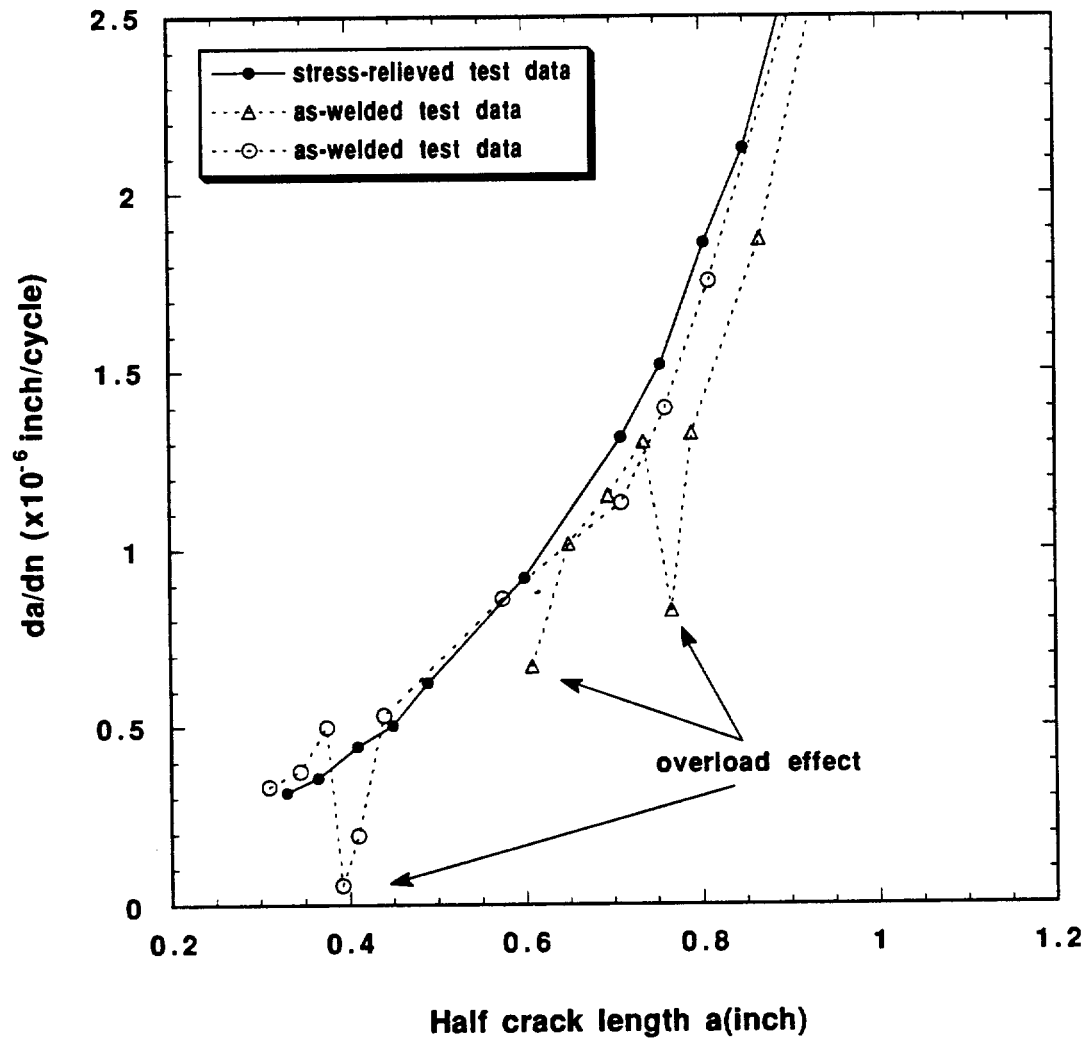


Figure 4.13 Overload Effect on Crack Growth Rate

4.5 Stress concentration factor

Table 4.11 shows the strain gage measurement results of the average stress concentration factors corresponding to three different gage widths. With a second order approximation for $f(x)$ in equation (3.5), we have $f(x) \approx a_1x + a_2x^2$. The equation (3.4) becomes:

$$f_t - 1 = [K(x) - 1](1 + a_1x + a_2x^2)$$

From experimental results, we have:

$$f_t - 1 = (1.8 - 1)(1 + 0.25a_1 + 0.25^2a_2)$$

$$f_t - 1 = (1.5 - 1)(1 + 0.51a_1 + 0.51^2a_2)$$

$$f_t - 1 = (1.2 - 1)(1 + 1.52a_1 + 1.52^2a_2)$$

By solving these equations, the coefficients were determined to be $a_1 = 5.272$, $a_2 = 0.126$ and the stress concentration factor at weld end toe was determined to be $f_t = 2.86$. This result is consistent with the result reported in the literature [8]. The average stress concentration factor $K(x)$ is then:

$$K(x) = \frac{2.86 - 1}{1 + 5.272x + 0.126x^2} + 1$$

Figure 4.14 shows the plotted $K(x)$ curve. Because of the differences in welding conditions, the SCF values for different welds may differ. However, for design purposes, this experimental result provides reliable evidence. To be reasonably conservative, a value $f_t = 3$ may be used for practical fatigue design in this type of weld.

Table 4.11 Average Stress Concentration Factor Measurement

x(mm)	0.25	0.51	1.52
K(x)	1.80	1.50	1.20

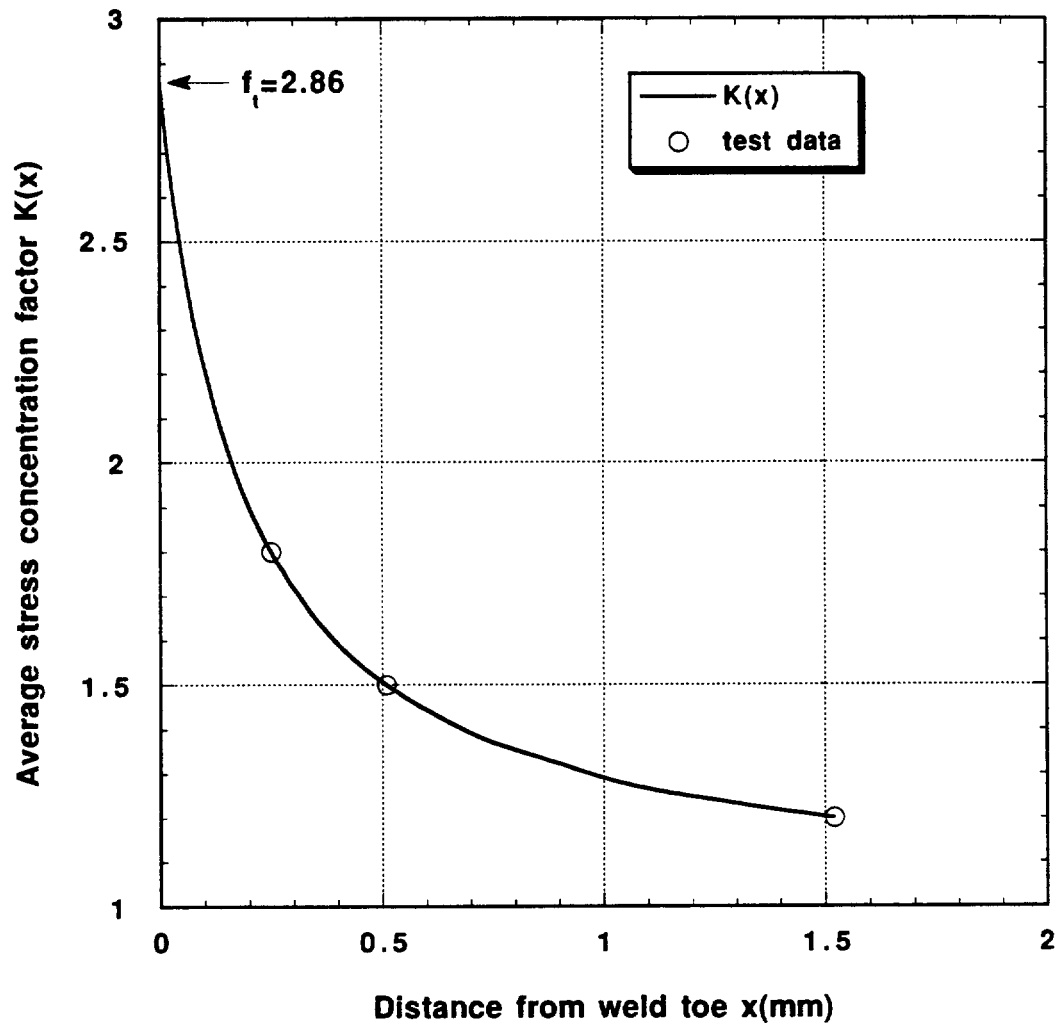


Figure 4.14 Stress Concentration Factor Measurement

4.6 Metallurgical analysis

4.6.1 Microstructure and microhardness analysis

Figure 4.15 shows the microstructure from a section of as-welded A515 steel. The microstructure in the parent metal of A515 steel is ferrite and pearlite. The microstructure in the weld was found to be parallel laths of ferrite and intragranular polygonal ferrite. The microstructures in the heat affected zone (HAZ) were found to be of two forms. One is in the overheated region which shows a mixture of bainite and proeutectoid ferrite, and the other is in the annealed region which shows a fine recrystallized structure. Figure 4.16 shows the microstructure from a section of stress-relieved weld. Its microstructure is similar to that of the as-welded A515 steel.

Table 4.12 shows the microhardness measurement results. It is seen that in the weld material, the hardness is consistent for both the as-welded and stress-relieved samples as well as for both the longitudinally and transversely sectioned samples. In the base material, the hardness of the as-welded sample is slightly higher than that of the stress-relieved sample, and the hardness of the transversely sectioned sample is slightly higher than that of the longitudinally sectioned sample. In the heat affected zone, the stress relieved sample generally showed a significant reduction in hardness due to the heat treatment, and the difference between the hardness of longitudinally and transversely sectioned samples was small and insignificant. In conclusion, the applied heat treatment will not cause any significant influence on the mechanical properties of the weld material and the base material, but it will cause a significant decrease in the hardness of the heat affected zone and this might affect some

of the mechanical properties in this region.

4.6.2 Weld defect analysis

The major weld defects in this type of weld specimen were found to be randomly distributed slag inclusions, Figure 4.17, porosity, Figure 4.18, and lack of fusion, Figure 4.19. Some slag inclusions and areas of lack of fusion were found to form crack like intrusions at the weld end toes, Figures 4.17 and 4.19.

4.6.3 Visual fracture surface analysis

Figures 4.20 - 4.23 show the fracture surface features and fatigue crack profiles from different viewing angles. It was found that the crack always started at the location right at the weld end toe, which is the maximum stress concentration site. Most parts of the crack surfaces are flat, smooth and straight except for the initiation and final fracture sites which show a rough and inclined fracture appearance. Figure 4.20 gives a top view of the crack profile. It can be seen that the major crack started at the weld toe end and then propagated along a line slightly beneath the weld end toe.

The fatigue crack growth process can be divided into four stages. The first stage is the crack initiation stage in which a semi-elliptic crack develops from a local defect at the weld end toe. There is usually a large amount of plastic deformation involved during the early crack growth stage, Figure 4.21. The crack is inclined to the nominal load direction and is driven to propagate within the heat affected zone, Figure 4.22. The second stage is the semi-elliptic crack growth stage, Figure 4.23. The crack propagates in a semi-elliptic mode until the crack breaks through the specimen thickness. The crack growth

direction in this stage is perpendicular to the nominal tensile load and the crack surface is flat and smooth, with less evidence of plastic deformation. The third stage is the through-thickness crack propagation stage. The crack propagates in a near central through-thickness mode until it is nearly across the specimen width. The crack surface in this stage is similar to that in the second stage. The fourth stage is the unstable crack growth stage. The crack growth life is short and the crack surface is again inclined and is about 45 degrees to the loading direction, Figure 4.20. The final crack length in the third stage was found to be about 4 inches.

Table 4.13 shows the measurement results of the semi-elliptic crack profiles from different test specimens, where $2a$ is the surface crack length and b is the crack depth. It was interesting to find that the ratio of b/a was approximately a constant under the same nominal cyclic load and it increased when the load increased. It was also found that residual stress had no consistent effect on the b/a ratio but the bending stress had slight influence on the b/a ratio. The b/a ratio had a tendency to decrease with an increase of bending stress.

4.6.4 SEM crack surface analysis

Figures 4.24-4.26 show the SEM analysis results of the fractured fatigue crack surfaces. At the initiation stage, the crack surface shows a few ripples originating from the weld toe, Figure 4.24. This implies that the crack initiation could originate from different sites simultaneously. At high magnification, Figure 4.25 shows that the crack originated from some intrusions under the weld end toe and that there was large plastic deformation involved in the pro-

cess. At the later stable crack growth stage, striation was observed within some of the grains and sub-cracks were also identified on the major crack surface, Figure 4.26.

Table 4.12 Microhardness Measurement (in Knoop Hardness)

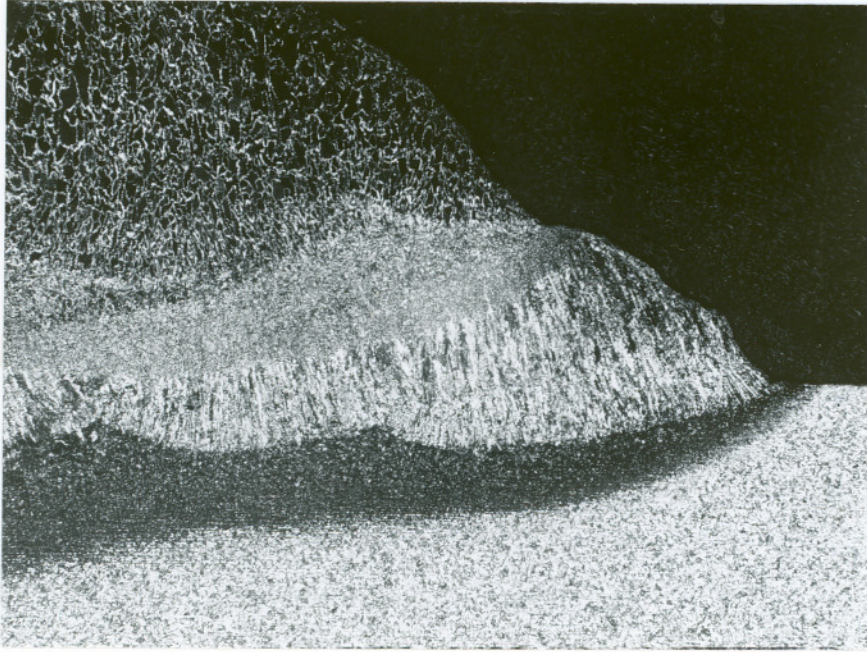
location condition	as-welded		stress-relieved	
	longitudinal	transverse	longitudinal	transverse
weld	161 - 194	165 - 205	168 - 186	162 - 209
HAZ -overheated	250 - 258	252 - 262	190	191 - 201
HAZ -recrystallized	214 - 226	239 - 243	182 - 199	172 - 190
base material	133 - 178	173 - 200	129 - 148	137 - 190

Table 4.13 Geometrical Features of Fatigue Crack

specimen #	2(A-W)	4(S-R)	5(A-W)	6(A-W)	9(S-R)
load (Ksi)	0 - 10	0 - 10	0-13	0-13	0-13
bending stress (Ksi)	1.5	0.0	7.0
2a (inch)	0.91	1.32	1.11	0.80	1.08
b (inch)	0.31	0.44	0.41	0.30	0.38
b/a	0.68	0.67	0.74	0.75	0.70

Note: A-W: As-welded, S-R: Stress-relieved

a).



b).

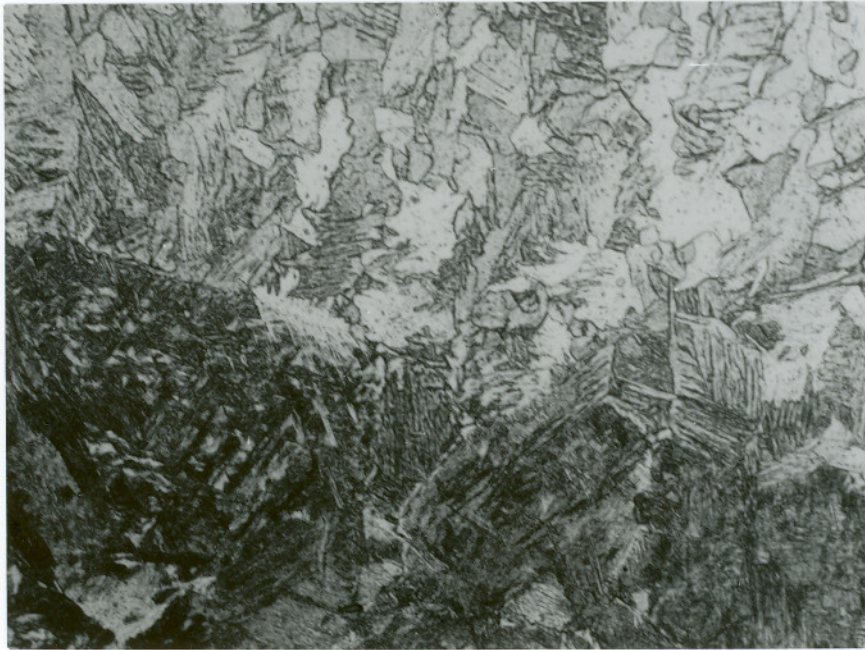


Figure 4.15 Microstructure of As-welded A515 Weld Joint

a). Microstructure in weld section (10×)

b). Microstructure in base material (400×)

c).



d).

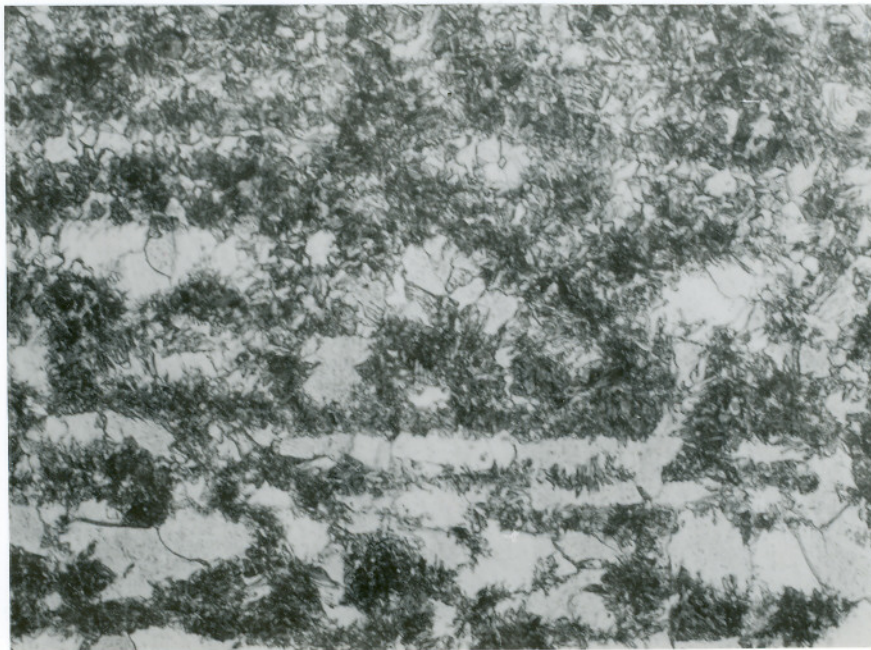


Figure 4.15 (Continued)

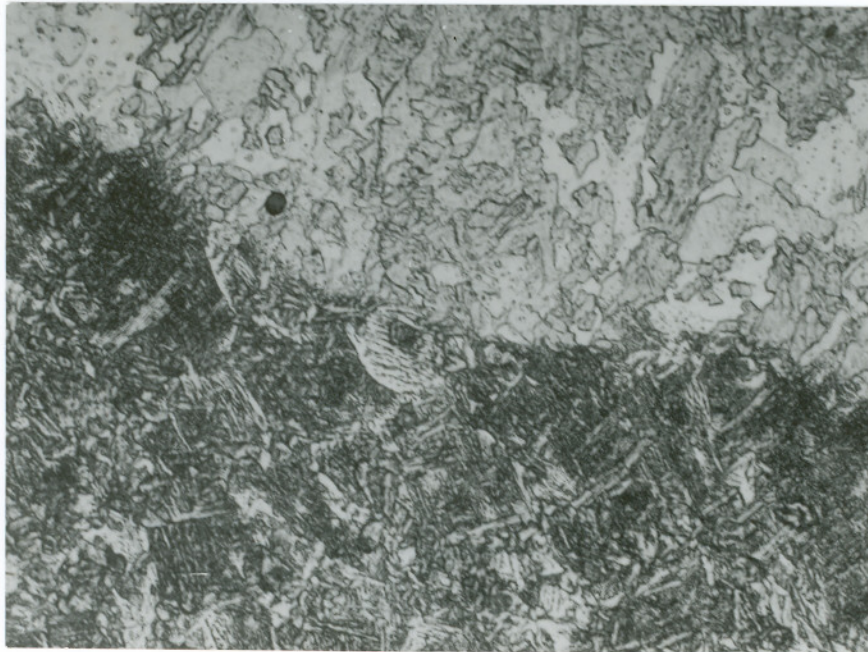
c). Microstructure in weld and in overheated HAZ (400 \times)
d). Microstructure in recrystallized HAZ (400 \times)

a).



Figure 4.16 Microstructure of Stress-relieved A515 Weld Joint
a). Microstructure in base material (400×)

b).



c).

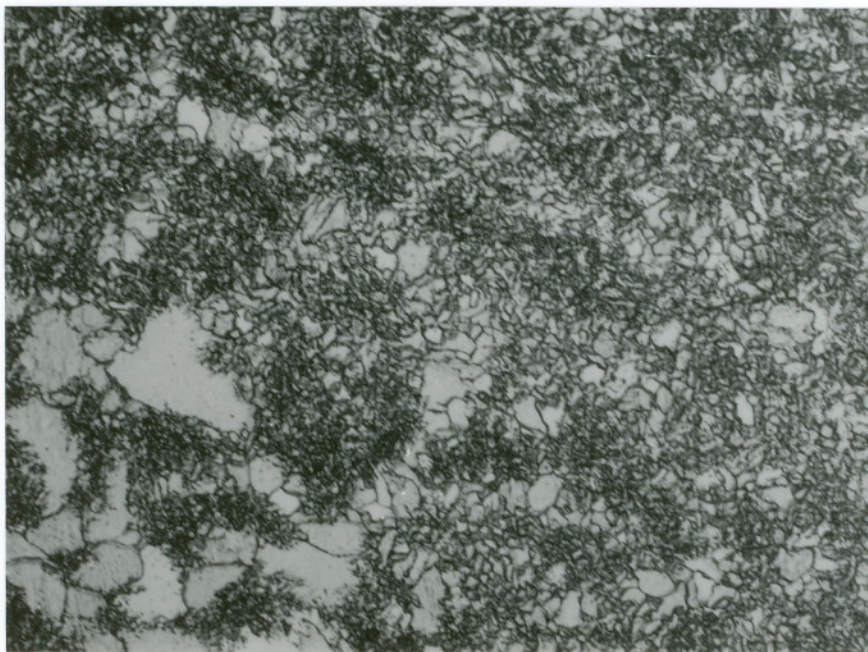
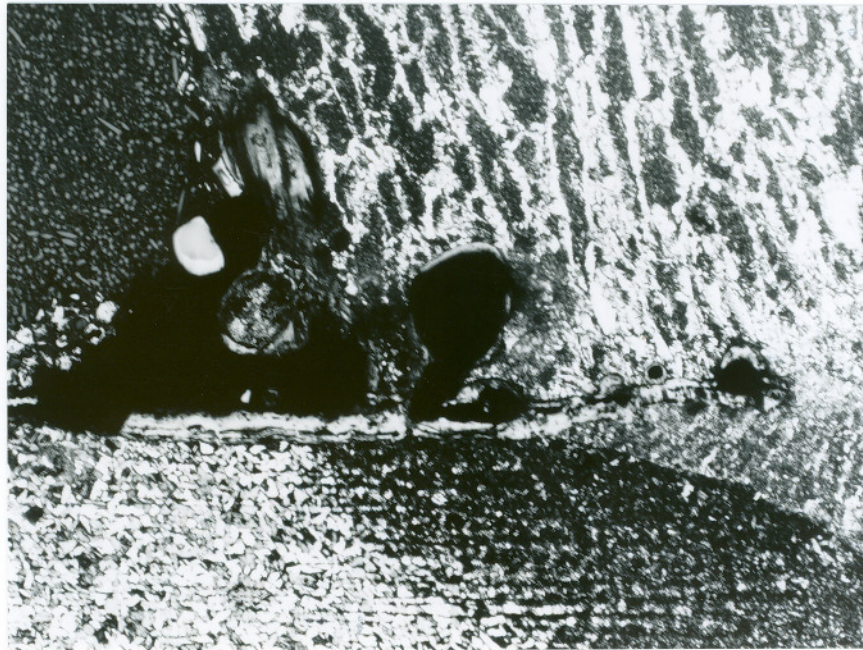


Figure 4.16 (Continued)

b). Microstructure in weld and in overheated HAZ (400 \times)
c). Microstructure in recrystallized HAZ (400 \times)

a).



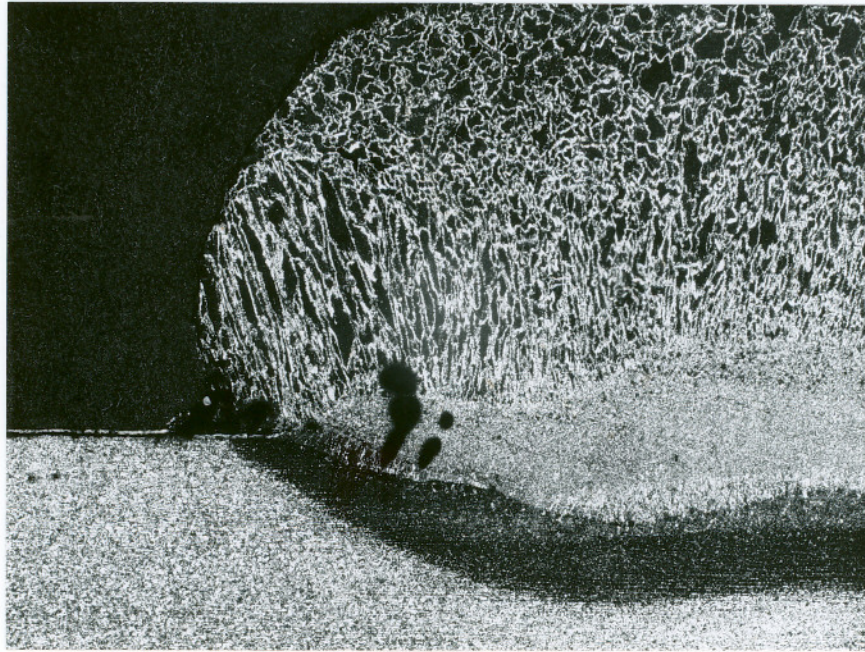
b).



Figure 4.17 Weld Defect (slag inclusion)

a). Slag inclusion at weld end toe (50×)
b). Slag inclusion at weld end toe (200×)

a).



b).

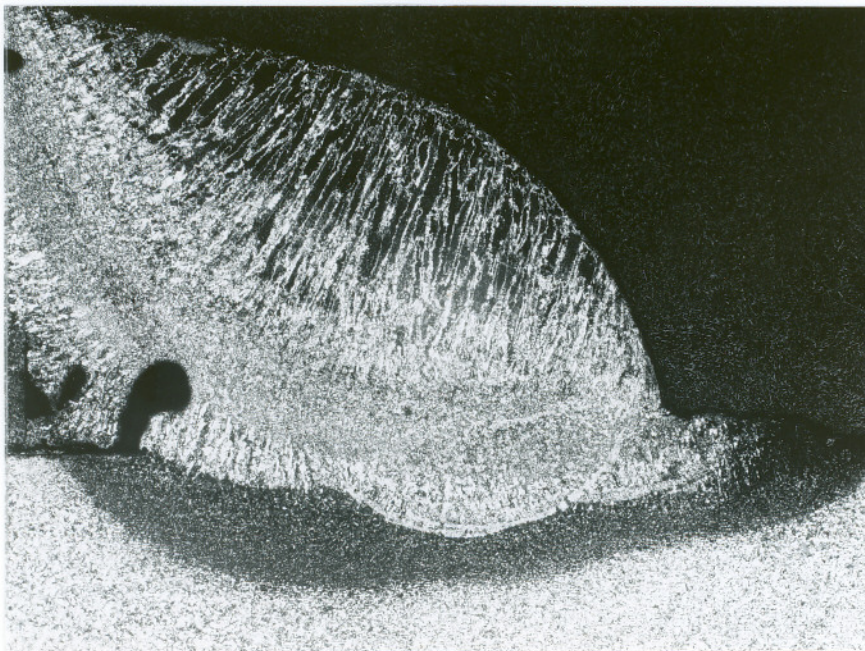
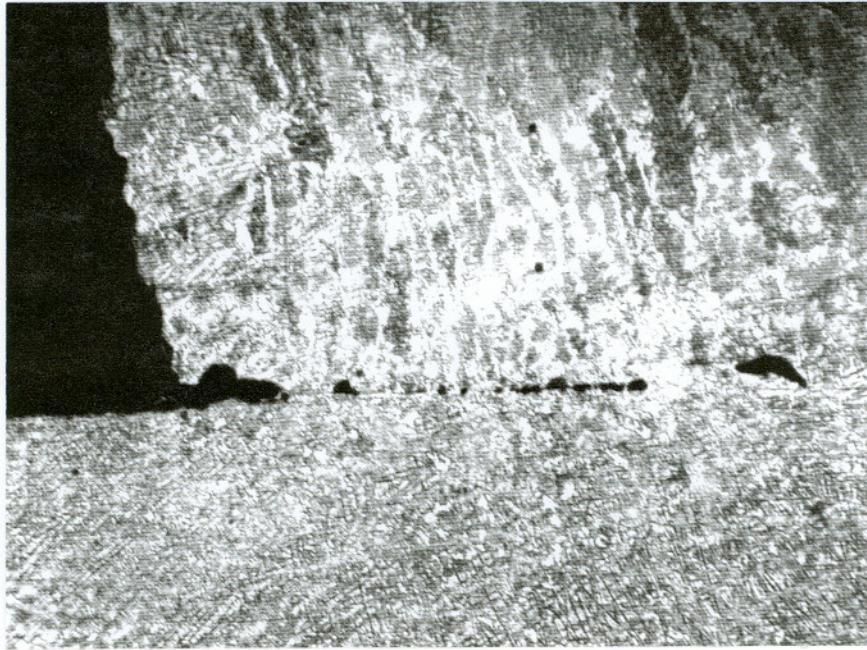


Figure 4.18 Weld Defect (porosity)

- a). Porosity in longitudinally sectioned weld (10 \times)
- b). Porosity in transversely sectioned weld (10 \times)

a).



b).

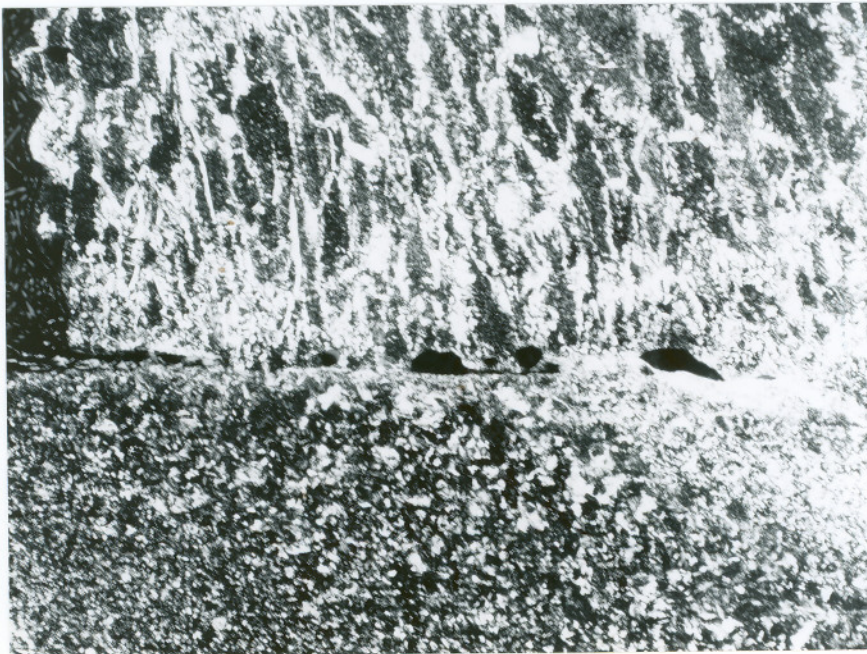


Figure 4.19 Weld Defect (lack of fusion)

- a). lack-of-fusion in longitudinally sectioned weld (50 \times)
- b). lack-of-fusion in transversely sectioned weld (50 \times)

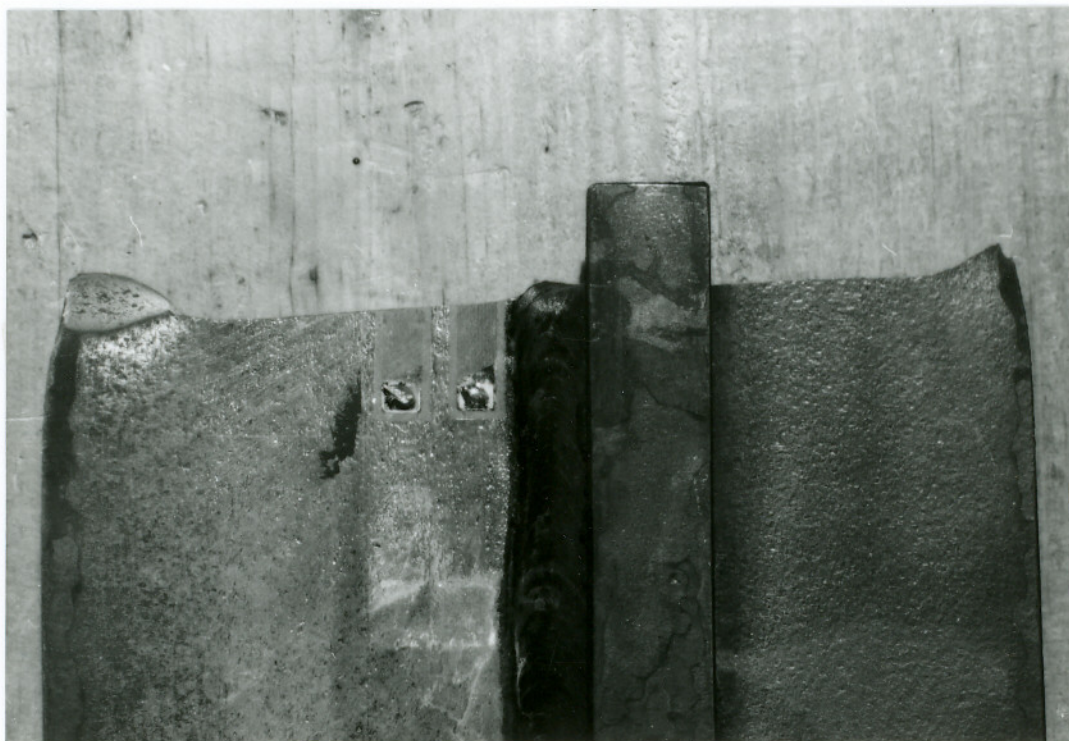


Figure 4.20 Fracture Surface Feature (top view, 1×)

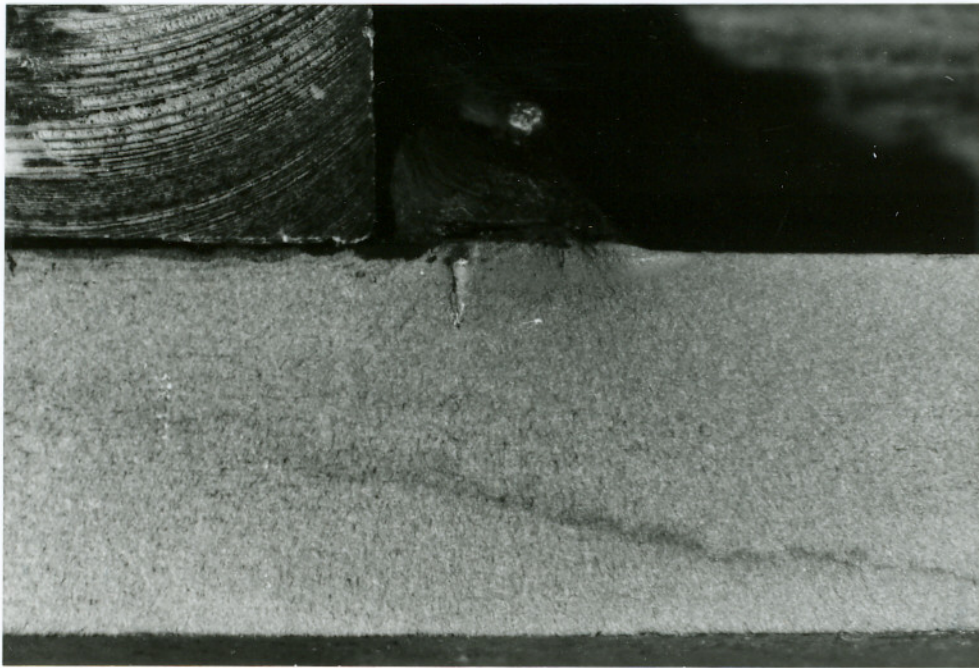
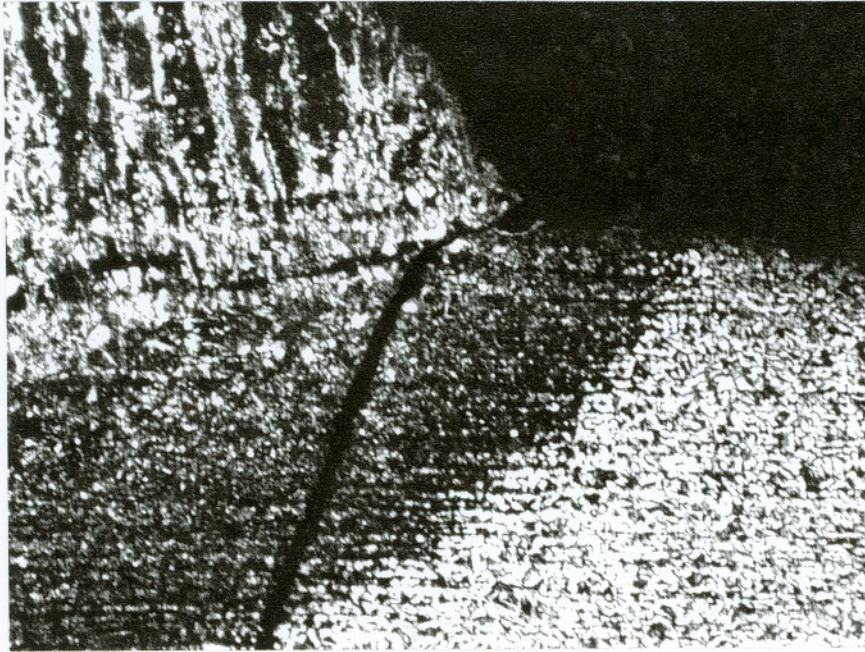


Figure 4.21 Fracture Surface Feature (surface view of initiation site, 4×)

a).



b).



Figure 4.22 Fracture Surface Feature (section view)

a). Crack initiation at weld end toe (50 \times)

b). Crack initiation at weld end toe (200 \times)

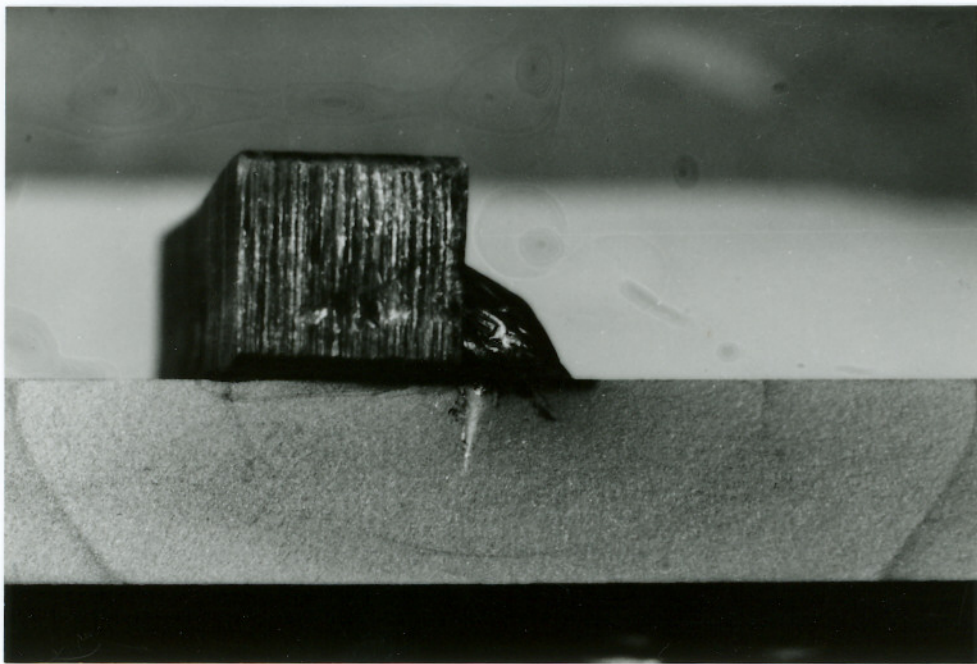


Figure 4.23 Fracture Surface Feature (surface view of crack profile, 2×)

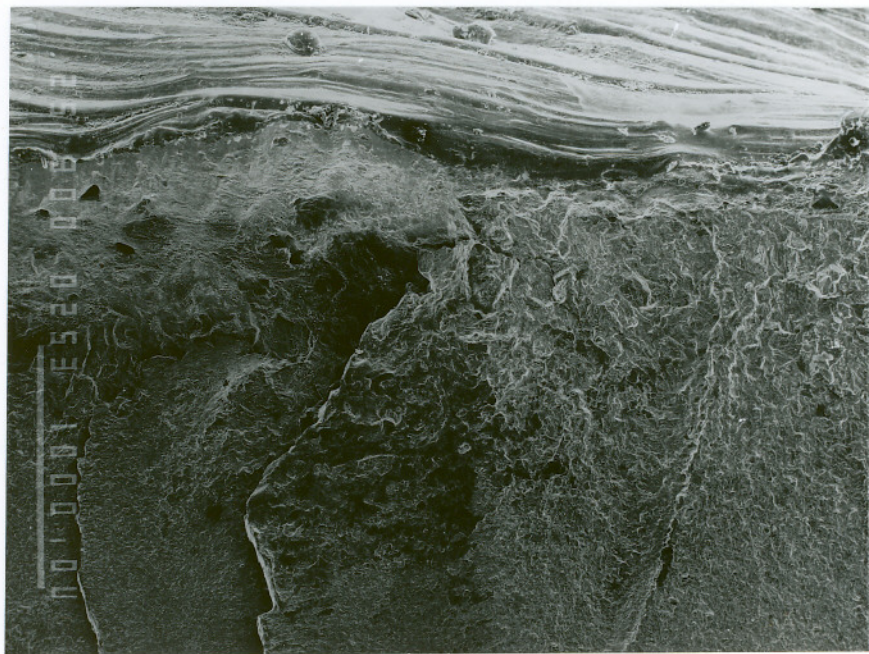
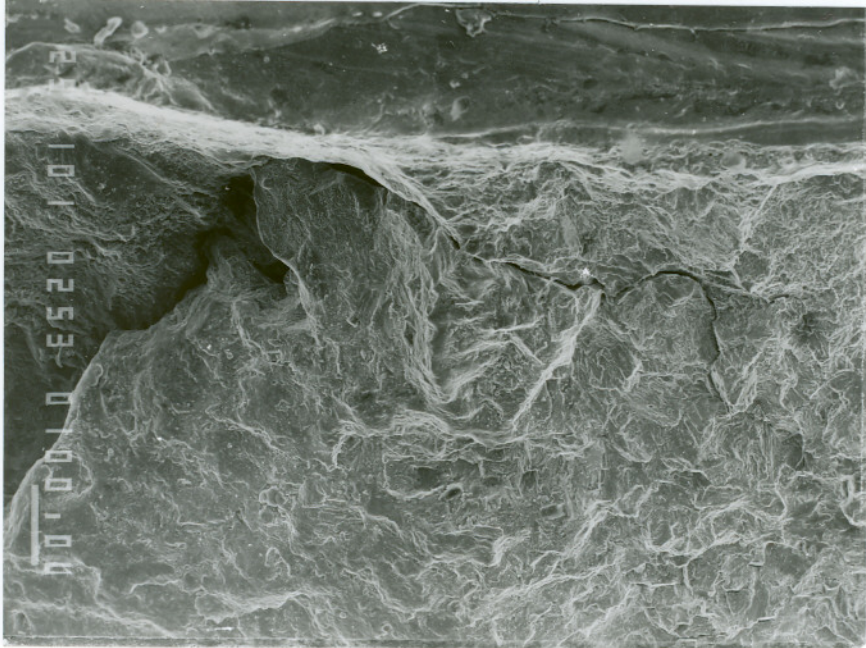


Figure 4.24 SEM Picture of Crack Initiation Site (30×)

a).



b).

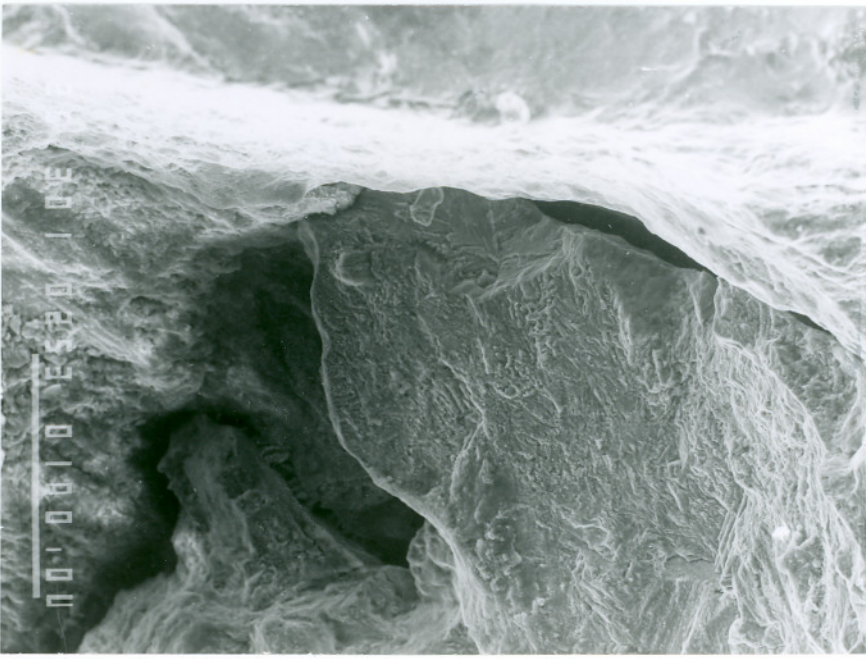
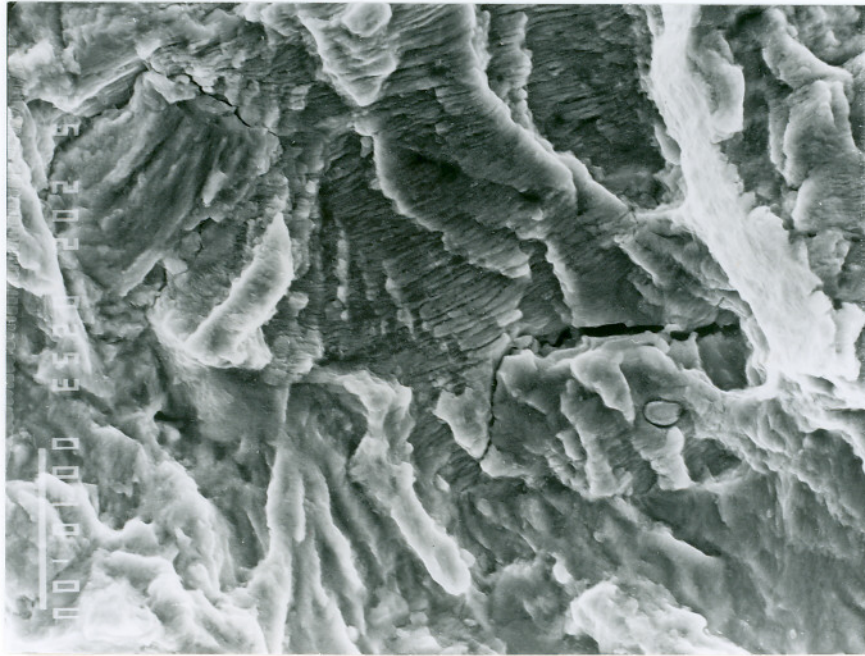


Figure 4.25 SEM Picture of Magnified Initiation Site
a). (100×) b). (300×)

a).



b).

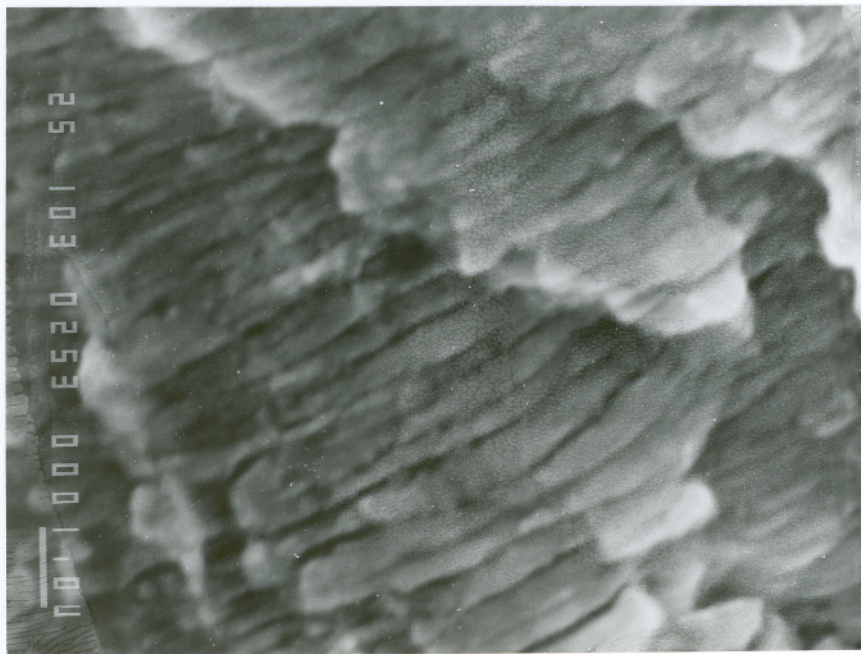


Figure 4.26 SEM Picture of Crack Surface
a). (2,000 \times) b). (10,000 \times)

CHAPTER 5 CALCULATION

5.1 Stress intensity factor

5.1.1 Semi-elliptic crack

Figure 5.1 shows the configuration of a plate with a central semi-elliptic surface crack. The stress intensity factor of a semi-elliptic crack can be determined in a variety of ways [75-80]. The most popular methods are the finite element method and the weight function method. The following equation is the numerical approach of the finite element analysis result obtained by Newman and Raju [80]. The accuracy is within 5% of the finite element result.

$$K_I = \frac{\sigma \sqrt{\pi b}}{E(K)} F_s \quad (5.1)$$

where:

$$F_s = [M_1 + M_2(bt)^2 + M_3(bt)^4] g f_\phi f_w \quad (5.2)$$

$$M_1 = 1.13 - 0.09(b/a) \quad (5.3)$$

$$M_2 = -0.54 + \frac{0.89}{0.2 + (b/a)} \quad (5.4)$$

$$M_3 = 0.5 - \frac{1}{0.65 + (b/a)} + 14(1 - b/a)^{24} \quad (5.5)$$

$$g = 1 + [0.1 + 0.35(bt)^2](1 - \sin\phi)^2 \quad (5.6)$$

$$f_{\phi} = [(b/a)^2 \cos^2 \phi + \sin^2 \phi]^{1/4} \quad (5.7)$$

$$f_w = [\sec \left(\frac{\pi a}{2W} \sqrt{bt} \right)]^{1/2} \quad (5.8)$$

$$E(K) = [1 + 1.464(b/a)^{1.65}]^{1/2} \quad (5.9)$$

The parameters a , b , t , W , ϕ are defined as in Figure 5.1. The necessary conditions for the application of the above equation are:

$$\frac{b}{t} < 1, \quad 0.2 \leq \frac{b}{a} \leq 1 \quad \text{and} \quad \frac{a}{W} < 0.5$$

From the fracture surface analysis results in Table 4.13, the ratio b/a was assumed to be unchanged in the semi-elliptic crack propagation mode. The stress intensity factor as a function of surface crack length was then calculated by a computer program given in Appendix 3. Different conditions were selected by taking $b/a=0.75$ for load 0 to 13 Ksi, taking $b/a=0.68$ for load 0 to 10 Ksi and taking $b/a=0.61$ for load 0 to 7 Ksi. Since the crack profile information under load 0 to 7 Ksi was not available from the test data, the selected b/a ratio was based on the linear extrapolation of the result in Table 4.13. The so obtained stress intensity factor, as a function of $1/2$ the crack length, is plotted in Figure 5.2. The calculation is complete when the semi-elliptic crack reaches the through-thickness of the specimen.

5.1.2 Through-thickness crack

When a through-thickness crack develops, its stress intensity factor can no longer be predicted by equation (5.1). Since there is no a general equation for the stress intensity factor calculation under such conditions, the equation for a central, through-thickness cracked finite plate was then used as an approximation. The following equation is based on the result of Feddersen and Tada [80]

$$K_I = \sigma \sqrt{\pi a} F_I(\alpha) \quad (5.10)$$

where:

$$\alpha = \frac{2a}{W} \quad (5.11)$$

$$F_I = (1 - 0.025\alpha^2 + 0.06\alpha^4) \sqrt{\sec(\alpha\pi/2)} \quad (5.12)$$

where a is 1/2 the crack length, W is the plate width. (here, the definition of W differs from the one given in equation (5.8)).

The associated program is given in Appendix 4. The calculated stress intensity factors as a function of 1/2 crack length under loads of 0 to 7 Ksi, 0 to 10 Ksi and 0 to 13 Ksi are plotted in Figure 5.2 to show the correlations.

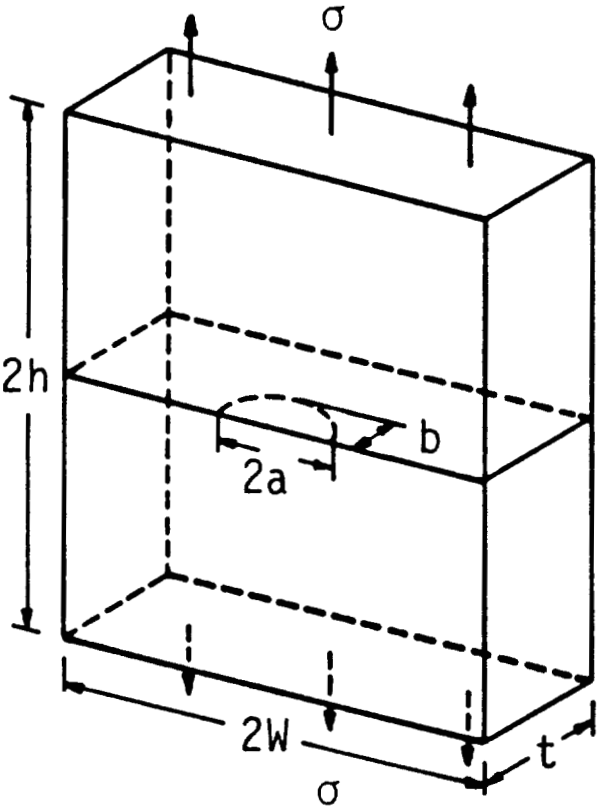


Figure 5.1 Center Semi-elliptic Crack Configuration

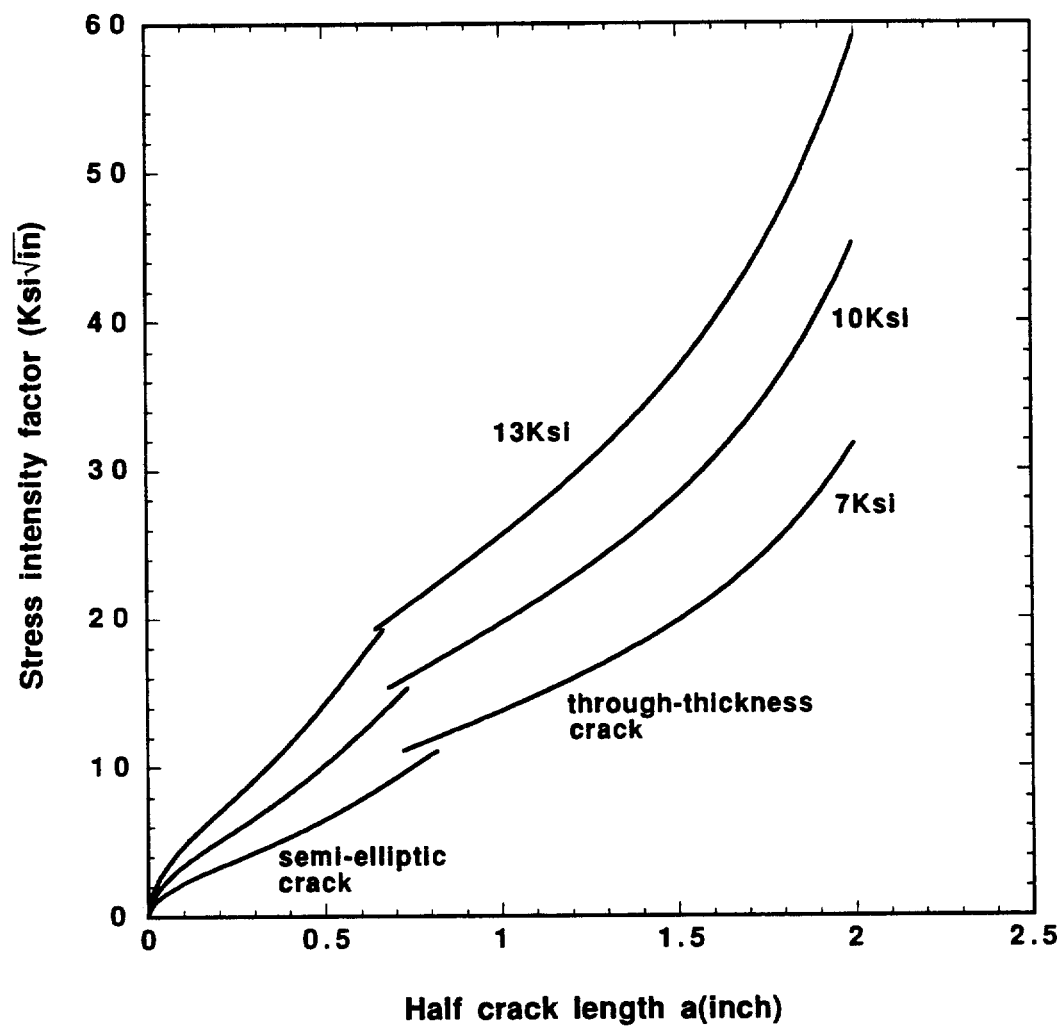


Figure 5.2 Calculated SIF as a Function of Crack Length

5.2 Fatigue crack propagation

From the crack propagation measurement results, Table 4.10, and stress intensity factor calculation results, Figure 5.2, the crack propagation behavior of A515 steel can be determined. Figure 5.3 shows the so determined $\frac{da}{dN} - \Delta K$ relationship in a log-log plot based on the test data from specimens 7 and 8. The relationship is approximately a straight line and therefore, corresponds to a region II crack propagation and is satisfied by the Paris law. Based on the best fitted linear regression line, the coefficients in the Paris law, equation (2.3), were determined to be approximately $m=2.0$ and $C=3.2 \times 10^{-9}$ for the crack growth rate with units of (inch/cycle) and the stress intensity factor with units of (Ksi $\sqrt{\text{in}}$). Specimen 7 is an as-welded specimen loaded under 0 to 7 Ksi and specimen 8 is a stress-relieved specimen loaded under 0 to 13 Ksi. Since no overloads were applied during these tests, the data should be more accurate than those from other specimens. Due to the effect of tensile welding residual stress, specimen 7 could be subjected to a higher true stress ratio than specimen 8. However, consider that the data from specimen 7 follows well the linear extension of the data from specimen 8, and that the data from a high stress ratio could also correspond to region II crack propagation even if the corresponding stress intensity factor range is low (Figures 2.8 and 2.9), it is, therefore, believed that the data from specimen 7 are valid for use in determining the crack propagation behavior.

The crack propagation life was determined based on the integration of the Paris equation:

$$N = \int_{a_i}^{a_f} \frac{da}{C(\Delta K)^m}$$

For a given initial 1/2 crack length a_i and a final 1/2 crack length a_f , the life for either a semi-elliptic or a through-thickness crack can be determined accurately by calculating the crack increment for each load cycle. The program for the calculation of the semi-elliptic crack propagation life is shown in Appendix 5, and the program for calculation of the through-thickness crack propagation life is shown in Appendix 6. According to the result in section 4.6, the final 1/2 crack length for a through-thickness crack is approximately 2 inches and for a semi-elliptic crack is $0.5(a/b)$ inch depending on the b/a ratio. The initial crack length is not directly obtained, and some analysis is required to select a reasonable value. For through-thickness crack propagation, the crack lengths of both surfaces of the specimen are actually different (the crack length on the welding surface is larger than the crack length on the back surface). From physical considerations, the stress state at the welding surface crack tip should be continuous when a semi-elliptic crack transfers to a through-thickness crack, and it is the stress state that determines the stress intensity factor. So, the stress intensity factor at the welding surface crack tip should be a continuous function of the load cycles. The initial length for the through-thickness crack is then chosen to be such a value so that it is of the same stress intensity factor value from equation (5.10) as that of the final semi-elliptic crack from equation (5.1). In this way, the welding surface crack length will show a reduction at the moment of crack transference from the semi-elliptic mode to the through-thickness mode. For semi-elliptic crack propagation, the initial crack length

needs to be chosen by a numerical iteration approach to coincide with some typical results from experimental fatigue testing. Figure 5.4 shows the comparisons of the test result and calculation result for the load conditions of 0 to 13 Ksi. With the initial $1/2$ crack length is chosen to be 0.1 inch, the test data are well fitted to the calculation curve.

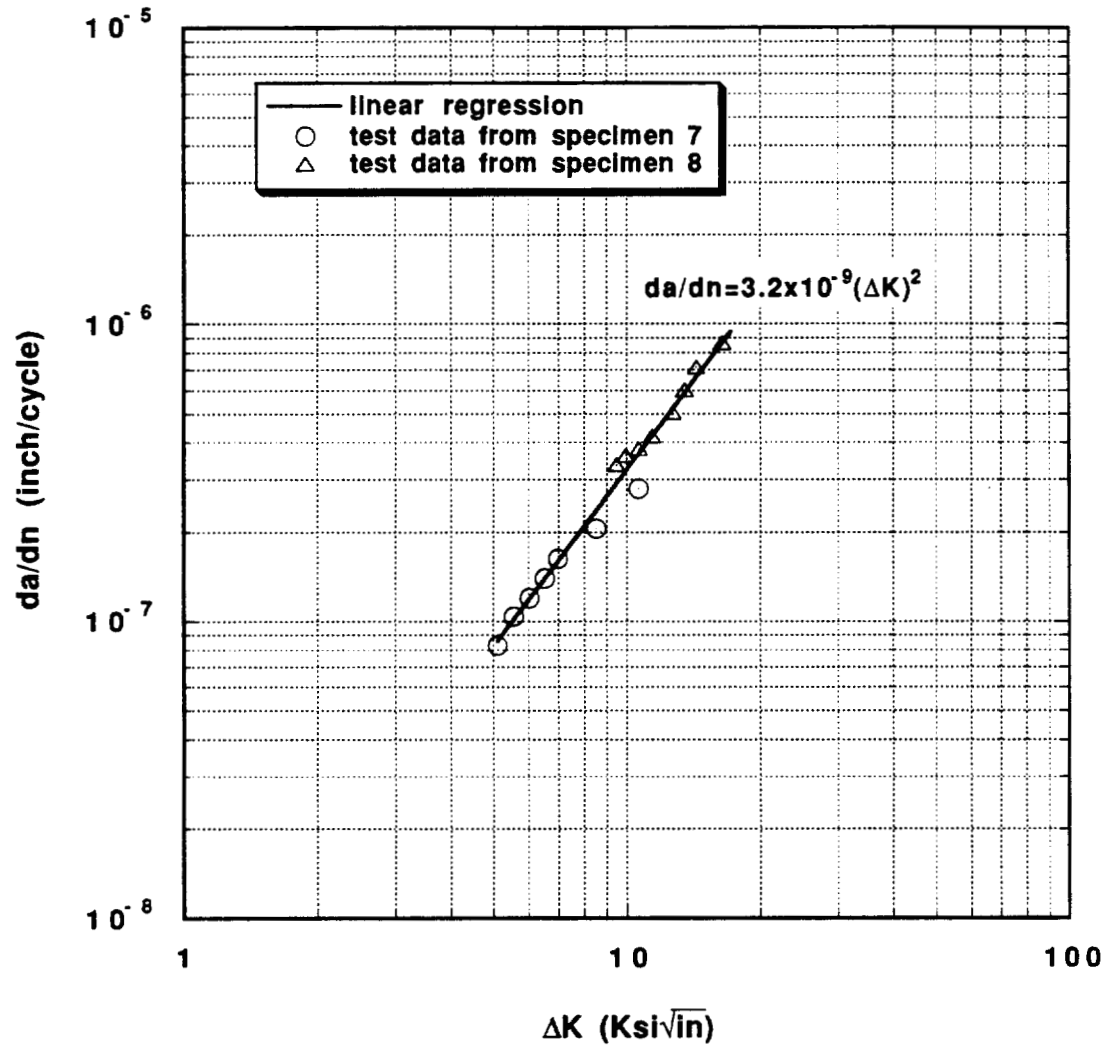


Figure 5.3 Crack Propagation Property of A515 Steel

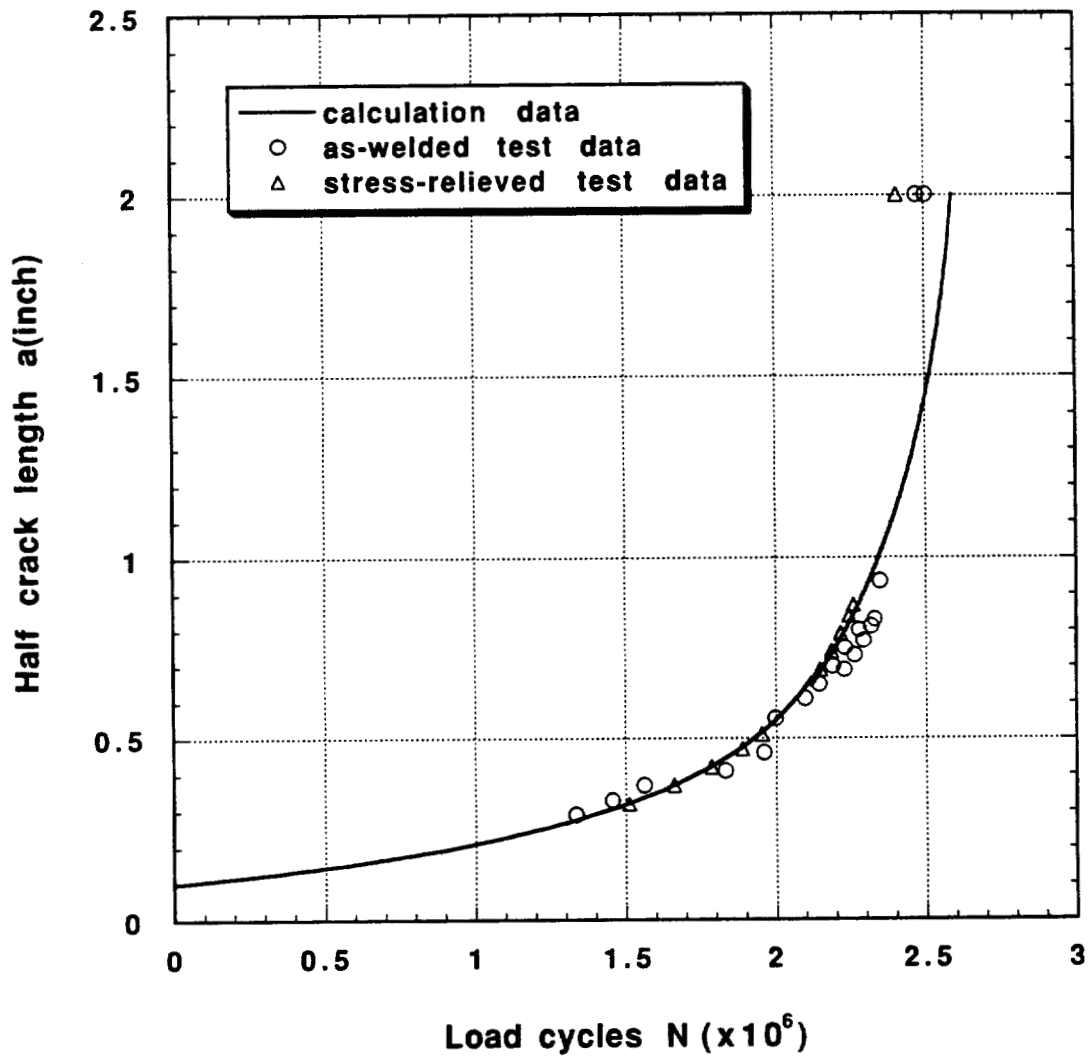


Figure 5.4 Crack Propagation Calculation under Load 0 to 13 Ksi

CHAPTER 6

DISCUSSION

6.1 Residual stresses

6.1.1 Measurement method

Figure 4.5 shows that the residual stress measurements from the sectioning method follow the same pattern as those obtained from the hole-drilling method. Theoretically, the sectioning method is considered the most accurate method for the measurement of surface residual stress. However, because of the laborious machining and caution required for its use, its application is limited to laboratory test conditions. The hole-drilling method is the most popular measurement method in both laboratory and field applications. Compared to the sectioning method, the hole-drilling method has proven to be accurate, only semi-destructive, less time consuming, convenient and economical.

The applied calibration test for the high stress application of the hole-drilling technique shows that accurate residual stress measurement can be obtained under uniaxial load conditions. Strictly speaking, the calibration test should also be carried out under biaxial tension-tension and biaxial tension-compression load conditions to ascertain the accuracy of the hole-drilling technique under general biaxial stress conditions. Considering that under uniaxial load conditions, the stress concentration factor (SCF) is 3, which lies between $SCF=2$ for biaxial tension and $SCF=4$ for pure shear, it is expected that the

calibration method used in section 4.2 is a reasonable first order approach to the general biaxial calibration of the effects of plastic deformation. Because of the limitations in the currently available experimental conditions, a general quantitative evaluation on the accuracy of the hole drilling technique is still not available. However, it is believed that the hole-drilling method is reliable to provide residual stress information even if the measurement error is higher than 5% under some circumstances.

6.1.2 Residual stress measurement

The residual stress state near the weld end toe was found to be biaxial tension-compression and the residual stress state near the weld center toe was found to be biaxial tension-tension. These results can be qualitatively explained using Figure 6.1, which is a variation of Figure 2.5. Consider a skip welded plate as a combination of three distinct plates, in which two plates have center welds and one plate is unwelded. After welding, the two plates containing center welds may both create residual stresses and bending distortions as in Figure 2.5. Since these three parts are physically connected, the effect of the bending distortion of the center welded plates on the unwelded plate is equivalent to the application of bending moments to the sides of the unwelded plate. This will cause compressive stress in the transverse direction on the top surface (welding surface) of the plate, Figure 6.1. On the other hand, the effect of longitudinal shrinkage of the two skip welds on the unwelded plate is equivalent to applying concentrated tensile loads at the central ends of the unwelded plate. This will generate tensile stresses along the centerline in the longitudinal direction of the unwelded plate. Therefore, the total effect is to

cause tension-compression residual stresses at the front of weld end toes. The result, a build up of tension-tension residual stresses near the weld center toe, is consistent with the result shown in Figure 2.5, which is considered the typical text book case for welding residual stresses.

Residual stress measurements from both types of simple weld specimens show similar distribution features to that from the pad-on-plate weld specimens. This means that residual stress is insensitive to the welding conditions. This result is consistent with the results reported previously [1]. The attempt to compare the experimentally determined residual stress pattern and the theoretically predicted residual stress pattern given in Figure 1.3 failed. Because very limited experimental measurements were available within a 1/4 inch (6mm) diameter area at the weld end toe, no clear pattern could be drawn in that area so comparisons based on experimental results could only be made at a few isolated spots. As a conclusion, both experimental results and computed results showed that there are high tensile longitudinal residual stresses near the weld end toe, although the experimental results showed that the residual stress state near the weld ends is biaxial tension-compression rather than biaxial tension-tension as the calculation predicted. For fatigue crack growth under longitudinal cyclic loading, a tension-compression residual stress state favors the crack propagation perpendicular to the weld. From this point, the experimental results confirmed that the weld end toe is the most critical location for fatigue crack growth. This is consistent with the theoretical predictions.

Welding residual stress is usually of high stress gradient near a weld. Because there are restrictions for the measurements of both hole-drilling and sectioning methods in accessing the weld (the closest measurement point they

can reach is still about 3 mm away from the weld fusion line), both methods were unable to pick up the peak residual stress value exactly at the weld toe. This may cause a loss of the detailed residual stress information. However, considering that the measured residual stresses at the weld end toe (with coordinates $x=0$ and $y=0$) are actually the residual stress located at the front path of the potential fatigue crack, even if the measured stress is not the true stress at the weld toe, it is still significant in the analysis of the effect of residual stress on fatigue crack propagation.

In practice, the welding conditions for each weld bead may be slightly different. This lack of identical conditions will cause differences in the profiles of different welds, as shown in Figure 6.2. Irregular geometry will certainly cause distortions to the local residual stress patterns and it will be a source of difficulty in determining the coordinates of each measurement point. As a result, two measurement points with the same coordinates might have considerably different relative locations with respect to the actual weld. When all the data from different welds are presented together, the obtained stress distribution pattern may suffer from some unexpected measurement error. Also, when a residual stress distribution gradient exists, the measurement result may not correctly reflect the true residual stress at the chosen coordinates of the measurement point. So, the measurement results from both the sectioning and hole drilling methods are subject to certain measurement errors. It is important to acknowledge these sources of potential error when performing residual stress analysis.

6.1.3 Specimen width effect

The test results in Figure 4.6 show that a simple weld specimen with a minimum width of 4 inches (100mm) is required to maintain the welding residual stress pattern of the pad-on-plate weld specimens. This result is consistent with the results of Gurney [54], and is also consistent with the minimum dimensional requirement (found by Maddox) for maintaining the stress concentration pattern at a weld end toe [55]. In order to be conservative, a 5 inch (125mm) wide specimen was considered appropriate for fatigue testing.

6.1.4 Residual stress relaxation effect

The residual stress relaxation test results in Figure 4.9 show that if the maximum applied stress is at least 14 Ksi (100 MPa), the longitudinal tensile residual stresses near the weld end toe and the weld center toe will drop significantly after only a few hundred of load cycles. Similar test results were obtained by Berge from similar material and with a similar specimen design [8]. The yield strength of A515 is about 45Ksi. From the experimental results in sections 4.3 and 4.5, the measured tensile residual stress at the weld toe is approximately 50% of the yield strength and the measured stress concentration factor at the weld end toe is approximately 3. Theoretically, plastic deformation will occur at the weld end toe when the nominal stress load is about 8 Ksi. Since no real material possesses an ideal elastic-plastic behavior and there is some effect attributable to the hardening of the material after the nominal yield point is reached, significant plastic deformation will occur only until a high enough tensile stress is applied. This gives a semi-quantitative explanation as to why a higher tensile stress load level, 14 Ksi, is required to cause a signi-

ficant longitudinal welding residual stress relaxation effect at the weld toes.

The test results in Figure 4.9 are able to give a reasonable explanation as to why there is no difference between the fatigue lives of as-welded and stress-relieved specimens in Maddox's report, as discussed in section 2.5. Most of the test data in Table 2.3 were obtained at load levels of 14 Ksi and above, so the effect of residual stress is eliminated after hundreds of load cycles. To study the effect of welding residual stress on the fatigue strength of the longitudinally fillet welded mild steel, therefore, the load conditions should be limited to a maximum tensile load of less than 14 Ksi. Otherwise, the maximum stress, σ_{\max} , should be considered a major factor in the evaluation of the fatigue behavior of weld joint because of its direct effect on residual stress relaxation. The stress ratio, R, has a similar effect as maximum stress, but its significance is not as obvious.

As discussed in section 6.1.2, the transverse residual stress originated from the bending distortion of the plate, so the slight longitudinal plastic deformation at the weld end toe due to longitudinal cyclic load is unlikely to have a substantial effect on bending distortion. Therefore, the transverse residual stress is not sensitive to the longitudinal cyclic load.

6.1.5 Heat treatment effect

The test results in Table 4.8 show that the effective stress relief condition to apply is to anneal the specimen at 650°C for one hour. This result is consistent with previous observations [63]. According to Theining's result [81], this stress relief condition is equivalent to annealing the specimen at 600°C for 15 hours. Therefore, some literature reported post heat-treatment tensile residual

stress is believed to be attributable to the lack of annealing time.

The results in Figure 4.16 show that there are no significant changes in the microstructure after heat treatment, but the results in Table 4.12 show that there is some influence of the heat treatment on the hardness of the heat affected zone. A decrease in hardness usually corresponds to an increase in the toughness of the material. From this point of view, the post welding heat treatment may help to improve the toughness of the heat affected zone and, therefore, to improve the overall toughness of a welded structure. However, the significance of such a change should be evaluated under practical conditions. From the fatigue test results described in section 4.4, it was shown that the applied heat treatment conditions will not cause any significant influence on the fatigue crack initiation and the fatigue crack propagation under the applied test conditions.

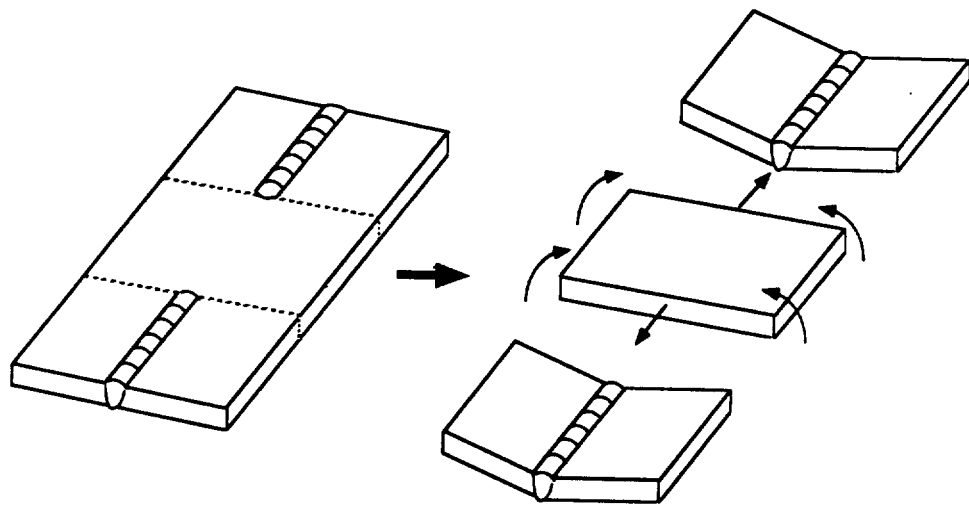
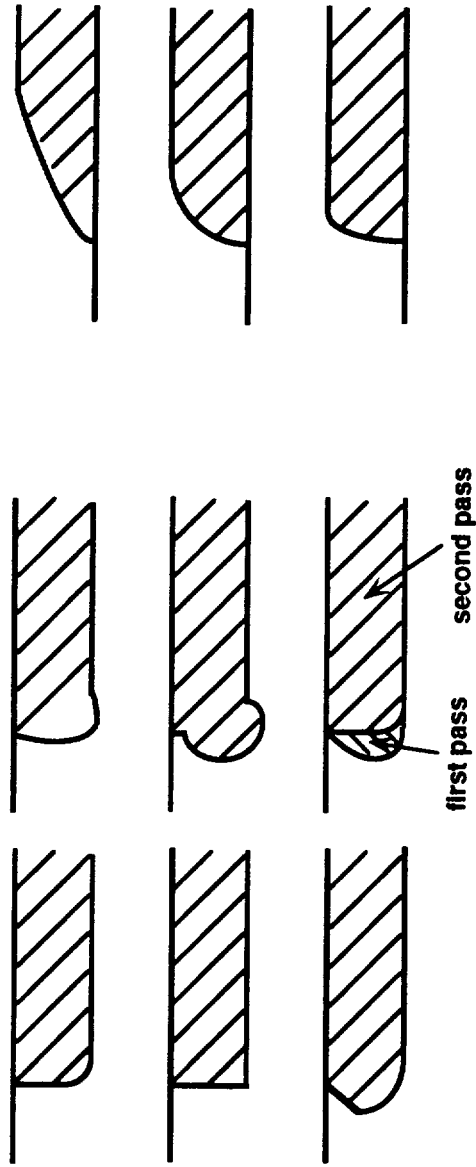


Figure 6.1 Residual Stress in Skip Weld Specimen



a). Vertical view b). Lateral view

Figure 6.2 Different Weld Profiles

6.2 Fatigue test

6.2.1 S-N test result

The test results in section 4.4 show that under load 0 to 13 Ksi, as-welded and stress-relieved specimens have a similar fatigue life. This means that there is no significant detrimental effect attributable to the welding residual stress and random weld defects under these load conditions.

Under load 0 to 10 Ksi, the test results for as-welded specimens show consistent fatigue lives. This suggests that the effect of random weld defects is insignificant. The results from stress-relieved specimens show a large scatter in fatigue life but do not show a consistent effect of residual stress on fatigue strength. On the one hand, this implies that residual stress is not critical to fatigue strength. On the other hand, it implies that random weld defects could be more significant under conditions of low mean stress.

Under load 0 to 7 Ksi, one as-welded specimen had a finite fatigue life and the other showed no crack after 11 million cycles. This implies that this load condition is in the region of the endurance limit. The random weld defect effect is believed to be the dominant factor that controls the fatigue strength under such low load conditions.

Under load -7 to 7 Ksi, the fatigue life of an as-welded specimen is similar to the fatigue life under load 0 to 13 Ksi. This means that under a compressive nominal stress load, the existence of tensile residual stress can cause a crack to propagate at a rate similar to that under a tensile nominal stress load. So, under the effect of tensile residual stress, the whole nominal stress load range is the effective stress range to cause crack growth.

Under load -10 to 10 Ksi, stress-relieved specimens consistently showed an increase in fatigue life over the as-welded specimens. The fatigue life of one stress-relieved specimen is similar to that of the stress-relieved specimens which were loaded under 0 to 10 Ksi. This means that for a residual stress free specimen, only tension nominal stress load range is the effective stress load range to cause crack growth. However, the fatigue life of the other stress-relieved specimen did not strongly support this conclusion. More test data are necessary for conclusive remarks.

6.2.2 Welding residual stress effect

Based on the above analysis, it is believed that under cyclic load with a high effective stress range or high mean stress, fatigue crack growth is controlled by the load and some consistent factors. Under cyclic load with low effective stress range or low mean stress, the fatigue crack growth is also controlled by some random factors. The welding residual stress has significant detrimental effect on fatigue strength when the load is in tension-compression mode, but it has no significant effect on the fatigue strength when the load is in tension-tension mode and the load range is 13 Ksi and the above. The welding residual stress has no consistent effects on the fatigue strength when the load is in tension-tension mode and the load range is below 13 Ksi.

6.2.3 Literature comparison

Figures 6.3 and 6.4 are the replotted Figures 2.12 and 2.13 respectively, and they show the comparisons between the current S-N test data and the S-N test data obtained by Gurney and Maddox. The current test data are found to be well fitted with Gurney's S-N test result, Figure 6.3. This confirms that the

test data are typical for mild steels. Figure 6.4 shows that there is a slight deviation between the current test data and Maddox's results. By examining the test conditions in Maddox's report [6], it was found that the as-welded specimens used in his test were spot heated at the weld ends to create the worst possible residual stress conditions. Also, since Maddox's test data involved different stress ratios, it is therefore not surprising that his S-N data generally shows a lower fatigue strength than that of the current test data.

6.2.4 Effect of weld toe notch and weld defect

Test results showed that all the fatigue cracks originated at the weld end toe and that some crack-like slag inclusions and lack of fusion defects were found at the weld toes. It seems true that these slag inclusions and lack of fusion defects are the most critical defects for crack initiation. Since these defects are usually randomly distributed around a weld, their effects on fatigue strength of a welded joint are expected to be of a random nature. However, This is inconsistent with the test result, in that there is no random factor effect when the applied load or mean stress is high. It is, therefore, believed that the relatively consistent weld toe notch effect is the major factor responsible for fatigue failure. The existence of the weld toe notch plays the role of a pre-crack. When the load is high, this notch effect is so overpoweringly significant that the effects of other random factors are insignificant in comparison. When the load is low, both the crack tip plastic zone and crack tip residual stresses are small. The notch affected zone is probably of similar dimension to the random defect affected zone. Therefore, the random defects play a major role in the fatigue crack growth process. Porosity and other types of defects may also

play a role of stress concentration that affect local stress conditions, but they are not critical to the crack initiation in the tested specimens.

6.2.5 Crack profile analysis

Since it is the stress that controls the crack growth mechanism, it is generally believed that the profile of a fatigue crack is determined by the profile of the real stresses around the crack. Test results in Table 4.13 show that the semi-elliptic crack profile in a stable growth stage are approximately unchanged, which suggests that the crack profile is previously determined by the stress conditions at the crack initiation stage. For the tested longitudinally fillet welded specimens, the initial stress state is determined by the weld toe stress concentration, nominal cyclic load, bending stress, residual stress and weld defects. The results in Table 4.13 show that under the tested conditions, the nominal cyclic load and bending stress have little effect on the crack profile, and that residual stresses have no effect on the crack profile. Considering that the effect of weld defects on the crack geometry should be inconsistent, it is, therefore, believed that it is the weld toe notch effect that determines the basic crack profile, and that other factors will cause slight changes in the original profile.

6.2.6 Tank car problem

For the tank car structures, the design service life is about 30 years with an average mileage of about 20,000 mile/year. The total life mileage is then approximately 600,000 miles. According to the tank car life load estimation result in [1], the average load frequency is of the order of 1 cycle/mile with a tensile stress load range between 4 to 10 Ksi and of the order of 0.1 cycle/mile

for tensile stress load range between 10 to 13 Ksi. So the total significant life load cycle is about 600,000 cycles which is well below the 2,000,000 cycles of the through-thickness fatigue life of the tested as-welded specimen under load 0 to 13 Ksi. So, under these conditions, residual stress relief is not necessary. However, the test result also shows that the fatigue life of an as-welded specimen under load of -10 to 10 Ksi is of the order of between 600,000 to 1,000,000 cycles. Considering that the result in [3] showed that the tank car is also subjected to compressive stress loads of considerable magnitude, a detailed life load analysis is then required to evaluate the fatigue performance of the tank car shell based on the principle of fitness for purpose. Unfortunately, the real life load of the tank car is not available and no final conclusion on the effect of welding stress on the fatigue safety of the tank car structure can be given at this time.

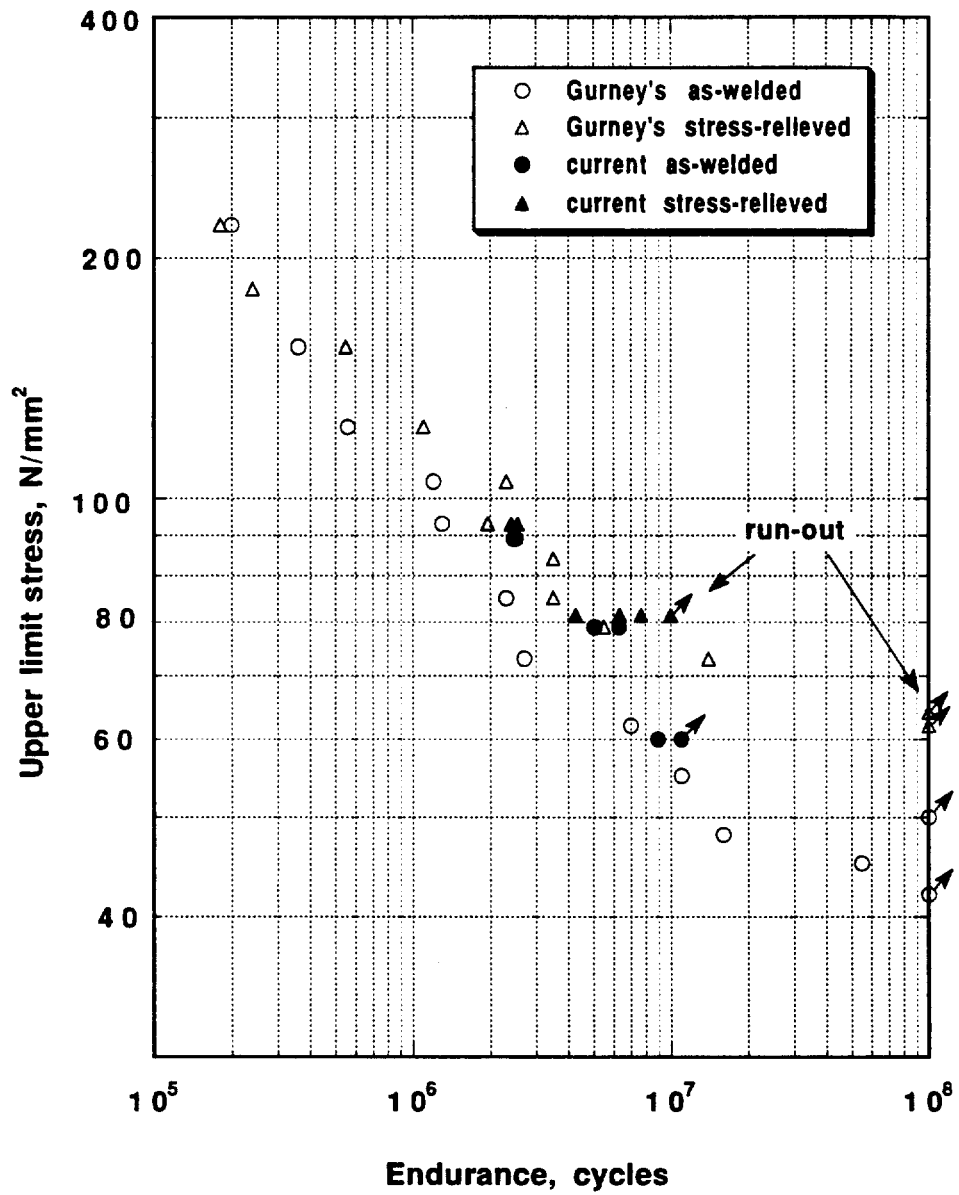


Figure 6.3 Comparison of S-N Test Result and Gurney's result
(replotted from [5])

6.3 Fatigue crack propagation

6.3.1 The concept of an equivalent crack

To explain the whole fatigue crack growth process quantitatively, detailed analysis of short crack growth behavior is required for crack initiation and near threshold crack propagation. This topic is beyond the scope of the current study. The behavior of short cracks is different from that of long cracks. Short crack propagation cannot be predicted well from linear elastic fracture mechanics theory. Propagation is usually much faster than a long crack under the same stress intensity factor, and it is more sensitive to local microstructure. It is difficult to monitor a short crack experimentally [82]. Because the available experimental evidence is limited, it is impractical to carry out an analysis for the current study.

For engineering applications, it is practical to ignore the detailed crack growth mechanisms and to make some assumptions to simplify the problem. Based on the fatigue test results and the crack propagation results, it was found that a concept of equivalent crack length can be introduced to make the problem easier to analyze. By simply considering the overall effect of crack initiation and near threshold crack propagation as the effect of an imaginary 'equivalent crack', the fatigue strength and long crack propagation behavior of a welded structure is then equivalent to that of a pre-cracked unwelded structure, Figure 6.5. The advantage of the equivalent crack concept is that it ignores the complicated crack initiation and near threshold crack growth stages, and considers only the region II crack propagation stage. The fatigue process can then be well described by the linear elastic fracture mechanics

approach. If such an idea can be proved to be effective, the process of fatigue design and fatigue life prediction of welded structures is considerably simplified. For any welded joint of interest, the only experimental work that would be required would be to use a few simple specimens to determine the equivalent crack geometry and crack propagation behavior of the material. The rest of the analysis would be just simple calculation.

6.3.2 Determination of equivalent crack

Since most fatigue cracks which formed at the weld toe are of semi-elliptic geometry, it was assumed that the equivalent crack for a welded joint is semi-elliptic. Strictly speaking, since an equivalent crack is used to substitute for the crack initiation and near threshold crack propagation processes, its geometry should be determined by all the factors which relate to the crack initiation conditions. This will cause too many factors to be involved and too much inconvenience in analysis. Based on the test results in Table 4.13, it was assumed that the effect of residual stress on the profile of a semi-elliptic crack is negligible. Since the bending stress due to welding distortion is not a consistent factor and since there is not enough related test data for analysis, it was also assumed that the effect of bending stress on the profile of a semi-elliptic crack is negligible. Then, according to the analysis in section 6.2.5, the length and depth of the equivalent crack would depend upon the weld toe notch effect, nominal load conditions and weld defects. The weld toe notch effect, which determines the stress concentration conditions, is expected to have a major contribution to the basic equivalent crack geometry. The load conditions, which drive the crack growth, are expected to have an effect on the detail of the equivalent

crack profile. Weld defects, which are randomly distributed around the weld toe, are expected to have additional effect on the equivalent crack length. For simplicity, it was further assumed that the weld toe notch effect had a major contribution on the equivalent crack length and the nominal load had a major contribution on the b/a ratio of the equivalent crack. If the effect of weld defects are temporarily ignored, then, the length of the equivalent crack depends only on the weld toe notch effect and is the same under different load conditions, and the b/a ratio of the equivalent crack depends only on the nominal load and will not change during the whole semi-elliptic crack growth process.

With the aid of equivalent crack, the fatigue life of the tested specimens was considered to be comprised of only two stages instead of the four stages as mentioned in section 4.6. Stage 1 is crack propagation in a semi-elliptic mode from the initial equivalent crack length to the through-thickness point and stage 2 is crack propagation in through-thickness mode from the through-thickness point to the final fracture. The fatigue life in stage 1 is about 6/7 of the total life and the life in stage 2 is about 1/7 of the total life, Figure 4.13. From the results in section 5.2, the constants in Paris law are determined to be $C=3.2 \times 10^{-9}$ and $m=2$ for A515 steel. Literature reports show that for most ferrite-pearlite steel, the constant m is about 3 [13]. Figure 6.6 is a replottting of the test results from literature and it shows the comparisons with the current test result. From Figure 6.6, it was found that

- a). The current test data fall within the error band of the data from literatures.
- b). The current data were obtained in low stress intensity factor region but

the data from literature were obtained in high stress intensity factor region.

- c). The current data were obtained from semi-elliptic cracks and the data from literature were obtained from either through-thickness cracks or from edge cracks.

Since there are also some other literature reports that show that the power exponent for mild steel is about $m=2$ [83], to obtain the best result, both the C and m constants from the test and from the literatures were used to calculate the crack growth life.

Since the S-N test results were consistent for all the specimens tested under load 0 to 13 ksi, the crack initiation conditions of these specimens should be similar and the effect of random weld defects should be insignificant. So, these test conditions are satisfied with most of the above assumptions of the equivalent crack concept. To use the data obtained under this test condition as reference and follow the calculation process described in section 5.2, the so determined initial crack length is then the required equivalent crack length. This determined equivalent crack length was then able to be used to predict the crack propagation life for other load conditions. Since no crack profile data are available for conditions under load -10 to 10 Ksi, both b/a ratios for loads 0 to 10 Ksi and for loads 0 to 20 Ksi (obtained from linear extrapolation) were used in the calculation for comparison. Table 6.1 and Table 6.2 give the calculation results of crack growth lives of semi-elliptic cracks and through-thickness cracks. The results for loads 0 to 13, 0 to 10 and 0 to 7 Ksi are also plotted in Figures 6.7 and 6.8 to compare with the experimental data. It was found that the determined $1/2$ equivalent crack length is

0.10 inch for using $m=2$ and is 0.12 inch for using $m=3$. Both constants give a reasonable prediction of the final fatigue life. From the profile of the crack growth curve, it is seen that the calculation result from constants $m=2$ and $C=3.2 \times 10^{-9}$ gives a better match with the experimental data for the semi-elliptic crack, Figure 6.7, and the calculation from constants $m=3$ and $C=3.6 \times 10^{-10}$ gives a better match for the through-thickness crack propagation, Figure 6.8. It is, therefore, suggested that $m=2$ be used for a semi-elliptic crack propagation prediction and $m=3$ be used for a through-thickness crack prediction. Theoretically, the crack propagation behavior of semi-elliptic cracks and through-thickness cracks should be the same; however, this is not supported by the current test data. Further work is required to provide an explanation for this.

For the tested specimens, the semi-elliptic crack propagation life is about 6/7 of the total fatigue life. For the tank car fatigue problem, a through-thickness crack is considered a total failure of the structure. Therefore, the power exponent should be taken as $m=2$. The result in Figure 6.9 shows that to take $m=2$ corresponds to a faster crack growth rate in the short crack region than to take $m=3$, provided that the initial crack length is the same. To take $m=2$ corresponds to a conservative prediction for the fatigue life.

The reason that the fatigue life of the specimen loaded under 0 to 7 Ksi was shorter than the prediction, Figure 6.7, is probably due to some unexpected, random weld defects since their effects have been neglected so far. With the application of the concept of the equivalent crack, only the effect of those relatively consistent factors, such as weld toe notch effect, are taken into account by the prediction. To predict the effect of those random weld defects

on fatigue life, we can either carry out detailed analysis to determine the corresponding equivalent crack length or simply apply an appropriate safety coefficient to the current results.

With the equivalent crack length concept, the post welding weld defect erasing method, such as weld toe grinding, can be considered a process that decreases the initial equivalent crack length, and therefore, would be an effective way to improve the fatigue strength of the welded structure.

Also, this equivalent crack concept could be useful in fatigue life prediction for unwelded structures if they are subjected to consistent crack initiation conditions. As a conclusion, for the tested longitudinal fillet weld, an equivalent crack with a $1/2$ length about 0.1 inch (2.5 mm) was proved to be associated with the weld end toe and it can be used to reasonably predict the fatigue life of the welded joint.

The above analysis is based on the assumptions that the length of equivalent crack is determined only by the weld toe notch effect and the b/a ratio of equivalent crack is determined only by the nominal load. These assumptions may not be true in general and detailed experimental evidence is required for further analysis of this issue. However, from the results in Figure 6.7, it is seen that under the tested conditions, these assumptions do give a simple and reasonable prediction of the fatigue crack propagation behavior. Considering that the effect of weld defects on the scatter in fatigue life prediction could be more significant than the effect of the accuracy of equivalent crack geometry, it is, therefore, believed that it is valid to use these assumptions in engineering applications.

6.3.3 Crack propagation analysis

The published fatigue data for A515 steel are limited [84,85] and no accurate crack propagation properties are available for comparison. In order to evaluate the obtained test data, comparisons were made with the crack propagation data of A516 steel. Figure 6.10 is a replotting of Figure 2.8 and it also shows the current test results. It was found that the test data from specimen 8 fit well with the A516 data in region of high stress intensity factor range ($\Delta K > 10 \text{MPa}\sqrt{\text{m}}$) and that the test data from specimen 7 fit well with A516 data in region of low stress intensity factor range ($\Delta K < 10 \text{MPa}\sqrt{\text{m}}$) with a high stress ratio of $R=0.75$. Due to the restraint of weld geometry, the crack propagation gage measurement, as mentioned in section 3.4, was actually made when the 1/2 surface crack length was greater than 0.3 inch at which the crack was growing out of the weld, Figure 4.20. If A515 steel has a similar crack propagation behavior as A516 steel, the results in Figure 6.10 would imply that the as-welded specimen is subjected to the effect of welding residual stress even when the surface crack length is of a considerable size, and that the effect of welding residual stress on the crack growth rate is significant in the region of low stress intensity factor range. According to the analysis in section 2.4, the effect of mean stress on the fatigue crack propagation of mild steel is significant when the stress intensity factor range is less than $10 \text{MPa}\sqrt{\text{m}}$ ($9 \text{Ksi}\sqrt{\text{in}}$). From Figure 5.2, it is seen that this stress intensity factor range value approximately corresponds to a semi-elliptic crack with 1/2 surface length of 0.5 inch under a load 0 to 10 Ksi. From Figure 6.7, it is seen that such a crack length approximately corresponds to 90% of the fatigue life for a semi-elliptic crack and 80% of the fatigue life for a total failure. So, based on these analyses, it is

expected that some consistent effects of welding residual stress on the fatigue strength of the tested specimens will be seen under a load 0 to 10 Ksi. However, this is not supported by the experimental results. There are two possible reasons that could cause this result. One is that the crack propagation behavior of A515 steel could be different from the A516 steel. The other is that the welding residual stress relaxation effect could be significant at the weld end toe under load 0 to 10 Ksi since no residual stress measurement at the exact weld toe is available. From currently available test data, the only conclusion which can be made is that under a tension-tension cyclic load, the effect of welding residual stress on the fatigue strength of welded joints is secondary compared with the effect of weld defects. However, there is still no complete explanation for all the experimental results.

6.3.4 Future work

Because the crack propagation data of A515 steel at a low stress intensity factor range is still limited, to carry out further analysis it is necessary to determine the detailed crack propagation properties, and to carry out fatigue testing for some other type of welded joint and/or under some other load conditions in order to prove the general applicability of the equivalent crack concept. It is suggested that further testing be carried out to determine the crack propagation property of A515 steel following the standard procedures for fatigue crack growth measurement [86], to determine the effect of nominal load on the geometry of semi-elliptic crack and to study the fatigue behavior of transverse fillet welded and butt welded specimens.

Table 6.1 Semi-elliptic Crack Propagation Life Calculation

			m=2 C=3.2×10 ⁻⁹	m=3 C=3.6×10 ⁻¹⁰
Δσ (Ksi)	b/a	a _f (inch)	a _i =0.1 (inch)	a _i =0.12 (inch)
S=7	0.61	0.819	10.20×10 ⁶	20.72×10 ⁶
S=10	0.68	0.735	4.19×10 ⁶	5.62×10 ⁶
S=13	0.75	0.667	2.12×10 ⁶	2.09×10 ⁶
S=20	0.68	0.735	1.05×10 ⁶	0.70×10 ⁶
	0.87	0.575	0.72×10 ⁶	0.43×10 ⁶

Note: a_i is the initial crack length, a_f is the final crack length.

Table 6.2 Through-thickness Crack Propagation Life Calculation

Δσ (Ksi)	a _i (inch)	a _f (inch)	m=2 C=3.2×10 ⁻⁹	m=3 C=3.6×10 ⁻¹⁰
7	0.723	2.0	1.43×10 ⁶	0.84×10 ⁶
10	0.681	2.0	0.75×10 ⁶	0.32×10 ⁶
13	0.644	2.0	0.47×10 ⁶	0.16×10 ⁶

Note: a_i is the initial crack length, a_f is the final crack length

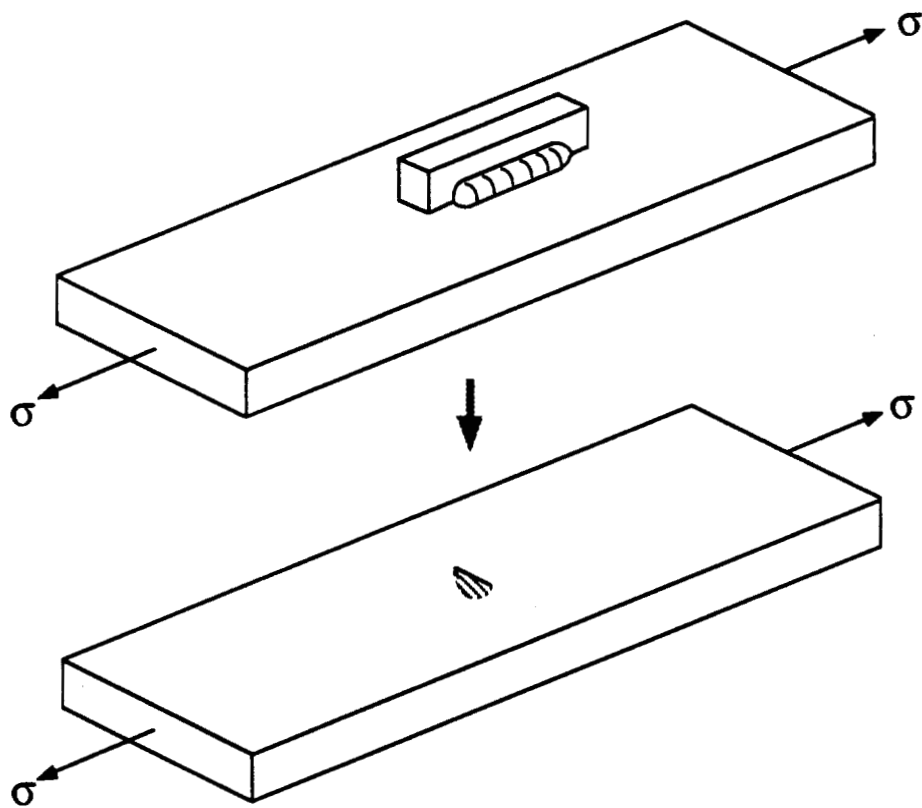
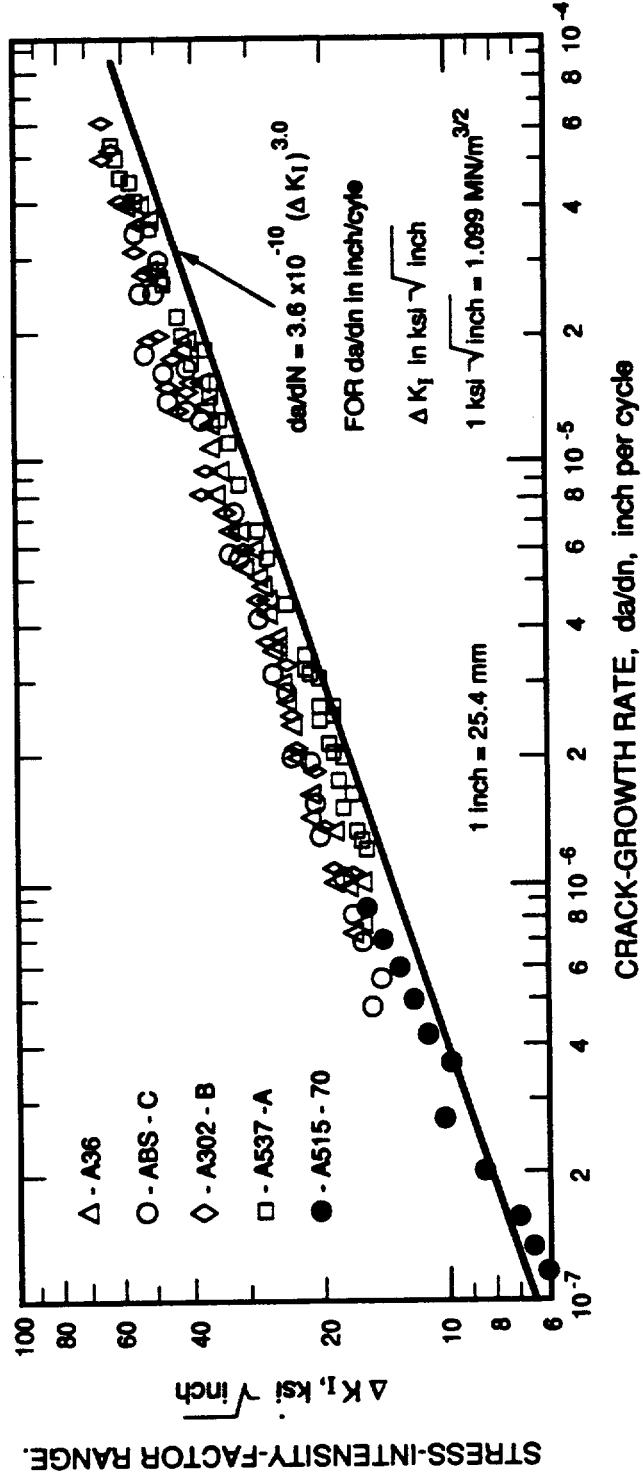
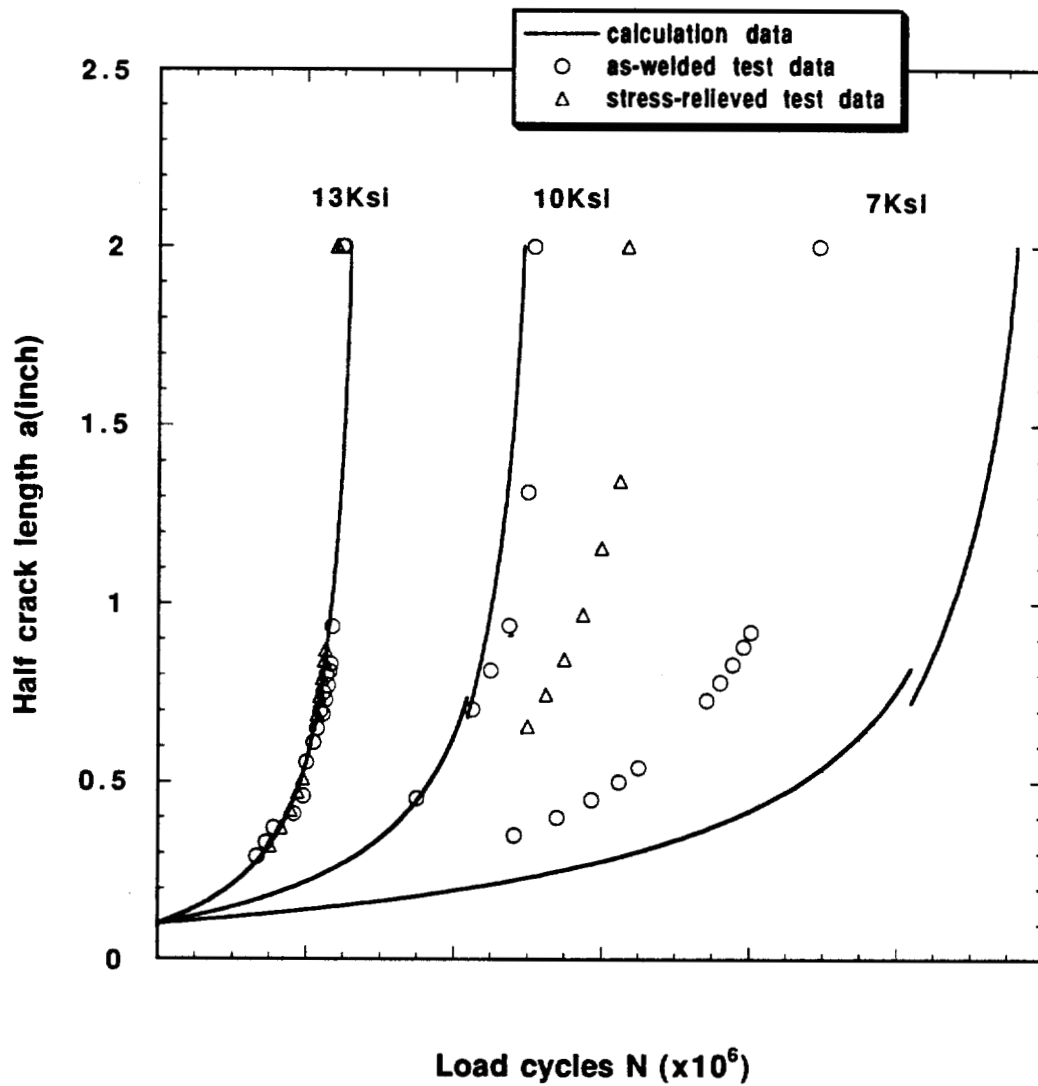


Figure 6.5 Equivalent Crack Concept



Summary of fatigue-crack-growth data for ferrite-pearlite steels.

Figure 6.6 Comparison with General Ferrite-pearlite Steels
 (replotted from [13])

Figure 6.7 Crack Propagation Calculation with $m=2$

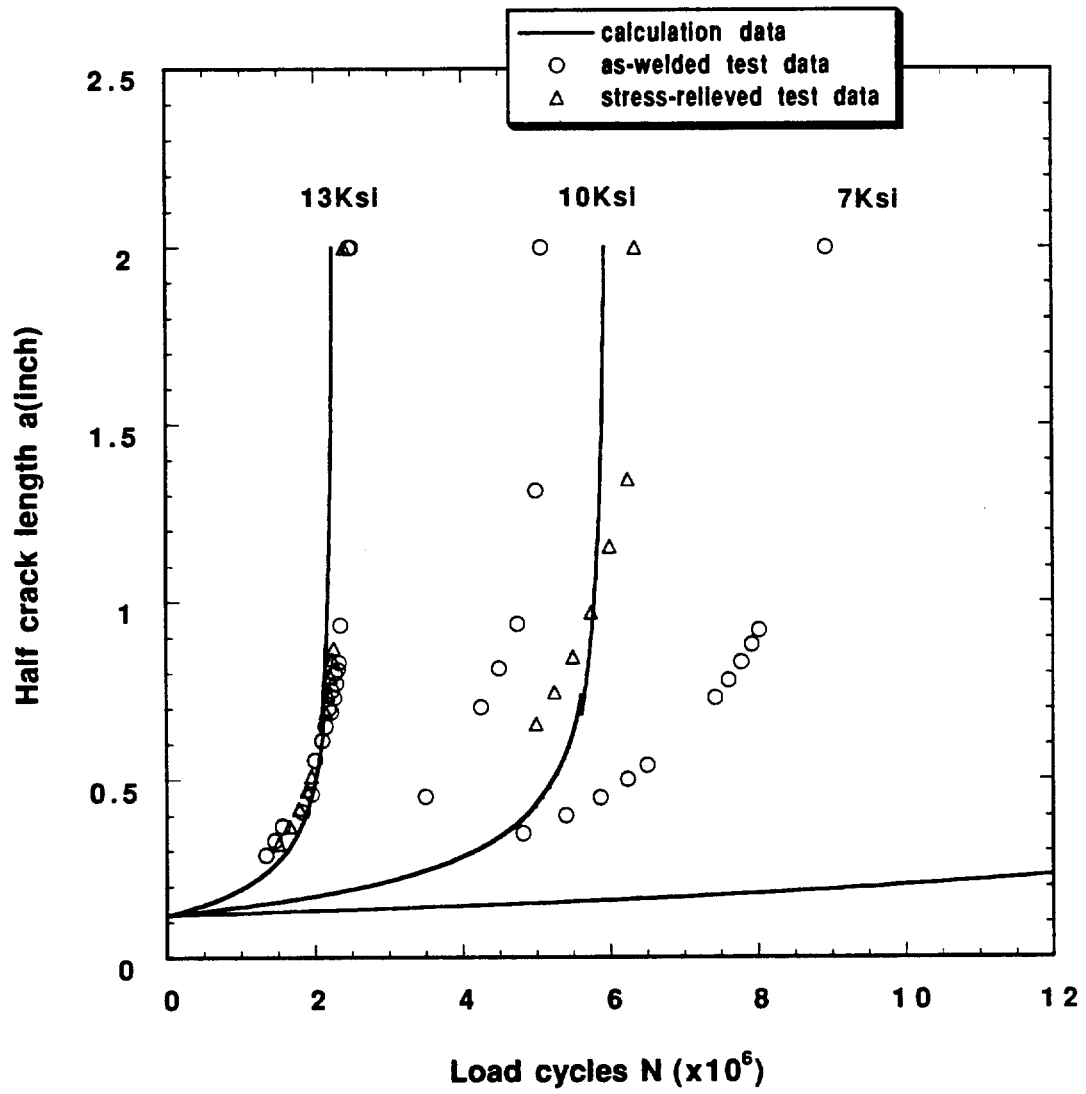


Figure 6.8 Crack Propagation Calculation with $m=3$

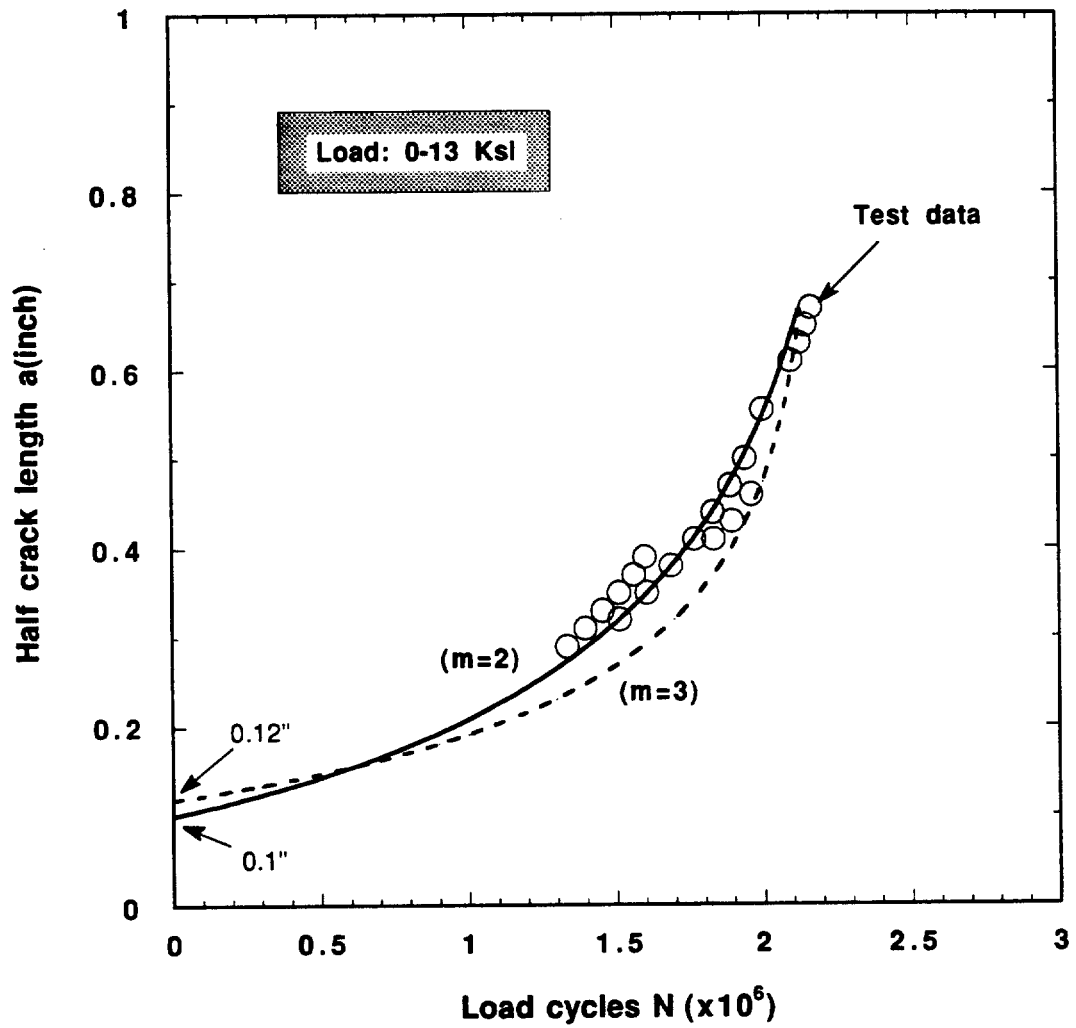


Figure 6.9 Crack Propagation Calculation Comparison

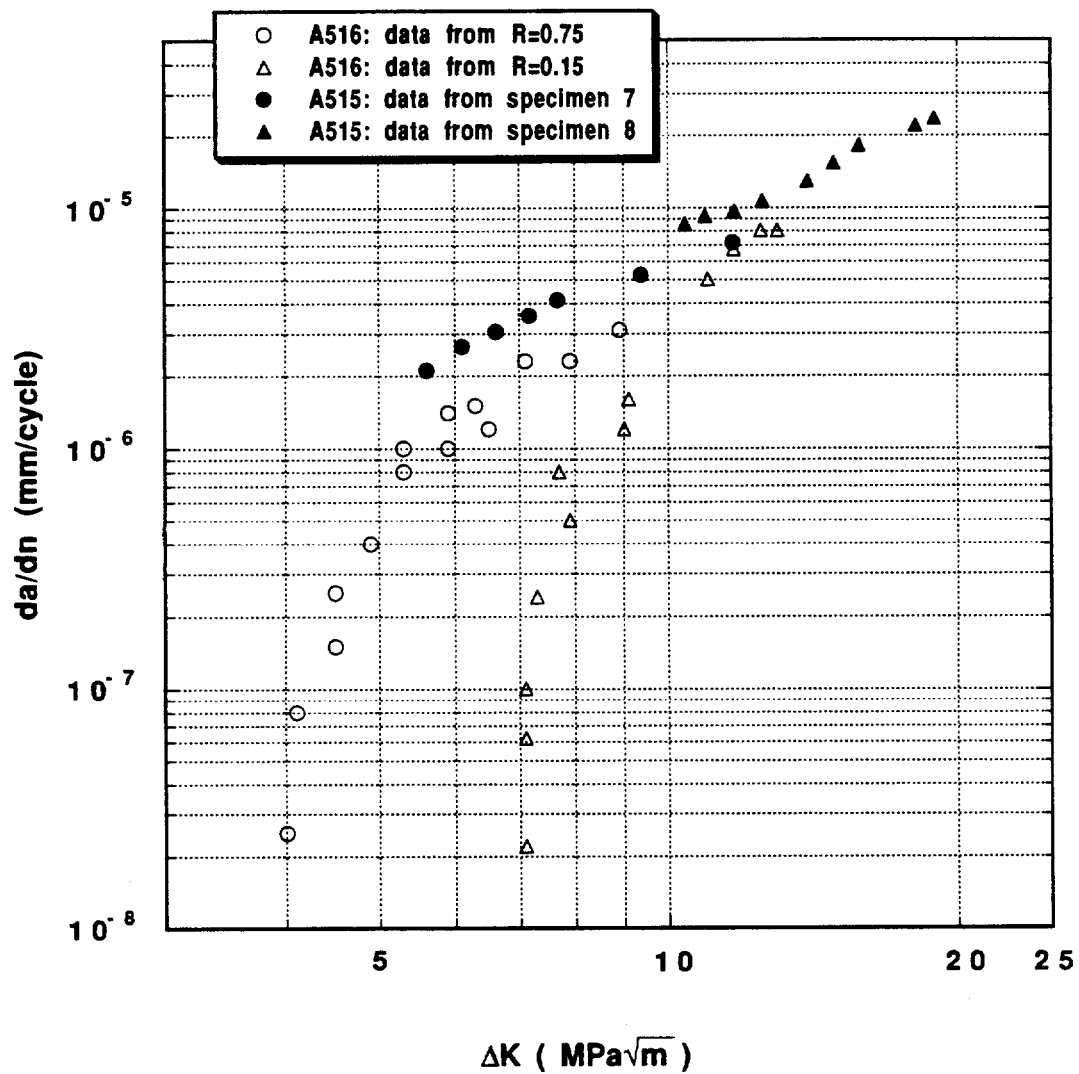


Figure 6.10 Comparison with A516 Steel
(replotted from [49])

CHAPTER 7

CONCLUSION

1). Consistent residual stress patterns near the fillet weld toe were found from both hole drilling and sectioning measurement results. Welding residual stresses were found to be biaxial tension-tension near the weld toe at the weld center and biaxial tension-compression near the weld toe at the weld end.

2). Simple weld specimens with widths greater than 4 inch (100mm) showed a similar residual stress state near weld ends as the pad-on-plate weld specimens. A 5 inch width simple specimen was considered appropriate for fatigue testing.

3). Cyclic load with maximum tensile stress greater than 14 Ksi (100 MPa) will cause a significant relaxation of longitudinal welding residual stress at weld ends of simple weld specimens. To study the effect of residual stresses on fatigue behavior of a longitudinally fillet welded structure, the applied cyclic load should be below 14 Ksi.

4). The effective thermal stress relief condition was found to be annealing the as-welded specimen at 650°C for one hour. Under this condition, tensile residual stress will be relieved completely and there is no significant heat treatment effect on the microstructure of the material.

5). Under pulsed tension cyclic load, no significant effect of residual stress on fatigue strength was found. Under alternating cyclic load, the stress-

relieved specimen showed a significant increase in fatigue life over the as-welded specimen.

6). The crack propagation behavior of welded A515 grade 70 steel was found to be accurately predicted by the Paris equation. The power exponent in the equation was found to be $m=2$ for the surface crack propagation of a semi-elliptic crack.

7). The concept of an equivalent crack has been discussed as an aid for engineering fatigue analysis. With this concept, the fatigue process of a welded joint is simplified to be a crack propagation process which is appropriately predicted by the linear elastic fracture mechanics approach. The tested fillet welded joint was found to be associated with a semi-elliptic equivalent crack of about 0.2 inch in length.

8). The fillet weld end toe, which is associated with a stress concentration factor of about 3, was found to be the most critical factor for fatigue crack initiation. The effects of weld defects are not critical to the fatigue strength under cyclic load with high amplitude or high mean stress. However, the effects of weld defects are significant under cyclic load with low amplitude or low mean stress.

9). Based on current experimental results, the effect of welding residual stress on the fatigue strength of tension-tension cyclic loaded welded joints is secondary when it is compared with the effect of random weld defects.

REFERENCE

1. Tong, P., et al "DOT 111A/100W tank car special retrofit stiffener integrity assessment", *Task Force Report*, U.S. DOT Transportation Systems Center, Cambridge, MA, 1987
2. Orringer, O., J. E. Gordon, A. B. Perlman "On some problems of stress concentration in railroad tank car shell", *App. Mech. Rail Transportation Symposium*, Ed. by H. H. Barr et al, ASTM, 1988
3. "Residual stress relief study" *Project Review*, Advanced Technology and Research Corporation, August, 1989
4. Ohta, A., E. Sasaki, M. Kamakura, M. Nihei, M. Kosuge, M. Kanao, M. Inagaki "Effect of Residual Tensile Stresses on Threshold Level for Fatigue Crack Propagation in Welded Joints of SM50B Steel" *Transactions of JWRI*, Vol. 12, No. 1, April 1981
5. Gurney, T. R. *Fatigue of Welded Structures*, 2nd edition, Cambridge University Press, 1979
6. Maddox, S. J. "Influence of tensile residual stress on the fatigue behavior of welded joints in steel" *Residual Stress Effects in Fatigue*, ASTM STP 776, 1982
7. Reemsnyder, H. S. "Development and application of fatigue data for structural steel weldments" *Fatigue Testing of Weldments*, Ed. by D. W. Hoepfner, ASTM STP 648, 1978
8. Berge, S., O. I. Eide "Residual stress and stress interaction in fatigue testing of welded joints" *Residual Stress Effects in Fatigue*, ASTM STP 776, 1982
9. Munse, W. H. *Fatigue of Welded Steel Structures*, Welding Research Council, New York, 1964
10. Masubuchi, K. *Analysis of Welded Steel Structure*, Pergamon Press, New York, 1980
11. Cottell, G. A. "Fatigue failures, with special reference to fracture characteristics" *British Engine Technical Report*, Vol. II, pp. 221-256, 1954
12. Engel, L., H. Klingele *An Atlas of Metal Damage*, Prentice-Hall, 1981

13. Rolfe, S. T., J. M. Barsom *Fracture and Fatigue Control in Structures - Applications of Fracture Mechanics*, Prentice-Hall, 1977
14. Forrest, P. G. *Fatigue of Metals*, Pergamon Press, 1962
15. Frost, N. E., K. J. Marsh, L. P. Pook *Metal Fatigue*, Oxford University Press, 1974
16. Bannantine, J. A., J. J. Comer, J. L. Handrock *Fundamentals of Metal Fatigue Analysis*, Prentice-Hall, 1990
17. McClintock, F. A., A. S. Argon *Mechanical Behavior of Material*, Addison-Wesley, MA, 1966
18. Parlane, A. J. A. "The determination of residual stresses: a review of contemporary measurement techniques", *Residual Stress in Welded Construction and Their Effect*, Welding Institute Conference, London, 15-17 Nov. 1977
19. Fukuda, S., Y. Tsuruta "An experimental study of redistribution of welding residual stress with fatigue crack extension" *Transactions of JWRI*, Vol. 7, No. 2, 1978
20. Itoh, Y. Z., S. Suruga, H. Kashiwaya "Prediction of fatigue crack growth rate in welding residual stress field" *Engineering Fracture Mechanics*, Vol. 33, No. 3, pp. 397-407, 1989
21. Fukuda, S., S. Watari, K. Horikawa "An experimental study of welding residual stress upon fatigue crack propagation based on observation of crack opening and closure" *Transactions of JWRI*, Vol. 8, No. 2, 1979
22. Ohta, A., M. Kosuge, T. Mawari, S. Nishijima "Fatigue crack propagation in tensile residual stress fields of welded joint under fully compressive cycling" *Int. J. Fatigue*, Vol. 10, No. 4, pp. 237-242, 1988
23. Greasley, A., S. G. W. Naylor "Influence of welding residual stresses on fatigue crack growth under compressive loading" *Engineering Fracture Mechanics*, Vol. 24, No. 5, pp. 717-726, 1986
24. Bernard, P. J., T. C. Lindley, C. E. Richards "Mechanisms of overload retardation during fatigue crack propagation", *Fatigue Crack Growth under Spectrum Loads*, ASTM STP 595, 1976
25. Maddox, S. J. "The effect of plate thickness on the fatigue strength of fillet welded joint", Edison Welding Institute, 1987
26. Boler, R. "Influence of residual stress on fracture of weldments" *The Mechanics of Fracture*, conference proceedings, Dec. 2-6, 1985
27. Broek, D. *Elementary Engineering Fracture Mechanics*, 4th edition,

Martinus Nijhoff, 1986

28. Bodger, P. H., F. Watkinson, Lim, M., Weldl, R. G. Baker "The Initiation of cracking in the fatigue of non-carrying fillet welds" *Fatigue Performance of Welded High Strength Steels*, Welding Institute, 1974
29. Reemsnyder, H. S. "Development and application of fatigue data for structural steel Weldments" *Fatigue Testing of Weldments*, Ed. by D. W. Hoepfner, ASTM STP 648, 1978
30. Iida, K. "Fatigue strength of defective butt welded joints" *Significance of Defects in Welded Structures* Ed. by T. Kanazawa, A. S. Kobayashi, University of Tokyo Press, 1974
31. Martins Ferreira, J. A., C. A. Moura Branco "Influence of the radius of curvature at the weld toe in the fatigue strength of fillet welded joints" *Int. J. Fatigue*, Vol. 11, No. 1, pp. 29-36, 1989
32. Maddox, S. J. "Assessing the significance of flaws in welds subject to fatigue" *Welding Research Supplement* pp. 401s-409s, September 1974
33. Lassen, T. "The effect of the welding process on the fatigue crack growth" *Welding Research Supplement*, pp. 75s-81s, February, 1990
34. Jakubczak, H., G. Glinka "Fatigue analysis of manufacturing defect in weldments" *Int. J. Fatigue*, Vol. 8, No. 2, pp. 51-57, 1986
35. Smith, I. F. C. "Advances in defect assessment for fatigue" *Metal Construction*, November 1982
36. Gurney, T. R. "Revised fatigue design rules", *Metal Construction*, January, 1983
37. Graville, B. A., F. Watkinson, Lim "Research program to investigate the fatigue of high strength steel: initiation in fillet welds" *Fatigue Performance of Welded High Strength Steels*", Report Series, Welding Institute, 1974
38. Signes, E. G., R. G. Baker, J. D. Harrison, F. M. Burdekin "Factors affecting the fatigue strength of welded high strength steels", *Brit. Welding J.*, Vol. 14, No. 3, pp. 108-116, 1967
39. Kapadia, B. M. "Influence of residual stresses on fatigue crack propagation in electrosag welds" *Fatigue Testing of Weldments*, Ed. by D. W. Hoepfner, ASTM STP 648, 1978
40. Radaj, D. *Design and Analysis of Fatigue Resistant Welded Structures*, Halsted Press, 1990
41. Maddox, S. J. "Improving the fatigue strength of welded joints by

peening" *Metal Construction*, April, 1985

42. Booth, G. S. "Improving the fatigue strength of welded joints by grinding techniques and benefits" *Metal Construction*, July, 1986
43. Booth, G. S. "The fatigue life of ground or peened fillet welded steel joints -the effect of mean stress" *Metal Construction*, February, 1981
44. Zheng, X. "A further study on fatigue crack initiation life - mechanical model for fatigue crack initiation" *Int. J. Fatigue*, Vol. 8, No. 1, pp. 17-21, 1986
45. Lawrence, F. V., R. J. Mattos, Y. Higashida, J. D. Burk "Estimating the fatigue crack initiation life of welds" *Fatigue Testing of Weldments*, Ed. by D. W. Hoepfner, ASTM STP 648, pp. 135-158, 1978
46. Maddox, S. J. "The effect of mean stress on fatigue crack propagation - a literature review" *International Journal of Fracture*, Vol. 11, No. 3, pp. 389-408, June 1975
47. Vosikovsky, O., L. P. Trudeau, A. Rivard "Effect of residual stresses on fatigue crack growth threshold" *Int. J. Fracture*, Vol 16, 1980
48. Geary, W., J. E. King "Residual stress effects during near-threshold fatigue crack growth" *Int. J. Fatigue*, Vol. 9, No. 1, pp. 11-16, 1987
49. Taylor, D. *A Compendium of Fatigue Thresholds and Growth Rates*, EMAS, 1985
50. Zhao, X. "The effect of stress ratio on fatigue threshold" *Int. J. Fatigue*, Vol. 12, No 2, 1990
51. Woodtli, J., W. Muster, J. C. Radon "Residual stress effects in fatigue crack growth" *Engineering Fracture Mechanics*, Vol. 24, No. 3, pp. 399-412, 1986
52. Glinka, G. "Effect of residual stresses on fatigue crack growth in steel weldments under constant and variable amplitude loads" *Fracture Mechanics* Ed by C. W. Smith, ASTM STP 677, pp. 198-214, 1979
53. Crooker, T. W., D. J. Krause "The influence of stress ratio and stress level on fatigue crack growth rate in 140Ksi YS steel", *Report of NRL Progress*, Naval Research Laboratory, Washington D.C., Dec. 1972
54. Gurney, T. R. "Some recent work relating to the influence of residual stresses on fatigue strength" *Residual Stress in Welded Construction and Their Effect*, Welding Institute Conference, London, 15-17 Nov. 1977
55. Maddox, S. J. "Fatigue of stress-relieved fillet welds under part-compressive loading" *Research Report*, Welding Institute, Nov. 1982

56. Harrison, J. D. "The effect of residual stresses on fatigue behavior", *Residual Stresses and Their Effect*, The welding Institute, 1981
57. Horikawa, K., Y. Takada "Influence of welding residual stresses on fatigue crack initiation life" *Transactions of JWRI*, Vol. 13, No. 1, pp. 163-166, 1984
58. Verreman, Y., J. Masounave, J. P. Bailon "fatigue life prediction of welded joints using the effective stress intensity factor range" *The Mechanism of Fracture*, conference proceedings, 1985
59. Nelson, D. V. "Effects of residual stress on fatigue crack propagation" *Residual Stress Effects in Fatigue*, ASTM STP 776, 1982
60. Shi, Y. W., B. Y. Chen, J. X. Zhang "Effects of welding residual stresses on fatigue crack growth behavior in butt welds of a pipeline steel", *Engineering Fracture Mechanics*, Vol. 36, No. 6, pp. 893-902, 1990
61. Parker, A. P. "Stress intensity factors, crack profiles, and fatigue crack growth rate in residual stress fields" *Residual Stress Effects in Fatigue*, ASTM STP 776, 1982
62. Wu, X. R. "The effect of welding residual stress on brittle fracture of plates with surface cracks" *Engineering Fracture Mechanics*, Vol. 19, No. 3, pp. 427-439, 1984
63. Horikawa, K., S. Fukuda, Y. Kishimoto "Fatigue crack growth rate in welded joints after stress relief heat treatment" *Transactions of JWRI*, Vol. 10, No. 2, pp. 91-95, 1981
64. Takahashi, E., K. Iwai, K. Satoh "A method of measuring triaxial residual stress in heavy section butt weldments", *Transactions of the Japan Welding Society*, Vol. 10, No 1, April 1979
65. Misra, A. "Examination of the ring method for determination of residual stresses" *SESA*, July, 1981
66. Nelson, D. V., J. T. McCrickerd "Residual stress determination through combined use of holographic interferometry and blind-hole drilling", *Experimental Mechanics*, December, 1986
67. Rund, C. O. "A review of selected nondestructive methods for residual stress measurement", *NDT international*, February, 1982
68. Stahlkopf, K, G. R. Egan, G. Dau "Recent advances in residual stress measurement", *Residual Stress in Welded Construction and Their Effect*, Welding Institute Conference, London, 15-17 Nov. 1977
69. Prask, H. J., C. S. Choi "Residual stress measurements in armament system components by means of neutron diffraction", *Residual Stress in*

Design, Process and Materials Selection, Proceedings of ASM's conference on residual stress, 1987

70. Dove, R. C., P. H. Adams "Experimental Stress Analysis and Motion Measurement", Charles E. Merrill Books, Inc., 1964
71. "Errors due to transverse sensitivity in strain gages" *Technique Note*, No. 507, Measurement Group Inc., 1987
72. "Standard test method for determining residual stress by the hole-drilling strain-gage method", *Annual Book of ASTM Standards*, Vol. 03.01, E837-89, 1989
73. Boag, J. M., M. T. Flaman, J. A. Herring "Considerations of using the hole drilling method for measuring residual stresses in engineering components" *Residual Stress in Design, Process and Materials Selection*, Proceedings of ASM's conference on residual stress, 1987
74. Makhnenko, V. I., R. Yu. Mosenkis "Calculating the coefficient of concentration of stresses in welded joints with butt and fillet welds" *Automatic Welding*, August 1985
75. McFadyen, N. B., R. Bell, O. Vosikovsky "Fatigue crack growth of semi-elliptical surface cracks" *Int. J. Fatigue*, Vol. 12, No. 1, pp. 43-50, 1990
76. Vainshtok, V., I. Varfolomeyev "Stress intensity factor analysis for part-elliptical cracks in structures" *Int. J. Fracture*, Vol. 46, pp. 1-24, 1990
77. Tada, H., P. C. Paris "The stress intensity factor for a crack perpendicular to the welding bead" *Int. J. Fracture*, Vol. 21, pp. 279-284, 1983
78. Fett, T. "An estimation of local stress intensity factors for semi-elliptical surface cracks" *Engineering Fracture Mechanics*, Vol. 34, No. 4, pp. 883-890, 1989
79. Niu, X., G. Glinka "The weld profile effect on stress intensity factors in weldments" *International Journal of Fracture*, No. 35, pp. 3-20, 1987
80. *Stress Intensity Factors Handbook*, Ed. by Y. Murakami et al, Pergaman Press, 1987
81. Thelning, K-E *Steel and Its Heat Treatment* 2nd edition, Mackays of Chatham Ltd., 1984
82. Smith, R. A. "Short fatigue cracks" *Fatigue Mechanisms: Advances in Quantitative Measurement of Physical Damage*, ASTM STP 811, pp. 264-279, 1983
83. Smith, I. F. C., R. A. Smith "Fatigue crack growth in a fillet welded joint" *Engineering Fracture Mechanics*, Vol. 18, No. 4, pp. 861-869, 1983

84. *Structural Alloys Handbook*, Metals and Ceramics Information Center, Battelle, 1990
85. Seeley, S. S., L. Katz, J. R. M. Smith "Fatigue crack growth in low alloy steel submerged arc weld metals, *ASTM STP 648*, Ed. by D. W. Hoepfner, pp. 261-284, 1978
86. "Standard test method for measurement of fatigue crack growth rate", *Annual Book of ASTM Standards*, Vol. 03.01, E647-88a, 1989

APPENDIX

Appendix 1 Program for sectioning residual stress measurement

```

C   Fortran program for sectioning residual stress measurement
    real R1,R2,R3,D1,D2,D3,S1,S2,SX,SY,SXY,SX1,SY1,SXY1,
*   GA,AG,P,Q,A,B
    i=1
10  PRINT*, " SECTIONING RESIDUAL STRESS CALCULATION "
    A=-1.4768
    B=-2.6832
    print*, "Input resistance: R0,R45,R90=?"
    read (*,*),R1,R2,R3
C   Input resistance value of gage 0, 45, 90 from screen
    print*, "Input resistance change: D1,D2,D3=?"
    read (*,*),D1,D2,D3
C   Input resistance change value of gage 0, 45, 90 screen
    D1=(D1/R1)*1000
    D2=(D2/R2)*1000
    D3=(D3/R3)*1000
    SX1=0.5*30*((1/A+1/B)*D1+(1/A-1/B)*D3)
    SY1=0.5*30*((1/A-1/B)*D1+(1/A+1/B)*D3)
    SXY1=(0.5*30*(D2-0.5*(D1+D3)))/B
    print*, "Input direction: ANGLE=?"
    read (*,*),AG
C   Input the angle between the interested direction X and the gage 0
    GA=AG*3.1415926/180
    SX=SX1*((COS(GA))**2)+SY1*((SIN(GA))**2)+SXY1*SIN(2*GA)
    SY=SX1*((SIN(GA))**2)+SY1*((COS(GA))**2)-SXY1*SIN(2*GA)
    SXY=0.5*(SY1-SX1)*SIN(2*GA)+SXY1*COS(2*GA)
    P=SY-SX
    Q=-2*SXY
    S1=0.5*(SX+SY)+SQRT((((SX-SY)/2)**2+SXY**2)
    S2=0.5*(SX+SY)-SQRT((((SX-SY)/2)**2+SXY**2)
    SEQ=SQRT(0.5*((S1-S2)**2+S1**2+S2**2))
    if (P.NE.0) go to 300
    if (Q) 220,240,260
220  GA=1.5707963/2
    go to 320
240  GA=0.0
    go to 320
260  GA=-1.5707963/2
    go to 320

```

```
300 GA=0.5*ATAN(Q/P)
    if (P.LT.0) go to 320
    if (Q) 305,306,307
305 GA=GA+1.5707963
    go to 320
306 GA=1.5707963
    go to 320
307 GA=GA-1.5707963
    go to 320
320 AG=GA*180/3.1415926
    if (i.NE.1) goto 370
    write (1,350)
350 format (//,11x,'* * * THIS IS THE STRESS STATE * * *',/)
    write (1,360)
360 format (1x,'#',3x,'STRESS-1',2x,'STRESS-2',2x,'ANGLE',2x,
* 'STRESS-X',2x,'STRESS-Y',2x,'STRESS-XY',2x,'STRESS-EQ')
370 write (1,400)i,S1,S2,AG,SX,SY,SXY,SEQ
400 format (/ ,I2,4x,f5.1,5x,f5.1,4x,f5.1,4x,f5.1,5x,f5.1,5x,f5.1)
C Print out the principle stresses, the stress components in the x
C axis defined coordinates and the equivalent stress to file fort.1
    i=i+1
    goto 10
    stop
    end
```

Appendix 2 Program for hole-drilling residual stress measurement

```

C   Fortran program for hole-drilling residual stress measurement
C   with high stress effect modification
integer I,J
real R1,R2,R3,D1,D2,D3,S1,S2,SX,SY,GA,AG,P,Q,AA,BB
dimension A(50),B(50)
do 10 J=1,20
A(J)=-29.90
B(J)=-64.00
10  continue
A(21)=-30.2
A(22)=-30.5
A(23)=-30.8
A(24)=-31.1
A(25)=-31.4
A(26)=-31.70
A(27)=-32.00
A(28)=-32.29
A(29)=-32.59
A(30)=-32.89
A(31)=-33.30
A(32)=-33.73
A(33)=-34.14
A(34)=-34.56
A(35)=-34.98
A(36)=-35.40
A(37)=-35.82
A(38)=-36.24
A(39)=-36.66
A(40)=-37.08
A(41)=-37.50
A(42)=-37.92
A(43)=-38.33
A(44)=-38.75
A(45)=-39.17
A(46)=-39.59
A(47)=-40.01
A(48)=-40.43
A(49)=-40.85
A(50)=-41.27
B(21)=-64.64
B(22)=-65.28
B(23)=-65.92
B(24)=-66.56
B(25)=-67.20
B(26)=-67.84
B(27)=-68.48
B(28)=-69.12

```

```

B(29)=-69.76
B(30)=-70.40
B(31)=-71.30
B(32)=-72.19
B(33)=-73.09
B(34)=-73.98
B(35)=-74.88
B(36)=-75.78
B(37)=-76.67
B(38)=-77.57
B(39)=-78.46
B(40)=-79.36
B(41)=-80.26
B(42)=-81.15
B(43)=-82.05
B(44)=-82.94
B(45)=-83.84
B(46)=-84.74
B(47)=-85.63
B(48)=-86.53
B(49)=-87.42
B(50)=-88.32
J=1
20 I=20
PRINT*, "HOLE-DRILLING RESIDUAL STRESS CALCULATION"
print*, "R1,R2,R3=?"
read (1,100),R1,R2,R3
C Input resistance value of gage x, 45, y from file fort.1
print*, "D1,D2,D3=?"
read (1,100),D1,D2,D3
C Input resistance change value of gage x, 45, y from file fort.1
100 format(1x,f8.3,1x,f8.3,1x,f8.3)
D1=(D1/R1)*1000000
D2=(D2/R2)*1000000
D3=(D3/R3)*1000000
30 AA=A(I)
BB=B(I)
S1=(D1+D3)/AA-SQRT((D1-D3)**2+(2*D2-D1-D3)**2)/BB
S2=(D1+D3)/AA+SQRT((D1-D3)**2+(2*D2-D1-D3)**2)/BB
SEQ=SQRT(0.5*((S1-S2)**2+S1**2+S2**2))
SA=ABS(I-SEQ)
if (SEQ.LT.20) go to 40
if (SA.LT.1) go to 40
if (SEQ.GE.50) go to 35
I=INT(SEQ)
go to 30
35 I=50
go to 30
40 P=D3-D1
Q=D1+D3-2*D2

```

```

    if (P.NE.0) goto 300
    if (Q) 200,220,240
200  GA=-1.5707963/2
    GOTO 320
220  GA=0.0
    GOTO 320
240  GA=1.5705963/2
    GOTO 320
300  GA= 0.5*ATAN(Q/P)
    if (P.GT.0) go to 320
    if (Q) 305,306,307
305  GA=GA-1.5705963
    go to 320
306  GA=1.5707963
307  GA=GA+1.5707963
    go to 320
320  AG=GA*180/3.1415926
    SX=S1*((COS(GA))**2)+S2*((SIN(GA))**2)
    SY=S1*((SIN(GA))**2)+S2*((COS(GA))**2)
    SXY=-0.5*(S2-S1)*SIN(2*GA)
    if (J.NE.1) goto 370
    write (2,350)
350  format (//,11x,'* * * THIS IS THE STRESS STATE * * **',/)
    write (2,360)
360  format (1x,'#',3x,'STRESS-1',2x,'STRESS-2',2x,'ANGLE',2x,
    * 'STRESS-X',2x,'STRESS-Y',2x,'STRESS-XY',2x,'STRESS-EQ')
370  write (2,400)J,S1,S2,AG,SX,SY,SXY,SEQ
400  format (/ ,I2,4x,f5.1,5x,f5.1,4x,f5.1,4x,f5.1,5x,f5.1,5x,f5.1,5x,f5.1)
C    Print out principle stresses, stress components in x-y
C    coordinates and the equivalent stress to file fort.2
    J=J+1
    goto 20
    stop
    end

```

Appendix 3 Program for stress intensity factor of semi-elliptic crack

```

C Fortran program for determination of stress intensity factor
C of surface semi-elliptical crack under tension load
real W, t, fi1, fi2, pi, a, b, a0, af, ba, in, M1, M2, M3, ga, gb,
* Ffa, Ffb, Fw, Fsa, Fsb, Ek, Ka, Kb, S
write (2,10)
10 format (/4x,'* * STRESS INTENSITY FACTOR OF
* SEMI-ELLIPTIC CRACK * ',/)
50 PRINT*, " STRESS INTENSITY FACTOR CALCULATION "
W=5.0
t=0.5
C Note: W is plate width, t is plate thickness
a0=?
af=?
ba=?
S=?
in=?
C Set initial and final crack length, b/a ratio, load, crack length increment
write (2,100) S, ba
100 format (5x,'S=',f5.2,10x,'b/a=',f5.2,/)
fi1=0.0
fi2=1.5708
fi3=0.7854
pi=3.1415926
Do 420 a=a0, af, in
b=a*ba
IF (b-t) 110, 450, 450
110 IF (a-0.25*W) 120, 450, 450
120 continue
130 IF (a-b) 160, 150, 150
150 M1=1.13-0.09*(b/a)
M2=-0.54+0.89/(0.2+(b/a))
M3=0.5-1/(0.65+(b/a))+14*((1-(b/a))**24)
ga=1+(0.1+0.35*(b/t)**2)*((1-SIN(fi1))**2)
gb=1+(0.1+0.35*(b/t)**2)*((1-SIN(fi2))**2)
Ffa=(((b/a)**2)*((COS(fi1))**2)+((SIN(fi1))**2))**0.25)
Ffb=(((b/a)**2)*((COS(fi2))**2)+((SIN(fi2))**2))**0.25)
Fw=SQRT(1/(COS(((pi*a)/W)*SQRT(b/t))))
Fsa=(M1+M2*((b/t)**2)+M3*((b/t)**4))*ga*Ffa*Fw
Fsb=(M1+M2*((b/t)**2)+M3*((b/t)**4))*gb*Ffb*Fw
Ek=SQRT(1+1.464*((b/a)**1.65))
GOTO 200
160 M1=(1+0.04*(a/b))*SQRT(a/b)
M2=0.2*((a/b)**4)
M3=-0.11*((a/b)**4)
ga=1+(0.1+0.35*(a/b)*(b/t)**2)*((1-SIN(fi1))**2)
gb=1+(0.1+0.35*(a/b)*(b/t)**2)*((1-SIN(fi2))**2)
Ffa=(((a/b)**2)*((SIN(fi1))**2)+((COS(fi1))**2))**0.25)

```

```
Ffb=(((a/b)**2)*((SIN(fi2))**2)+((COS(fi2))**2))**(0.25)
Fw=SQRT(1/(COS(((pi*a)/W)*SQRT(b/t))))
Ek=SQRT(1+1.464*((a/b)**1.65))
GOTO 200
200 Ka=(S*(SQRT(pi*b))*Fsa)/Ek
210 Kb=(S*(SQRT(pi*b))*Fsb)/Ek
370 write (2,400)a,b,Ka,Kb
400 format (4x,'a =',f6.3,6x,'b =',f6.3,9x,'Ka =',f6.2,9x,'Kb =',f6.2)
C Print out crack length, depth and their corresponding stress
C intensity factor values to file fort.2
420 continue
450 continue
stop
end
```

Appendix 4 Program for stress intensity factor of through-thickness crack

```

C      Fortran program for determination of stress intensity factor
C      of center through-thickness crack in finite wide plate under
C      tension Load
      real W, t, pi, a, a0, af, aa, in, S
      double precision Ka
      i=1
      write (3,10)
10     format (4x,'* * STRESS INTENSITY FACTOR OF
*     THROUGH-THICKNESS CRACK * *',/)
50     PRINT*, " STRESS INTENSITY FACTOR CALCULATION "
      W=5.0
      t=0.5
C      Note: W is plate width, t is plate thickness
      pi=3.1415926
      a0=?
      af=?
      in=?
      S=?
C      Set initial and final crack length, crack length increment and load
      Do 450 a=a0, af, in
      aa=(2*a)/W
100    format(1x,f5.2,1x,f6.3)
150    Ka=S*(SQRT(pi*a))*(1-0.025*(aa**2)+0.06*(aa**4))*
*     SQRT(1/(COS((pi*a)/W)))
      write (3,400) S, a, Ka
400    format (4x,'S =',f5.1,' (Ksi)',9x,'a =',f6.3,' (inch)',9x,'Ka =',f6.2)
C      Print out load, crack length and stress intensity factor to file fort.3
450    continue
      stop
      end

```

Appendix 5 Program for semi-elliptic crack propagation life

```

C   Fortran program for determination of fatigue crack propagation
C   life of surface semi-elliptical crack under tension Load
real W, t, pi, a0, ba, C, Cm, M1, M2, M3, ga, Ffa, Fw, Fsa, Ek, Ka, S
integer i, N, J
double precision a, b, da
write (4,10)
10  format (//,4x,"* * * Fatigue Crack Propagation Life * * *",//)
50  PRINT*, " Fatigue Crack Propagation Life Calculation "
    J=0
    N=0
    W=5.0
C   Note: W is plate width, t is plate thickness
    t=0.5
    pi=3.1415926
    C=?
    Cm=?
    S=?
    a0=?
    ba=?
C   Set constants in Paris law, stress range, initial crack length and b/a ratio
    i=1
    da=0.0
    a=a0
105  continue
    a=a+da
    b=a*ba
    IF (b-t) 110, 450, 450
110  IF (a-0.25*W) 120, 450, 450
120  goto 150
150  M1=1.13-0.09*ba
    M2=-0.54+0.89/(0.2+ba)
    M3=0.5-1/(0.65+ba)+14*((1-ba)**24)
    ga=1+(0.1+0.35*(b/t)**2)
    Ffa=SQRT(ba)
    Fw=SQRT(1/(COS(((pi*a)/W)*SQRT(b/t))))
    Fsa=(M1+M2*((b/t)**2)+M3*((b/t)**4))*ga*Ffa*Fw
    Ek=SQRT(1+1.464*(ba**1.65))
    GOTO 200
200  Ka=(S*(SQRT(pi*b))*Fsa)/Ek
    da=C*(Ka**Cm)
    N=INT(i/100000)
    IF (N-J) 408, 405, 405
405  J=J+1
    write (4, 406) N, a, b, Ka, da
406  format (1x,'N='I3,'X100000',4x,'a=',f7.5,4x,'b=',f7.5,4x,'Ka=',f7.4,
* 4x,'da=',E11.4)
408  continue

```

```
    i=i+1
    goto 105
450  goto 455
455  write (4,460) S, C, Cm, ba
460  format (/ ,1x,'S=',f5.1,6x,'C=',f15.12,6x,'m=',f5.2,6x,'b/a=',f5.2)
470  write (4,500) a0, a
500  format (/ ,1x,'Initial Crack Length =',f7.4,8x,'Final Crack Length =',f7.4)
570  write (4,600) i
600  format (/ ,1x,'Crack Propagation Life =',I8)
C    Print out setup informations, crack length at selected cycles, final
C    crack length and total crack propagation life to file fort.4
    print*,"Fractured"
    stop
    end
```

Appendix 6 Program for through-thickness crack propagation life

```

C   Fortran program for crack propagation life calculation
C   of center cracked plate
real a, a0, af, aa, w, pi, s, m, c
integer i, N, J
double precision da, k
i=0
J=0
w=5.0
C   Note: w is plate width
af=2.0
pi=3.1415926
c=?
m=?
a0=?
s=?
C   Set constants in Paris law, initial crack length and stress range
write (3, 25)
25  format (5x, '* * Through Thickness Crack Propagation life * *')
write (3, 50) s, a0, af, c, m
50  format (/ ,1x, 'S=', f4.1, 6x, 'a0=', f5.3, 6x, 'af=', f5.3, 6x, 'C=', f14.12,
*    6x, 'M=', f3.1, /)
a=a0
100 continue
aa=(2*a)/w
k=s*(SQRT(pi*a))*(1-0.025*(aa**2)+0.06*(aa**4))*
*  SQRT(1/cos((pi*a)/w))
da=c*(k**m)
N=INT(i/10000)
if (N-J) 150, 120, 120
120 J=J+1
write (3, 125) i, a, k, da
125 format (2x, 'N=', I7, 9x, 'a=', f5.3, 9x, 'Ka=', f6.2, 9x, 'da=', e11.4)
150 continue
a=a+da
i=i+1
if (a .GE. af) goto 200
goto 100
200 continue
write (3, 350) i
350 format (/ ,8x, 'The Fatigue Propagation Life is N=', I7)
C   Print out setup informations, crack length at selected cycles
C   and total crack propagation life to file fort.3
print *, "Fractured !"
stop
end

```